ULTRA-WIDEBAND WIRELESS BODY AREA NETWORK DESIGN AND OPTIMISATION

by

Jie Ding

Dissertation submitted in fulfilment of the requirements

for the degree of

DOCTOR OF PHILOSOPHY

Department of Engineering
Faculty of Science & Engineering
Macquarie University
Sydney, Australia

September 2015

ABSTRACT

Wireless body area networks (WBANs) recently have drawn significant attention in telemedicine and mHealth, which comprise intelligent devices on/in the human body to support various healthcare applications for patient care and disease treatment. Impulse radio ultra-wideband (IR-UWB) is a promising potential telemetry technique in WBANs. Owing to its simple electronics and low power emission, it is less likely to affect human tissues or cause interference to other medical equipment. In UWB based WBANs, spectral efficiency and energy efficiency are certainly two of the most important challenges.

In this thesis, we will study the spectral efficiency and energy efficiency optimization problems in relay-assisted UWB based WBANs under various practical transmission scenarios. The main work done in this thesis is summarized as follows:

(1) Research on energy-saving based relay selection in UWB based WBANs. With a pulse based energy consumption model, the energy-saving relay selection criterion is detailed and analyzed. We show that the relay location plays an important role in UWB based WBANs, which motivates us to explore the optimal relay location and power allocation for performance optimization under various scenarios.

(2) Spectral efficiency optimization and energy efficiency optimization in single-relay UWB based WBANs. To maximize the two metrics, we seek the relay with the optimal location together with the corresponding optimal power allocation. We show the necessity of utilization of a relay node in UWB based WBANs in some scenarios. With the joint optimal relay location and power allocation

scheme, the network spectral efficiency can be enhanced significantly compared to other transmission schemes. Up to 30 times improvement compared to direct transmission in terms of energy efficiency can be achieved when the battery of the source node is very limited.

(3) Research on tradeoff between energy efficiency and spectral efficiency in single-relay UWB based WBANs. To balance performance between energy efficiency and spectral efficiency and optimize the two metrics simultaneously with desirable preferences, a utility for the energy-spectral efficiency tradeoff is constructed. We show that the proposed utility can be a guideline with regard to the relay placement and power allocation in designing the energy-spectral efficient transmission in UWB based WBANs.

(4) Preliminary research on spectral efficiency and energy efficiency optimization in multiple-relay UWB based WBANs. We extend the single-relay case to the multiple-relay case. Distributed beamforming problems for the spectral efficiency and energy efficiency optimization are investigated, respectively. The preliminary results show that a considerable improvement can be achieved not only in energy efficiency but also in spectral efficiency by using multiple relays and the optimal relay location varies with the battery power limit of the source node.

STATEMENT OF CANDIDATE

I certify that the work in this thesis has not previously been submitted for a degree nor has it been submitted as part of the requirements for a degree to any other university or institution other than Macquarie University.

I certify that the thesis is an original piece of research and has been written by me.

In addition, I certify that all information sources and literature used are indicated in the thesis.

. . . . . .

Jie Ding

ACKNOWLEDGMENTS

First and foremost, I would like to express my sincerest gratitude to my supervisors, Prof. Eryk Dutkiewicz (Macquarie University, Australia) and Prof. Xiaojing Huang (University of Technology, Sydney), who have constantly encouraged me to strive for excellence in my career. This work would not have been completed without their remarkable insight, great knowledge, invaluable guidance and generous financial support.

I would also like to acknowledge my co-supervisor Dr. Gengfa Fang, my colleagues and friends Beeshanga Abewardana Jayawickrama, Yuyi Wei, Xianjun Yang, Yin Hui Chye, Perzila Ara, etc for their help and encouragement to my life and PhD studies.

This thesis was co-funded by Macquarie University and CSIRO. I would like to thank both organisations for their generous support, which have provided a rich and fertile environment for me to study and explore new ideas.

Finally, I am forever indebted to my parents, my wife and my newborn baby for their infinite love and support along this long but fulfilling road.

Contents

Abstract **iii**

Acknowledgments **ix**

Table of Contents **xi**

List of Figures **xv**

List of Tables **xix**

List of Publications **xxi**

1 Introduction **1**

1.1 Background 1

1.2 Research Objectives 3

1.3 Organization of Thesis 4

1.4 Contributions 6

2 Literature Review **9**

2.1 Outline 9

2.2 Overview of Ultra-Wideband Technology 9

2.2.1 Concept of Ultra-Wideband 10

2.2.2 Advantages of Ultra-Wideband 11

2.2.3 Transmissions of Ultra-Wideband 13
2.3 Overview of Wireless Body Area Networks 15
2.3.1 Definition of Wireless Body Area Networks 15
2.3.2 Properties of Wireless Body Area Networks 17
2.3.3 IEEE 802.15.6 Standard 18
2.4 Main Challenges in Ultra-Wideband based Wireless Body Area Networks . 22
2.4.1 Channel Modelling 22
2.4.2 Spectral Efficiency 25
2.4.3 Energy Efficiency 27
2.4.4 Tradeoff between Spectral Efficiency and Energy Efficiency 29
2.5 Summary 30

3 Energy-Saving based Relay Selection for UWB based WBANs 31

3.1 Introduction 31
3.2 System Model 32
3.2.1 Channel Model 33
3.2.2 System Metric 35
3.2.3 Energy Consumption Model 36
3.3 Minimized Energy Consumption for Cooperative Transmission 37
3.3.1 Energy Consumption of Cooperative Transmission 37
3.3.2 Optimal Power Allocation for Cooperative Transmission 38
3.4 Energy-Saving Relay Selection 39
3.5 Simulation Results 43
3.6 Summary 47

4 Spectral Efficiency Optimization in Single-Relay UWB based WBANs 49

4.1 Introduction 49

4.2 System Model 50
4.2.1 System Scenarios 50
4.2.2 Channel Models 52
4.3 Spectral Efficiency Optimization 54
4.3.1 Spectral Efficiency of Direct Transmission 54
4.3.2 Spectral Efficiency Optimization for On-Body Transmissions 56
4.3.3 Spectral Efficiency Optimization for In-Body Transmissions 65
4.3.4 Discussions 69
4.4 Simulation Results 71
4.4.1 Spectral Efficiency Evaluation for On-Body Transmissions 71
4.4.2 Spectral Efficiency Evaluation for In-Body Transmissions 77
4.5 Summary 81

5 Energy Efficiency Optimization in Single-Relay UWB based WBANs 85
5.1 Introduction 85
5.2 Energy Efficiency Optimization 86
5.2.1 Energy Efficiency Optimization for On-Body Transmissions 87
5.2.2 Energy Efficiency Optimization for In-Body Transmissions 92
5.3 Simulation Results 93
5.3.1 Energy Efficiency Evaluation for On-Body Transmissions 94
5.3.2 Energy Efficiency Evaluation for In-Body Transmissions 98
5.4 Summary 100

6 Joint Energy Efficiency and Spectral Efficiency Optimization in Single-Relay UWB based WBANs 103
6.1 Introduction 103
6.2 Utility for Tradeoff between Energy Efficiency and Spectral Efficiency . . . 104

6.3 Proposed Algorithms for Tradeoff Optimization . . . 106
6.3.1 Numerical Algorithm . . . 106
6.3.2 Sub-Optimal Algorithm . . . 107
6.4 Simulation Results . . . 109
6.5 Summary . . . 113

7 Spectral Efficiency Optimization and Energy Efficiency Optimization in Multiple-Relay UWB based WBANs 115
7.1 Introduction . . . 115
7.2 System Scenarios and Proposed Cooperative Model . . . 117
7.3 Distributed Beamforming Transmission . . . 118
7.4 Optimal Power Allocation for Spectral Efficiency Optimization . . . 121
7.5 Optimal Power Allocation for Energy Efficiency Optimization . . . 124
7.6 Simulation Results . . . 125
7.6.1 Spectral Efficiency of Proposed Distributed Beamforming Scheme . 126
7.6.2 Energy Efficiency of Proposed Distributed Beamforming Scheme . . 130
7.7 Summary . . . 133

8 Conclusions and Future Work 135
8.1 Research Summary . . . 135
8.2 Future Work . . . 138
8.2.1 Channel Modeling . . . 138
8.2.2 Error Resilience and Reliability . . . 139
8.2.3 Interference Mitigation . . . 139

Abbreviations 141

Bibliography 145

List of Figures

Figure 2.1 UWB EIPR level by FCC First Report and Order [1]. 10
Figure 2.2 UWB PSD and bandwidth comparison with different types of wireless systems [1]. 12
Figure 2.3 Block diagram of a typical UWB transmitter. 14
Figure 2.4 Examples of monitoring in WBAN [2]. 16
Figure 2.5 Interconnection of WBAN, WPAN, WLAN, and wide area networks [2]. 17
Figure 2.6 Network topology in IEEE 802.15.6 standard. 19

Figure 3.1 A simplified network model for WBANs. 33
Figure 3.2 Relay regions corresponding to different criterion rules when S and D are on the different sides of the human body (around the torso). 41
Figure 3.3 Relay regions corresponding to different criterion rules when S and D are on the same side of the human body (along the torso). 42
Figure 3.4 $\Delta\xi$ versus d with various relay locations when S and D are on the different sides of the human body (around the torso) and $Z = 10$dB. 44
Figure 3.5 $\Delta\xi$ versus d with various relay locations when S and D are on the same side of the human body (along the torso) and $Z = 10$dB. 45
Figure 3.6 Cooperation energy-gain versus desired Z when S and D are on the different sides of the human body (around the torso) and $d = 0.8$. 46

Figure 4.1 Proposed cooperative model for on-body transmissions in WBANs. 56

Figure 4.2 Proposed cooperative model for in-body transmissions in WBANs. . 65

Figure 4.3 SE performance of the proposed scheme with and without body motion in the around-torso scenario when $d_{SD} = 0.6$m and $d_r = 0.2$m. . . . 74

Figure 4.4 Average SE versus P_s for the along-torso scenario. 76

Figure 4.5 Average SE versus P_s in the around-torso scenario when $d_{SD} = 0.6$m and $d_r = 0.2$m. 77

Figure 4.6 Average SE versus d_{SD} in the around-torso scenario with different d_r and $P_s = 4$dBm. 78

Figure 4.7 Average SE versus P_s for the in-body scenario with different d_{SD} and $d_r = 5$cm. 80

Figure 5.1 Average energy efficiency versus P_s in the around-torso scenario with $d_{SD} = 0.6$m and $d_r = 0.2$m. 95

Figure 5.2 Average EE versus d_{SD} in the around-torso scenario with $P_s = 4$dBm. 96

Figure 5.3 Energy efficiency versus P_s in the along-torso scenario. 97

Figure 5.4 Average EE versus P_s in the in-body scenario with $d_{SD} = 0.3$m and $d_r = 5$cm. 99

Figure 5.5 Average EE versus d_{SD} in the in-body scenario with $P_s = 10$dBm and $d_r = 5$cm. 100

Figure 6.1 The normalized utility versus P_s with $w = 0.5$ in the around-torso scenario. 110

Figure 6.2 The normalized utility versus P_s with $w = 0.5$ in the in-body scenario.111

Figure 6.3 The normalized utility, EE, and SE with $\{x_r^o, y_r^o, P_1^o, P_2^o\}$ when $P_s =$ 0dBm in the around-torso scenario. 112

Figure 6.4 The normalized utility, EE, and SE with $\{x_r^o, y_r^o, P_1^o, P_2^o\}$ when $P_s =$ 0dBm in the in-body scenario. 112

Figure 7.1 Modified cooperative model for implant WBANs. 117

Figure 7.2 Average SE versus P_s with $L_r = 4$ in a 2-relay network. 126

Figure 7.3 Average SE versus P_s with different numbers of relays and relay locations when $L_r = 4$. 128

Figure 7.4 Average SE versus x_0 with different P_s in a 2-relay network. 129

Figure 7.5 Average SE versus P_s with different L_r in a 2-relay network. 130

Figure 7.6 Average EE versus P_s in a 2-relay network. 131

Figure 7.7 Average SE versus P_s in a 2-relay network. 132

Figure 7.8 Average EE versus P_s with different relay locations. 133

List of Tables

Table 3.1 UWB based WBAN CM3 Channel Model 34
Table 3.2 Simulation Parameters 43

Table 4.1 UWB based WBAN path loss (including shadowing) models 53
Table 4.2 Averaged optimal set $\left\{\mathrm{E}\{x_r^{se}\}, \mathrm{E}\{y_r^{se}\}, \mathrm{E}\{P_1^{se}\}, \mathrm{E}\{P_2^{se}\}\right\}$ for on-body transmissions 72
Table 4.3 Averaged optimal set $\left\{\mathrm{E}\{x_r^{se}\}, \mathrm{E}\{y_r^{se}\}, \mathrm{E}\{P_1^{se}\}, \mathrm{E}\{P_2^{se}\}\right\}$ in the around-torso scenario without body motion 73
Table 4.4 Averaged optimal set $\left\{\mathrm{E}\{x_r^{se}\}, \mathrm{E}\{y_r^{se}\}, \mathrm{E}\{P_1^{se}\}, \mathrm{E}\{P_2^{se}\}\right\}$ for in-body transmissions 79

Table 5.1 The proposed iterative algorithm 90
Table 5.2 $\left\{\mathrm{E}\{x_r^{ee}\}, \mathrm{E}\{y_r^{ee}\}\right\}$ and $\alpha = \mathrm{E}\{P_1^{ee}/P_2^{ee}\}$ for both scenarios 94
Table 5.3 Averaged optimal solution $\left\{\mathrm{E}\{x_r^{ee}\}, \mathrm{E}\{y_r^{ee}\}, \mathrm{E}\{P_1^{ee}\}, \mathrm{E}\{P_2^{ee}\}\right\}$ 98

Table 6.1 Averaged optimal solution $\left\{\mathrm{E}\{x_r^{o}\}, \mathrm{E}\{y_r^{o}\}, \mathrm{E}\{P_1^{o}\}, \mathrm{E}\{P_2^{o}\}\right\}$ for the utility optimization 109

Table 7.1 Examples of STBC matrix $\mathbf{B}$ for relays 120

List of Publications

As the major outcome of my PhD research work, a number of papers have been published or are currently under review. They are listed as following:

- **Journal Papers**

1. **Jie Ding**, Eryk Dutkiewicz, Xiaojing Huang, "Energy and Spectral Efficiency Optimization and Tradeoff in Single-Relay UWB Based Implant Body Area Networks," Submitted to *ACM/IEEE Transactions on Networks*.

2. **Jie Ding**, Eryk Dutkiewicz, Xiaojing Huang, "Joint Optimal Relay Location and Power Allocation for Ultra-Wideband Based Wireless Body Area Networks," *EURASIP Journal on Wireless Communications and Networking,* Vol. 2015, No. 1, April 2015.

- **Conference papers**

1. **Jie Ding**, Eryk Dutkiewicz, Xiaojing Huang, "Performance Evaluation of Virtual MIMO for UWB Based Body Area Networks," IEEE International Symposium on Medical Information and Communication Technology (ISMICT), 2013, pp. 28-32.

2. **Jie Ding**, Eryk Dutkiewicz, Xiaojing Huang, Gengfa Fang, "Energy-Efficient Cooperative Relay Selection for UWB based Body Area Networks," IEEE International Conference on Ultra-Wideband (ICUWB), 2013, pp. 97-102. (Won the "Merit of Certificate")

3. **Jie Ding**, Eryk Dutkiewicz, Xiaojing Huang, "Energy Efficient Cooperative Communication for UWB based In-body Area Networks," Proceedings of the International

Conference on Body Area Networks (ACM BodyNets), 2013, pp. 29-34.

4. **Jie Ding**, Eryk Dutkiewicz, Xiaojing Huang, "Carrier Frequency Offset Estimation for Non-contiguous OFDM Receiver in Cognitive Radio Systems," IEEE Global Communications Conference (GLOBECOM), 2013, pp. 4192-4197.

5. **Jie Ding**, Eryk Dutkiewicz, Xiaojing Huang, "Optimal Spectral Efficiency for Cooperative UWB based On-body Area Networks," IEEE Wireless Communications and Networking Conference (WCNC), 2014, pp. 1224-1229.

6. **Jie Ding**, Eryk Dutkiewicz, Xiaojing Huang, Gengfa Fang, "Spectral Efficiency Optimization with Distributed Beamforming in UWB Based Implant Body Area Networks," Proceedings of the International Conference on Body Area Networks (ACM BodyNets), 2014, pp.1-5.

7. **Jie Ding**, Eryk Dutkiewicz, Xiaojing Huang, Gengfa Fang, "Energy-Efficient Distributed Beamforming in UWB Based Implant Body Area Networks," IEEE Vehicular Technology Conference (VTC) Spring, 2015, pp.1-5.

8. **Jie Ding**, Eryk Dutkiewicz, Xiaojing Huang, Gengfa Fang, "Energy Efficient Cooperative Transmission in Single-Relay UWB Based Body Area Networks," IEEE International Conference on Communications (ICC), 2015, pp.1-5.

Chapter 1

Introduction

In this Chapter, the background is presented in Section 1.1, the research objectives of the thesis are addressed in Section 1.2, the organization of this thesis is described in Section 1.3 and the contributions of this thesis are summarized in Section 1.4.

1.1 Background

Wireless communications have been witnessed to evolve at an outstanding speed in recent years. With the advances in wireless technology and supporting infrastructure, a new concept has been extensively explored to provide unprecedented opportunity for ubiquitous real-time healthcare without constraining the activities of the patient, commonly referred to as wireless body area networks or WBANs for short. Generally, a WBAN consists of several small, intelligent nodes attached on or implanted in the human body. These nodes are used to monitor the physiological states of the patient periodically, e.g., measuring heartbeat or recording body activities, and provide real-time feedback to the user or medical personnel. Unlike traditional wireless sensor networks (WSNs), WBANs have some typical properties, e.g., limited energy resources for nodes, limited network size, ultra-low-power wireless connectivity among nodes, and considerable signal attenuation

around or in the human body. Thus, unique technical challenges need to be taken into account in WBANs to achieve affordable and efficient healthcare solutions to patient that will improve their quality of life.

Motivated by the increasing research and industry interest in WBANs, the IEEE 802.15 Task Group 6 has developed the first industrial standard encompassing physical (PHY) and medium access control (MAC) layers for WBANs. In the IEEE 802.15.6 standard, impulse radio ultra-wideband (IR-UWB) is employed as a PHY layer technology. Since IR-UWB uses simple short pulses to send data, it makes the transmitter design very simple, small size, and low power. Moreover, it is less likely to affect human tissues or cause interference to other medical equipment due to a relatively low power spectral density (PSD) emission. These advantages lead to the suitability of IR-UWB applications in WBANs.

In UWB based WBANs, nodes have stringent limitations in size and weight. In most cases, their energy resources are extremely limited and batteries may not be rechargeable and replaceable. In some applications, a node should operate while supporting a battery lifetime of months or even years without intervention. Thus, a long lifetime is crucial. On the other hand, low power transmissions in UWB based WBANs often lead to unsatisfactory transmission reliability and efficiency due to the strong propagation blockage around or inside the human body. Therefore, spectral efficiency (SE) and energy efficiency (EE) are two of the biggest concerns in UWB based WBANs. Developing and designing schemes for the SE and EE related enhancement are of significant interest to recent WBAN industry and research community.

1.2 Research Objectives

The aim of the research project has been to enhance SE and EE in UWB based WBANs and eventually address the performance optimization to provide an insight into the spectral-energy efficient design of healthcare applications.

In WSNs, the relay-assisted transmission is considered as an effective method to improve network performance. Therefore, the theme in this thesis is to propose novel relay deployment solutions in order to design a spectral-energy efficient WBAN. Conventionally, relay deployment was only implemented with power allocation schemes in the literature to optimize the WBAN performance. However, deploying relays optimally in terms of relay location is still an open issue. Thus, the first main objective of the thesis is to design a joint optimal relay location and power allocation scheme for the SE and EE optimization.

As an intrinsic characteristic, although optimal SE and EE can be achieved separately, they are not always achievable simultaneously and sometimes may even conflict. Therefore, the second main objective of the thesis is to balance the tradeoff between SE and EE in UWB based WBANs. The key for the balanced performance between SE and EE is to build up a valid utility function of these two metrics. Hence, developing a novel utility is a prime work herein.

In addition to the SE and EE optimization in single-relay UWB based WBANs, the SE and EE optimization are also worth studying in a multiple-relay case. With multiple-relay assistance, spatial diversity gain can be exploited and consequently network performance may be further improved. Thus, the third main objective of the thesis is to design effective transmission methods and achieve optimal SE and EE in multiple-relay UWB based WBANs.

The specific major tasks in this thesis are as follows:

- Investigate the performance of cooperative transmission in single-relay UWB based

WBANs to well understand the effect of relay location on the network performance and identify potential space for performance improvement compared to direct transmission.

- Build relay-location based cooperative network models and problem frameworks for the SE and EE optimization in single-relay UWB based WBANs.
- Provide solutions to seek the optimal relay location together with the optimal power allocation for the SE and EE optimization. Compare with the state-of-art transmission schemes in existing literature to demonstrate the expected performance improvement and advantages of our proposed joint optimal relay location and power allocation scheme.
- Develop a novel utility to balance the tradeoff between SE and EE in UWB based WBANs and verify the efficacy of the developed utility.
- Extend our research work from the single-relay case to a multiple-relay case. Design effective transmission protocols and propose algorithms to achieve optimal SE and EE in multiple-relay UWB based WBANs.

1.3 Organization of Thesis

This thesis is organized to have eight chapters, and each chapter consists of several sections to perform a detailed presentation on a specific topic. The brief contents of the chapters are given as follows.

Chapter 1 is Introduction. Section 1.1 presents the background of this thesis. Section 1.2 states the main objectives of this thesis. Section 1.3 introduces the organization of this thesis. Section 1.4 describes the main contributions of this thesis.

Chapter 2 is Literature Review. Section 2.2 introduces the UWB techniques. Section 2.3 details WBANs, including their definition, properties, and physical layer techniques. Section 2.4 summarizes the existing research and main challenges of UWB based WBANs. Along with a description of the challenges, the motivations of the research are stated in detail.

Chapter 3 studies the performance of cooperative transmission from a relay-location selection perspective in single-relay UWB based WBANs. Specifically, Section 3.2 describes the system model. In Section 3.3, the minimized energy consumption for cooperative transmission is presented with a realistic pulse-based energy consumption model. In Section 3.4, the energy-saving relay selection criterion is developed in detail. Simulation results are presented in Section 3.5. Summary of this Chapter is given in Section 3.6.

Chapter 4 optimizes spectral efficiency in single-relay UWB based WBANs. In Section 4.2, the system model is described, where the system scenario and considered channel models are presented, respectively. In Section 4.3, relay-location based network models are developed first, the spectral efficiency optimization problem in cooperative transmission is then formulated and the joint relay location and power allocation is derived accordingly. Simulation results are illustrated in Section 4.4. Summary of this Chapter is given in Section 4.5.

Chapter 5 optimizes energy efficiency in single-relay UWB based WBANs. With the same system scenario, channel models and proposed network models as presented in Chapter 4, the energy efficiency optimization problems are formulated and solved in Section 5.2. Simulation results are illustrated to evaluate the proposed joint optimal relay location and power allocation scheme in Section 5.3. Section 5.4 summarizes this Chapter.

In Chapter 6, joint optimal energy efficiency and spectral efficiency is studied in single-relay UWB based WBANs. In Section 6.2, a utility for the tradeoff between energy efficiency and spectral efficiency is proposed. In Section 6.3, proposed algorithms for the

tradeoff optimization are presented. Simulation results are given in Section 6.4. This Chapter is summarized in Section 6.5.

In Chapter 7, spectral efficiency optimization and energy efficiency optimization are investigated in multiple-relay UWB based WBANs. In Section 7.2, a system scenario and a multiple-relay based cooperative model are presented. In Section 7.3, distributed beamforming transmissions are described. Optimal power allocation schemes are proposed for spectral efficiency optimization and energy efficiency optimization in 7.4 and 7.5, respectively. Performance evaluation is given in Section 7.6. This Chapter is summarized in Section 7.7.

Finally, Chapter 8 summarizes the research of this thesis and gives the outlook for future work.

1.4 Contributions

The main contributions of this research work are listed as follows.

- The energy-saving based relay selection criterion is developed in single-relay UWB based WBANs. With a realistic nonlinear energy consumption model, the optimal power allocation with a given relay location is derived for single-relay cooperative transmission to minimize the total energy consumption. By comparing the energy difference between cooperative transmission and direct transmission, it is revealed that the relay location in different WBAN regions makes a big difference on the energy-saving performance of cooperative transmission. The relay location, therefore, plays a critical role from the system optimization point of view. This evidence motivates us to explore the optimal relay location and power allocation under various scenarios in UWB based WBANs.

- Spectral efficiency optimization and energy efficiency optimization are theoretically

derived in single-relay UWB based WBANs. Unlike the conventional optimization scheme where only power allocation is considered, a truly joint optimal scheme for spectral efficiency and energy efficiency optimization problems is proposed, in which the relay location and power allocation are optimized jointly for each problem. We prove that globally optimal solutions exist for both optimization problems and the derived closed-form expressions are provided. Numerical results verify the importance of the relay location in UWB based WBANs and reveal that the utilization of a relay node is essential for the spectral and energy efficient transmission.

- The tradeoff between energy efficiency and spectral efficiency is effectively balanced in single-relay UWB based WBANs. To balance performance between energy efficiency and spectral efficiency and optimize the two metrics simultaneously with desirable preferences, a utility for the energy-spectral efficiency tradeoff is constructed. Since the utility optimization problem is a non-concave fractional program, a numerical algorithm by combining sequential quadratic programming algorithm and scatter search is firstly proposed to obtain the globally optimal solution. Then, a low complexity algorithm based on a linear approximation is proposed to obtain the suboptimal solution. We show that the proposed utility can be a guideline with regard to the relay placement and power allocation in designing the energy-spectral efficient transmission in UWB based WBANs.

- Spectral efficiency optimization and energy efficiency optimization are studied in multiple-relay UWB based WBANs. We design a valid distributed transmission scheme to exploit the spatial diversity gain in the multiple-relay case. With the transmission scheme, both metric optimization problems can be formulated as a distributed network beamforming problem. Algorithms are proposed to solve the distributed beamforming problem in an effective manner. Simulation results verify

the effectiveness of the proposed algorithms and show that the proposed distributed transmission scheme is superior to other transmission schemes regarding spectral efficiency and energy efficiency.

Chapter 2

Literature Review

2.1 Outline

In this Chapter, we present an overview of UWB and WBANs, respectively. Main challenges of UWB based WBANs are comprehensively reviewed. The Chapter is organized as follows. Section 2.2 reviews the UWB techniques. Section 2.3 details WBANs, including their definition, properties, and physical layer techniques. Section 2.4 summarizes the existing research and main challenges of UWB based WBANs. Along with a description of the challenges, the motivations of the research are stated accordingly. Finally, the Chapter is concluded in Section 2.5

2.2 Overview of Ultra-Wideband Technology

When designing future short-range wireless systems, one needs to take into account the increasingly pervasive nature of communications and computing based on the vision that wireless systems beyond the third generation (3G) will enable connectivity for "everybody and everything at any place and any time". This ambitious idea assumes that the new wireless world will be the result of a comprehensive integration of existing and future

wireless systems, including wide area networks [3], wireless local area networks (WLANs) [4], wireless personal area networks (WPANs) [5] and WBANs, as well as ad hoc networks that link devices as diverse as portable and fixed appliances, personal computers, and entertainment equipment. As a result, UWB, as a short-range wireless technology, plays an important role in the realization of future pervasive and heterogeneous networking.

2.2.1 Concept of Ultra-Wideband

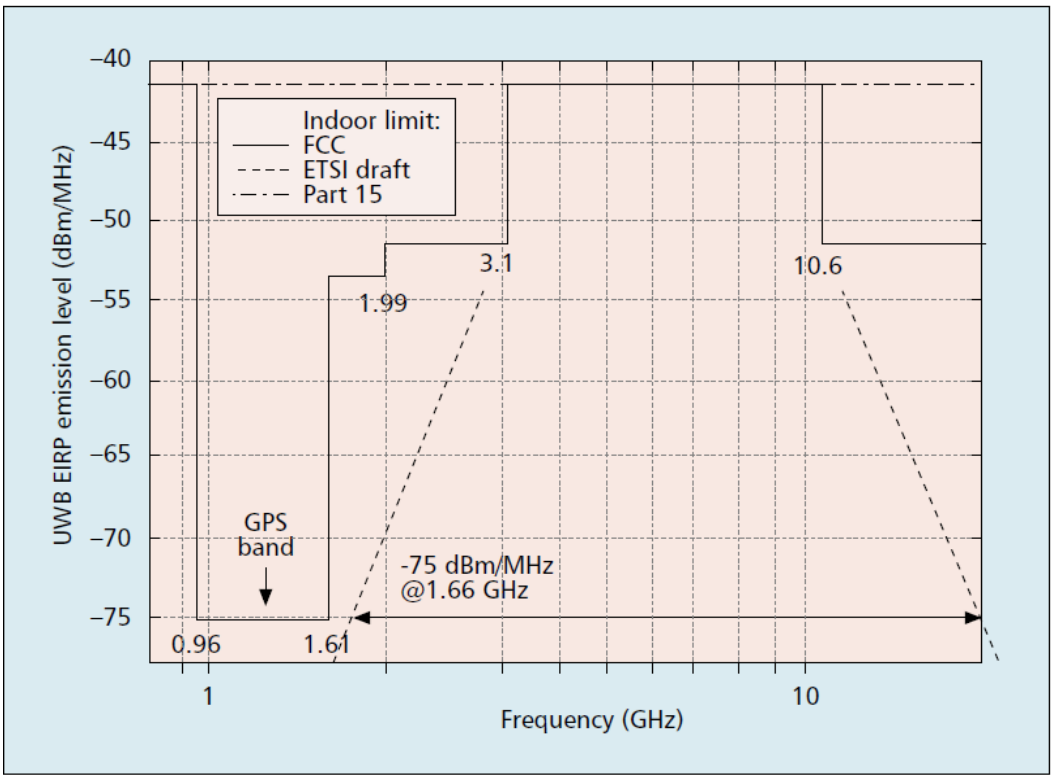

Figure 2.1: UWB EIPR level by FCC First Report and Order [1].

The FCC approved the use of UWB in February 2012 in the First Report and Order [6]. A generic definition used within the FCC and widely accepted by the industry [7] defines a UWB device as any device emitting signals with a fractional bandwidth greater than 0.2 or a bandwidth of at least 500MHz at all times of transmission. The fractional bandwidth

is defined by the expression $2(f_H - f_L)/(f_H + f_L)$, where f_H is the upper frequency and f_L the lower frequency at the -10dB emission point. The center frequency of the signal spectrum emitted by such a system is defined as the average of the upper and lower -10dB points (i.e., $f_C = (f_H + f_L)/2$). At the PHY layer, UWB communication systems operate by spreading rather small amounts of average effective isotropic radiated power (EIRP), which is always less than 0.56mW across a very wide band of frequencies relative to its center frequency. This quantity is easily calculated from the imposed PSD limit of -41.3dBm/MHz between 3.1 GHz and 10.6GHz, which is shown in Fig. 2.1 [1].

With the abundant frequency resources, there are mainly two approaches to the development of UWB systems [8, 9]: impulse-radio (IR) UWB and multi-band orthogonal frequency-division multiplexing (MB-OFDM) UWB. They have different advantages and can be applied in different fields. MB-OFDM UWB has been primarily used for high speed data applications such as streaming video and wireless USB [10]. Due to the high-performance electronics required to operate a MB-OFDM UWB radio, MB-OFDM UWB systems generally are not amenable to energy constrained applications. However, IR-UWB [11, 12], by using ultra-narrow pulses with a low duty cycle to carry information, can be designed for relatively low-complexity, low cost and low power consumption transmissions. Thus, IR-UWB is more suitable to be applied in WBANs [13]. In the sequel, we only consider IR-UWB for WBANs and the terms "IR-UWB" and "UWB" are used interchangeably throughout this thesis.

2.2.2 Advantages of Ultra-Wideband

In Fig. 2.2, the UWB PSD and bandwidth are compared with other types of wireless systems. As shown in the figure, with the properties of a large bandwidth and extremely low transmission power, UWB is able to offer several advantages over narrowband communications systems [1, 14, 15, 16]. The most important properties that make UWB systems

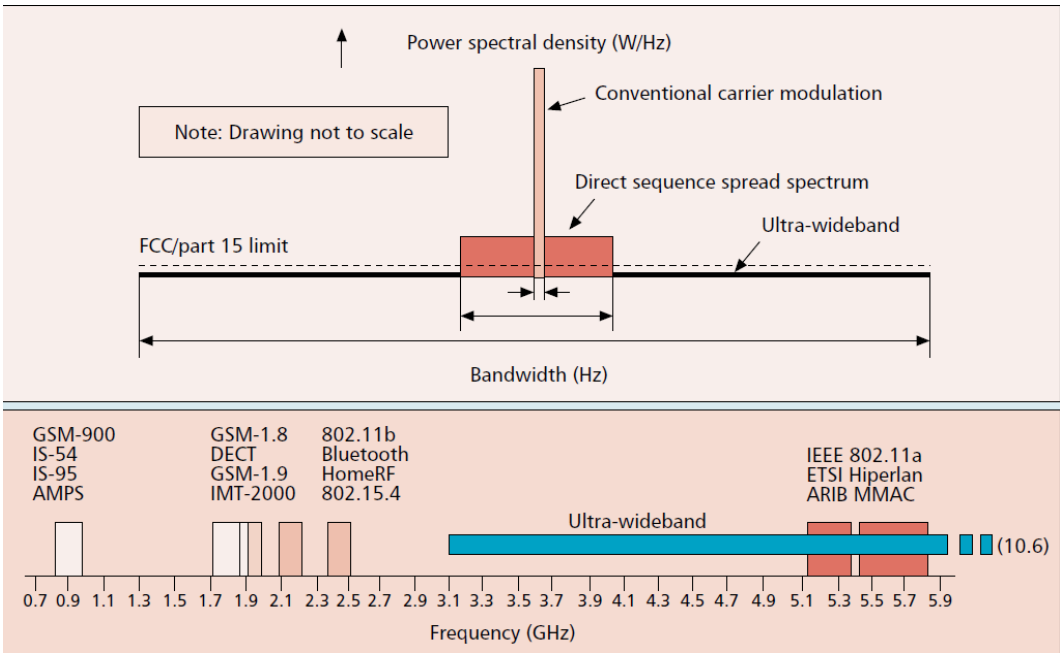

Figure 2.2: UWB PSD and bandwidth comparison with different types of wireless systems [1].

attractive are:

1. Low interference to other users [17, 18, 19, 20]. Because of the power restriction, UWB systems can reside below the noise floor of a typical narrowband receiver and coexist with current radio services with low or no interference. Conversely, the narrowband user represents only narrowband interference to UWB systems and this interference can be resolved using the inherent frequency diversity of UWB systems as long as the front end of the UWB receiver is not overloaded. Furthermore, owing to this characteristic, UWB technology can protect the transmission of sensitive data by reducing the probability of detection [20].

2. High channel capacity [17, 21]. One of the major advantages of the large bandwidth for UWB pulses is to provide high channel capacity. Based on Hartley-Shannon's capacity formula, channel capacity linearly increases with bandwidth. Thus, a high data rate transmission can be expected for UWB systems. However, due to the

extremely low power limitation on UWB transmissions, such high data rate is only valid for short ranges.

3. Simple transceiver architecture [22, 23]. Since the UWB technique employs a series of ultra-narrow pulses to transmit information, it means that the UWB transmission is carrierless and data is not modulated on a continuous waveform with a carrier frequency. For this reason, an UWB transceiver architecture is significantly simpler and thus cheaper to build compared to other traditional narrowband or wideband technologies.

Besides, UWB systems are able to cope with severe frequency-selective channels caused by wireless multipath propagation due to the fine multipath resolution (the transmission duration of a UWB pulse is shorter than a nanosecond in most cases). Furthermore, with time-hopping (TH) or direct-sequence (DS) techniques, multiple users can be accommodated harmoniously [11, 24, 25, 26].

2.2.3 Transmissions of Ultra-Wideband

As mentioned in the previous section, UWB transmission is carrierless and the UWB transmitter is simple and easy to build. A typical diagram of an UWB transmitter is shown in Fig. 2.3. As we can see, the major blocks for generating UWB signals are the pulse generator and data modulation [27].

In the pulse generator block, a UWB pulse signal can be generated by any one of a variety of wideband signals, such as Gaussian, chirp, wavelet, or Hermite-based short-duration pulses. Among these signals, the implementation of the first or the second order derivative of a Gaussian pulse, to generate a Gaussian monocycle or a Gaussian doublet, is considered an efficient approach for the UWB pulse generation [28, 29]. For example,

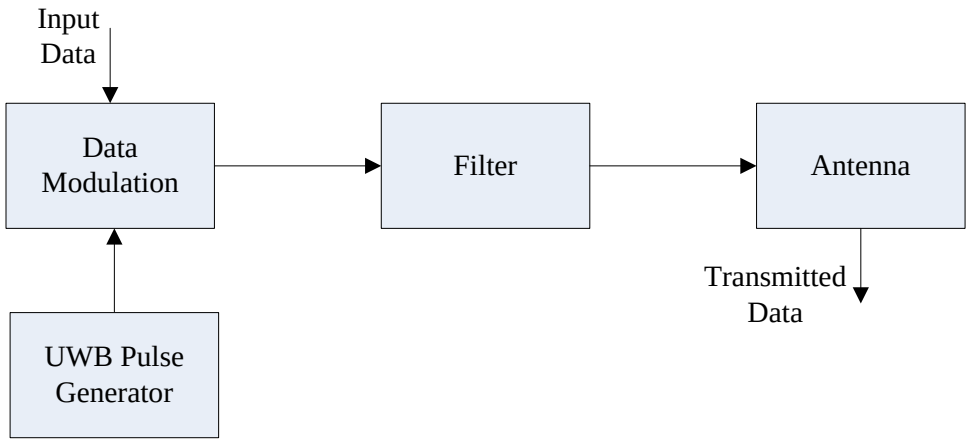

Figure 2.3: Block diagram of a typical UWB transmitter.

the Gaussian monocycle can be easily presented by

$$\omega(t) = \frac{t}{\tau} e^{-(\frac{t}{\tau})^2}, \tag{2.1}$$

where t represents time and τ is a time decay constant that determines the temporal width of the pulse.

In the data modulation block, binary modulation schemes are typically used rather than high-order modulation schemes. The most common modulation schemes employed in UWB are pulse-position modulation (PPM), binary phase-shift keying (BPSK) and on-off keying (OOK) [14,30]. With PPM, the transmitted data is encoded by the position of the transmitted pulses in time, referred to the nominal pulse position. With BPSK, the transmitted data is encoded with the polarity of the impulses. The polarity of the impulses is switched to encode a 0 or a 1. OOK is based on the principle of encoding information with the absence of the impulses, for example, the presence of a pulse represents a 1, while the absence of a pulse represents a 0.

In general, the UWB transmitted signal can be expressed as [31]

$$s_u(t) = \sqrt{P_u} \sum_i s(t - iT_s; d_i), \ d_i \in \{0, 1\}, \tag{2.2}$$

where P_u is the transmit power, T_s is the bit (symbol) duration, and $s(t - iT_s; d_i)$ is a unit-energy pulse waveform used to transmit the ith information bit d_i.

2.3 Overview of Wireless Body Area Networks

The aging population across the world and the rising expenses for health care have triggered the need to exploit new technological solutions to bring affordable and efficient healthcare to people that will improve their quality of life. Traditional wired connections for this purpose become too cumbersome and involve a high cost for deployment and maintenance. However, by using advanced wireless technologies, it not only gives patients greater experience in mobility but also increases their comfort by freeing them from the need to be connected to hospital equipments [32]. In order to fully exploit the benefits of wireless technologies in telemedicine and mobile health (mHealth), a new type of wireless network emerged: WBANs. This term was first mentioned by Van Dam et al. in 2001 [33].

2.3.1 Definition of Wireless Body Area Networks

A WBAN consists of several small, intelligent nodes attached on or implanted in the human body [2, 34, 35, 36, 37]. These nodes have wireless transmission capability. Typically, these nodes can be distinguished into two categories: sensor nodes and coordinator. Sensor nodes are used to monitor the physiological information (including measuring the heartbeat, body temperature or recording a prolonged electrocardiogram (ECG), as shown in Fig. 2.4) and provide the feedback to the coordinator worn on the body. The coordinator, as a sink in WBANs, analyzes the received data from sensor nodes and forwards it to a remote station for diagnostic and healthcare purposes. Notice that, different from sensor nodes with limited power resource and functionality, the coordinator is in charge of collecting all the information received from sensor nodes and handles interactions with

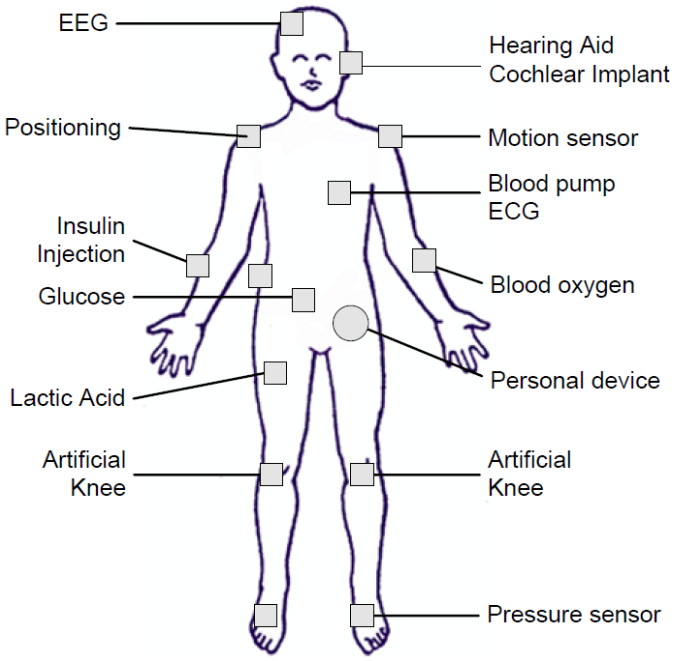

Figure 2.4: Examples of monitoring in WBAN [2].

other users. It is usually a personal device, e.g., a personal digital assistant (PDA) or a smart phone. Thus, it is much more powerful in functionality and computation capability compared to sensor nodes.

In Fig. 2.5, the interconnection of WBAN, WPAN [5], WLAN [4], and wide area networks [3] is displayed. As shown in the figure, the transmission range of WBANs is comparably shorter than other networks, which is restricted to a few meters. To make a connection to a remote station for real time diagnosis or to a medical database for record keeping, the data from the coordinator is transferred by means of WPAN or WLAN. The communication range of a WPAN can reach up to 10 meters for high data rate applications and up to several dozens of meters for low data rate applications. A WLAN has a typical communication range up to hundreds of meters.

Although WBAN is a promising candidate for healthcare, several design issues must be addressed in order to enable the deployment and adoption of WBANs [38,39,40,41]. At

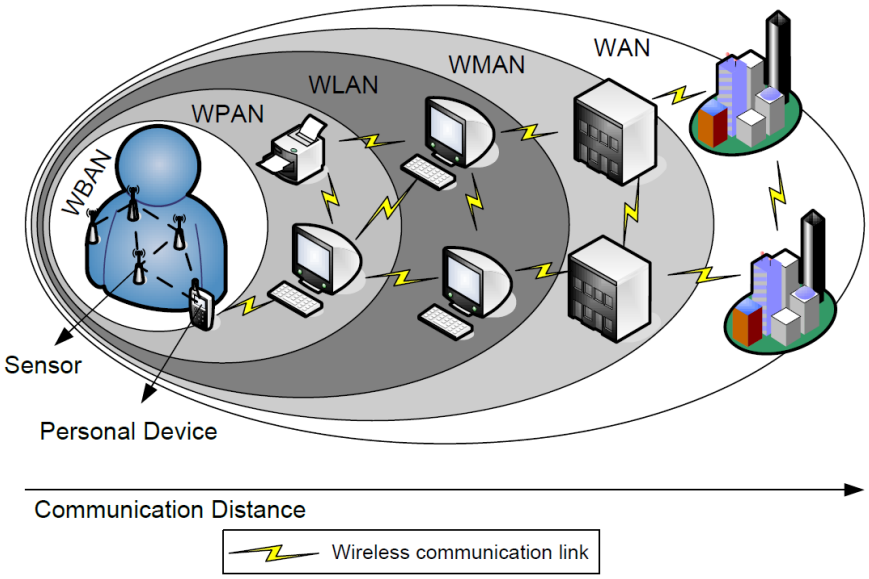

Figure 2.5: Interconnection of WBAN, WPAN, WLAN, and wide area networks [2].

the hardware level, sensor nodes must be small, non-invasive, wireless-enabled, and must be able to operate at an extremely low power level [38, 40]. From the communications perspective, it is crucial to design appropriate MAC protocols and PHY techniques to ensure higher spectral efficiency (SE), energy efficiency (EE), and adequate quality of service (QoS) [39,41]. At the application level, novel architectures should be implemented for the corresponding applications [38, 41].

2.3.2 Properties of Wireless Body Area Networks

Unlike conventional WSNs, WBANs have their own characteristics. Current protocols and PHY techniques designed for WSNs [42] are not always well suited to support a WBAN [2, 36, 43]. The following describes the differences between a WBAN and a WSN:

- Limited energy resources. Since sensor nodes must be small in size (often less than 1cm^3 [44]), their battery resources are very limited. Moreover, although a long lifetime of the node is expected (up to several years or even decades for implanted

nodes), its battery cannot be easily replaced and recharged. Hence, energy efficiency is a crucial parameter in WBANs.

- Equality. All nodes are equally important and nodes are only added when they are needed for an application. To guarantee a patient the best care and comfort, the number of nodes is usually kept to a minimum.

- Low power transmission. Low power transmissions are indispensable to keep interference to a minimum and to cope with health concerns [45].

- Strong propagation loss around/in the human body [46, 47]. The human body is considered as a very complicated and lossy medium. When the signals are transmitted around/through the human body, they may experience strong propagation loss and be attenuated considerably before reaching by the receiver;

- Mobility. Since patients may move around, nodes located on the human body can be in motion. In contrast, WSN nodes are usually considered to be stationary.

2.3.3 IEEE 802.15.6 Standard

Based on the description in the previous sections, it is a fact that the existing standards and technologies cannot meet the requirements and relevant communication regulations for WBAN applications. Therefore, an international standard should be provided for a short-range (i.e., about a human body range), low power, and highly reliable wireless communication for use in close proximity to, or inside a human body. For this purpose, IEEE 802.15 Task Group 6 was formed by the IEEE Standards Association. The IEEE 802.15 Task Group 6 aims to develop a communication standard optimized for low power devices and operation on, in or around the human body (but not limited to humans) to serve a variety of applications including medical, consumer electronics/personal entertainment and other [48].

In the IEEE 802.15.6 standard published in 2012, a general network topology [13] is introduced, which is illustrated in Fig. 2.6. As shown in the figure, there is one and only

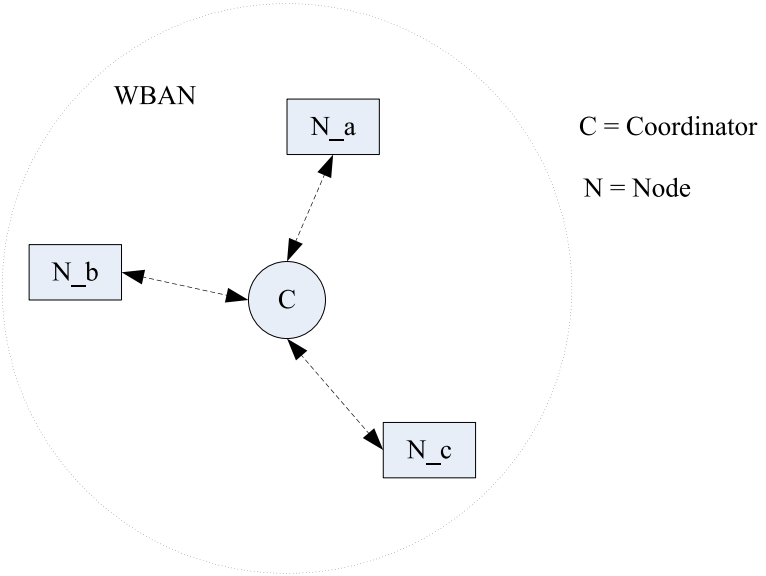

Figure 2.6: Network topology in IEEE 802.15.6 standard.

one coordinator in a WBAN, whereas the number of nodes in a WBAN ranges from zero to the maximum size of a WBAN. In a one-hop star WBAN, frame exchanges are to occur directly between nodes and the coordinator of the WBAN. In a two-hop extended star WBAN, the coordinator and a node exchange frames optionally via a relay-capable node.

The IEEE 802.15.6 standard also defines new MAC and PHY layers for WBANs [13, 49, 50]. For the MAC layer, a multiple access mode known as "improvised access" is supported in the standard, whereby the coordinator can inform nodes that they have been granted one-off exclusive time slots to transmit or receive information [51, 52]. Since this thesis only focuses on the WBAN PHY layer design and optimization, an ideal MAC layer protocol is assumed hereafter. Thus, we only briefly overview the PHYs supported in the IEEE 802.15.6 standard. For the PHY layer [13, 53, 54], three different PHYs are adopted in the IEEE 802.15.6 standard: narrowband, human body communications (HBC), and UWB.

1) *Narrowband PHY.* The narrowband PHY is responsible for activation/deactivation of the radio transceiver, clear channel assessment (CCA) within the current channel, and data transmission and reception. A compliant device shall be able to support transmission and reception in at least one of the following frequency bands: 402MHz to 405MHz, 420MHz to 450MHz, 863MHz to 870MHz, 902MHz to 928MHz, 950MHz to 958MHz, 2360MHz to 2400MHz, and 2400MHz to 2483.5MHz. At the transmitter, the transmit power is limited. For example, when operating in a low power low duty cycle mode on a center frequency of 403.65MHz, a transmitter shall be capable of transmitting at most −40dBm EIRP. When operating in a non low power low duty cycle mode in the 402MHz to 405MHz frequency band, a transmitter shall be capable of transmitting at most −16dBm EIRP. When operating in all other frequency bands, a transmitter shall be capable of transmitting at least −10dBm EIRP. During the transmission, a physical-layer service data unit (PSDU) shall be pre-appended with a physical-layer preamble and a physical-layer header in order to create a physical-layer protocol data unit (PPDU). At the receiver, the physical-layer preamble and physical-layer header serve as aids in the demodulation, decoding and delivery of the PSDU. Based on the recommendations of the standard, the narrowband PHY can be used for on-body and implant transmissions.

2) *HBC PHY.* The HBC PHY uses the electric field communication (EFC) technology. The band of operation is centered at 21MHz. Its PPDU is composed of a preamble, start frame delimiter (SFD), PHY header and a PSDU. The data patterns in the preamble and SFD are fixed. They are pre-generated and sent ahead of the packet header and payload. The SFD is transmitted only once while the preamble sequence is transmitted four times in order to ensure packet synchronization. When the packet is received by the receiver, it estimates the start of the packet by detecting the preamble sequence, and then it estimates the start of the frame by detecting the SFD. Based on the recommendations of the standard, the HBC PHY is used for on-body transmissions only.

3) *UWB PHY*. The UWB PHY is designed to offer robust performance for WBANs and to provide a large scope for implementation opportunities for high performance, robustness, low complexity, and ultra-low power operation. The signal power levels of UWB are in the order of those used in the narrowband, therefore providing safe power levels for the human body and low interference to other devices. The UWB PHY can be operated in two bands: low band and high band. Each band is divided into several optional channels and one mandatory channel and each channel is characterized by a bandwidth of 499.2MHz. As a regulation in the standard, a typical UWB device should support at least one of the mandatory channels. The UWB PHY PPDU is formed by concatenating the synchronization header (SHR), the physical layer header (PHR), and PSDU, respectively. The SHR contains a preamble and a SFD. The PHR conveys information about the data rate of the PSDU, length of the payload and scrambler seed. The information in the PHR is used by the receiver to decode the PSDU. Two operational modes are also defined in UWB PHY: default for medical and non-medical applications, and high quality of service for high-priority medical applications. Both modes shall support IR-UWB as mandatory PHY. Based on the recommendations of the standard, the UWB PHY is used for on-body transmissions only.

Although the narrowband option is usually chosen to realize the implant transmissions and IR-UWB is only considered as a PHY for on-body transmissions in IEEE 802.15.6, a number of studies indicate the feasibility of using IR-UWB for implant communications [55, 56, 57, 58]. In [55], the authors investigated a IR-UWB system for an integrated communication between an in-body implant device in the chest to the body surface. Bit error rate (BER) performance is evaluated accordingly. Results verify the effectiveness of the IR-UWB system for the implant applications. In [56], UWB transmitters based on the band-limited technique were developed and analyzed. The authors present the feasibility of applying an IR-UWB wireless scheme to both implantable neural recording

and wearable biomedical applications. In [57], to cope with the limited data rate from the narrowband modulation schemes for wireless capsule endoscopy, the authors developed an IR-UWB communication system with a PPM based detection scheme. Experimental evaluations indicate the validity of the proposed scheme and reliability of implant WBAN communications. In [58], based on the proposed IR-UWB system in [57], an experimental evaluation of the IR-UWB transmission performance in a living animal was performed. In a real implant WBAN environment, it is shown that the transmission performance is satisfactory and the IR-UWB is a good option as the implant transmission scheme.

In conclusion, the benefit of UWB for wearable and implant communications in W-BANs is quite obvious based on existing literature. Hence, the UWB based WBANs is a topic worth studying. In the next section, we summarize the key issues in UWB based WBANs. Along with a description of the issues, the motivations in this thesis are stated accordingly.

2.4 Main Challenges in Ultra-Wideband based Wireless Body Area Networks

To meet the broad range of requirements imposed by various applications, several issues need to be addressed and overcome in UWB based WBAN. For the main issues to be accounted for in the design of a UWB based WBAN, the impact of channel modelling, spectral efficiency and battery lifetime are of fundamental importance [34].

2.4.1 Channel Modelling

Channel model is important for the design and evaluation of the signalling techniques employed at the PHY in UWB based WBANs. The human body, as a lossy medium, has a great impact on radio propagation, leading to a specific and peculiar radio chan-

nel. Moreover, there is a very big difference in propagation characteristics with different transmission scenarios. The dynamic environment due to walking, running, and mobility further makes it difficult to derive a simple path loss model for WBANs. Thus, in order to realize systems optimised for body centric communications, a deep knowledge of the radio channel is of outmost importance and channel modelling is a main challenge.

A number of UWB based WBAN channel models have been proposed recently. This work was performed on different transmission scenarios, defined by the relative position of the nodes, as presented in [46]. Basically, there are two major transmission scenarios that are relevant for WBANs [59]: 1) On-body transmissions: transmissions between nodes on the human body and the coordinator (possibly including a relay), which is also on the human body. 2) In-body transmissions: transmissions between nodes implanted in the human body and the coordinator (possibly including a relay) on the human body.

Currently, the UWB based WBAN on-body propagation has attracted the most research interest and various investigations have been conducted in different frequency bands and environments [60,61,62,63,64,65,66]. All of these channel models are developed from a set of propagation measurements and are intended to provide a convenient basis for statistical modelling of the channel. In [62, 63, 65, 61], a static propagation condition is considered. Specifically, propagation modelling data was measured in a hospital room and an anechoic chamber in [62], respectively. In [63], measurements were done in an anechoic chamber. The channel models under line of sight (LoS) and non line of sight (NLoS) propagation conditions were both studied. Analysis indicates that the path loss of waves diffracting around the body is much higher than waves traveling along the front of the human body. In [65], time-domain UWB channel measurements were conducted to study the on-body radio propagation when the human body is in the sitting posture. In [61], the environmental reflections are measured for the channel modelling. Although this literature provides a comprehensive propagation characterization of various UWB

based WBAN architectures, the effect of body motion needs to be taken into account in practice [60, 64, 66]. Based on the observations in the literature, it is stressed that the distribution of received energy fluctuations due to the body motion (e.g., arm motions) can be approximately modelled as a Lognormal distribution. Furthermore, body motion to the front and side of the human body only has a small impact on the received power. More significant variations are observed when transmit and receive nodes are on the different sides of the human body.

On the other hand, only a limited contribution is available for the UWB based WBAN in-body channel modelling [67, 68, 69]. To the best of our knowledge, the state-of-the art UWB based WBANs in-body channel model through human tissues was developed in [69]. Herein, a general model with a broad frequency range from 1-6GHz is provided, in which the frequency-dependent material properties of the human tissues are taken into consideration. It is indicated that the path loss as a function of depth inside the chest can be modelled by a fitted mathematical function. The shadowing term, which accounts for the path loss variations caused by different material properties of the tissues, is modelled as a random variable.

In summary, based on the existing literature, the path loss of signals diffracting around the body is much stronger than signals traveling along the human body. The body motion to the front and side of the human body only has a small influence on the received power. A more significant impact is observed when transmit and receive nodes are on different sides of the human body. Furthermore, components through human tissues can be well described by a high path loss exponent and the shadowing due to the different material dielectric properties inside the human body can be modelled as a correlated Lognormal variable.

In the thesis, the channel models proposed in [64, 69] are used for the design of an efficient UWB based WBAN.

2.4.2 Spectral Efficiency

In wireless communication systems, spectral efficiency [bits/s/Hz] refers to the information rate that can be transmitted over a given bandwidth. It is a measure of how efficiently a limited frequency spectrum is utilized by the physical layer protocol [70]. A general expression of spectral efficiency can be given by

$$SE = \log_2(1 + SNR), \tag{2.3}$$

where SNR is the received signal-to-noise ratio (SNR). Since the received SNR is dominated by the transmit power and channel gain, spectral efficiency is also impacted by the two parameters. As the PSD emission for UWB signals is limited by the FCC regulations and the battery lifetime of WBAN nodes is required to last as long as possible, ultra-low power transmission is absolutely necessary in UWB based WBANs. On the other hand, from the overview of channel modelling in Section 2.4.1, it is noted that the UWB signals will experience strong propagation blockage when they travel around or inside the human body. Thus, ultra-low power transmissions with strong propagation blockage around or inside the human body may lead to unsatisfactory spectral efficiency, although UWB can provide a high channel capacity because of its wideband. Hence, spectral efficiency is a major challenge in UWB based WBANs which needs to be tackled.

As suggested in [59], the use of relays in WBANs to mitigate the effects of significant path loss and deep fades can improve spectral efficiency and transmission reliability. Therefore, applying the concept of cooperative communications to WBANs may offer several benefits. In fact, studies have been conducted in WSNs regarding spectral efficiency of relay assisted cooperative communications [71, 72, 73, 74, 75]. In [71], power allocation between a source and relay was optimized to maximize spectral efficiency in single-relay based cooperative networks. In [72], joint relay selection and power allocation strategy for multiuser amplify-and-forward (AF) networks was studied to maximize users' spectral ef-

ficiency. In [73], power allocation and relay selection schemes were proposed to achieve the maximum spectral efficiency and minimum outage probability for multiple relay assisted cooperative networks. In [74, 75], distributed beamforming strategies for multiple-relay cooperative transmission were developed to maximize the spectral efficiency subject to different power constrains under flat fading channels. These studies reveal that cooperative transmission is an effective way that can greatly improve spectral efficiency in WSNs.

Unlike WSNs, UWB based WBANs have some unique properties such as analog transmission, distinct channel characteristics, and limited network size, where the signal strength in a WBAN is mostly affected by the physical location of the nodes in relation to each other as well as the body tissues [59,76]. As a result, the aforementioned existing schemes and results on spectral efficiency in WSNs may be inefficient if they are applied to UWB based WBANs directly. Some related studies regarding cooperative transmission applied in WBANs have been recently reported in [65, 77, 78, 79, 80]. Particularly, channel modelling and system diversity for cooperative transmission in UWB based WBANs were investigated in [65]. In [77], cooperative scheduling schemes were proposed to decrease inter-BAN interference and increase packet reception rate of intra-BAN communications. In [78, 79], bit/packet error rate performance evaluation of two-hop links against direct transmission was presented in narrowband WBANs. In [80], the authors developed an improved form for switched combining with on-body cooperative communications to improve outage performance. Although these studies have demonstrated that cooperative communication can be effectively implemented in WBANs, the optimization and performance evaluation in term of spectral efficiency for cooperative communication is still an open issue in UWB based WBANs that have not been addressed yet. In this thesis, we maximize spectral efficiency in relay-assisted UWB based WBANs and give a comprehensive analysis for providing an insight into the design of an effective WBAN.

2.4.3 Energy Efficiency

Besides spectral efficiency, another key performance indicator in UWB based WBANs is energy efficiency. On one hand, as introduced in the previous section, WBAN nodes are generally battery-powered and the power available in the nodes is often restricted. In some mHealth applications, the battery lifetime is required to be up to several years without intervention (e.g., pacemakers require at least five years [81]). For implant nodes, the lifetime is especially crucial. In addition, frequent battery replacement or recharging is not realistic since it may cause stress and inconvenience to patient. On the other hand, significant path loss with deep fades may make communication difficult in WBANs, especially considering relatively low UWB transmission power. Consequently, the usage of energy resources may be inefficient. Therefore, energy efficiency is also a critical issue in UWB based WBANs.

One promising way to enhance energy efficiency in WBANs is energy harvesting during the operation of the system. Ideally, if the harvested energy is larger than the average consumed energy, systems could run eternally. However, only small amounts of energy can be harvested [82, 83]. For WBANs, energy can be scavenged from on-body sources such as body heat and body movement. In [84, 85], a thermoelectric generator is used to harvest energy from body warmth, which transforms the temperature difference between the environment and the human body into electrical energy. In [86, 87], accelerometers are used to investigate the generated power of a kinetic harvester based on data gathered at different body points. Nevertheless, the confined harvested energy and bulky size of harvesters limit the implementation of energy harvesting in practice.

Several energy-efficient MAC protocols have also been proposed for WBANs. In [88], an effective time-division multiple access (TDMA) strategy was described in a static network for vital signs monitoring. In [89], a cross-layer based battery-aware TDMA MAC protocol was proposed to prolong the battery lifespan of WBAN nodes, in which nodes can

decide whether or not to transmit their data in the assigned slot, depending on their battery status and buffer occupancy. In [90], a novel MAC protocol for WBANs is proposed to reduce the nodes' duty cycle, using out of band wake-up radio through a centralized and coordinated external wake-up mechanism. In [91], an energy-efficient traffic-aware dynamic MAC protocol for WBANs is established, which relies on the dynamic adaptation of the wake-up interval based on a traffic status register bank. While the MAC layer plays an important role for energy management, the design of wireless communication technologies in the PHY layer for energy efficiency is essential in WBANs.

In the PHY layer, the concept of cooperative communications has been successfully applied to WBANs in order to improve energy efficiency. In [92], energy efficiency of cooperative transmission was investigated with constrained outage probability. In [93], the optimal joint power allocation and coordinator deployment were derived to minimize the power consumption for various system requirements in WBANs. In [94], the reliability and energy efficiency of two-hop cooperative communication was assessed theoretically in terms of outage probability and bit error rate for medical services. Similar to spectral efficiency, cooperative communication can be implemented in WBANs in an effective manner to enhance energy efficiency. However, all aforementioned work only focuses on the single relay case in WBANs. The performance of multiple-relay cooperative communication needs to be evaluated for energy efficiency enhancement.

Additionally, the fact that the relay location is an influential parameter for system performance in WBANs has been reported in [94, 95, 96, 97]. In fact, signal strength is mostly affected by the relative physical locations of nodes as well as the movement of the human body. Therefore, deploying relay node optimally in terms of the relay location in UWB based WBANs is crucial. To the best of our knowledge, research on the energy efficiency optimization as well as the spectral efficiency optimization of cooperative communication related to the optimal relay location (RL) and power allocation (PA) in

UWB based WBANs has been rarely conducted, especially for scenarios involving both "on-body to on-body" and "in-body to on-body" propagation links.

Based on the above observations, therefore, our research work is motivated to develop a truly joint optimization scheme for the spectral efficiency and energy efficiency optimization problems, in which the relay location and power allocation are jointly optimized for each problem. For each optimization, single-relay and multiple-relay cases are taken into consideration, respectively.

2.4.4 Tradeoff between Spectral Efficiency and Energy Efficiency

In spite of the fact that spectral efficiency and energy efficiency are two important metrics in UWB based WBANs, optimizing one metric may not result in the other one being optimized. As pointed out in [98, 99], as an intrinsic characteristic, the optimal EE and SE are not always achievable simultaneously and sometimes may even conflict. Currently, the spectral-energy efficiency tradeoff has drawn significant attention from academic and industrial communities. In [100], the spectral-energy efficiency tradeoff problem was presented from the perspective of information theory with various channels. The closed-form approximations of the spectral-energy efficiency tradeoff relation were derived for the uplink of coordinated multi-point system [101] and for the multi-input-multi-output (MIMO) Rayleigh fading channel [102], respectively. From this work, it is clear that the tradeoff between spectral efficiency and energy efficiency is of prime significance for spectral and energy efficient wireless network design. However, very little work has been done towards the assessment of the spectral-energy efficiency tradeoff in cooperative UWB based WBANs.

Towards this goal, a utility for the spectral-energy efficiency tradeoff in single-relay UWB based WBANs is adopted in our research work. The spectral-energy efficiency

tradeoff optimization problem is tackled by proposed algorithms and the effectiveness of the proposed utility is consequently validated.

In the following Chapters, we will describe each optimization problem and the proposed corresponding scheme in detail.

2.5 Summary

In this Chapter, a comprehensive overview of UWB based WBANs has been summarized. The first section introduces the UWB technology, which plays an important role in the realization of future pervasive and heterogeneous networking. Some of its advantages and distinguishing properties in the transmission architecture are described. Clearly, UWB is a promising telemetry technique in WBANs, owing to its simple electronics and low power consumption. The second section provides an overview of WBANs as a specific emerging wireless technology for telemedicine and mHealth. Some of their unique components including taxonomy, requirements, simplified network architecture and key features of PHY layer are presented. Refering to the IEEE 802.15.6 standard and existing literature, it is clear that the UWB PHY indeed yields benefits and contributes strongly to wearable and implant communications in WBANs. UWB based WBANs is thus a topic worth studying. This Chapter ends in the section where the key issues in UWB based WBANs are emphasized. To design an efficient UWB based WBAN, the impact of the channel modelling, spectral efficiency and energy efficiency are of fundamental importance. Thus, our research work is dedicated to these issues and focused on development of novel optimal schemes to effectively maximize spectral efficiency and energy efficiency and eventually achieve a satisfactory spectral-energy efficiency tradeoff in UWB based WBANs.

Chapter 3

Energy-Saving based Relay Selection for UWB based WBANs

3.1 Introduction

As introduced in Chapter 2, cooperative transmission can offer several benefits in UWB based WBANs. In cooperative transmission, a relay location has a notable impact on the transmission performance. In this Chapter, the energy-saving performance of cooperative transmission is considered from a relay-location selection perspective. To save the energy of nodes as much as possible while maintaining a satisfactory transmission performance, we propose an energy-saving based relay selection criterion for UWB based WBANs. With the pulse-based energy consumption model in [103], the total energy consumption for single-relay cooperative transmission is established and the optimal power allocation is derived accordingly to minimize the total energy consumption at a given relay location. With the same desired spectral efficiency, the energy-saving relay based selection criterion is proposed and analyzed after considering the energy consumption difference between direct transmission and cooperative transmission. Simulation results verify the accuracy of our proposed criterion and show that, when the transmitter and receiver are

located on the same side of the human body without significant path loss, the transceiver circuit energy consumption dominates the total energy consumption, which implies that cooperative transmission does not necessarily save the energy and direct transmission is preferable in this case. However, at a suitable relay location and with large transmission distance, cooperative transmission can achieve a significant improvement on energy-saving compared to direct transmission when the transmitter and receiver are located on the different sides of the human body.

The Chapter is organized as follows. In Section 3.2, the system model is described. In Section 3.3, the minimized energy consumption for cooperative transmission is presented. In Section 3.4, the energy-saving relay selection criterion is detailed. Simulation results are presented in Section 3.5. Summary is given in Section 3.6.

3.2 System Model

In this Chapter, we consider a simplified UWB based WBAN model with one lightweight on-body node, one relay node, and one coordinator. In practice, to guarantee a patient the best care and comfort, the number of devices is usually kept to a minimum. Therefore, we only consider a single relay herein. The coordinator can collect physiological data from the on-body node and send them to the personal server wirelessly for further processing. As shown in Fig. 3.1, cooperative transmission is adopted where the relay node R can assist the source S in delivering its message to the coordinator D. With the distance d [m] between S and D, we denote $d_1 = \theta_1 d$ and $d_2 = \theta_2 d$ as the distance between S and R and the one between R and D, respectively, where $0 < \theta_1, \theta_2 < 1$ and $\theta_1 + \theta_1 \geq 1$.

The cooperation protocol is a typical TDMA protocol shown in Fig. 3.1. It consists of two time slots with equal pulse frame duration, in which S broadcasts its signal to D and R during the first time slot, and at the second time slot, R forwards its received signal to

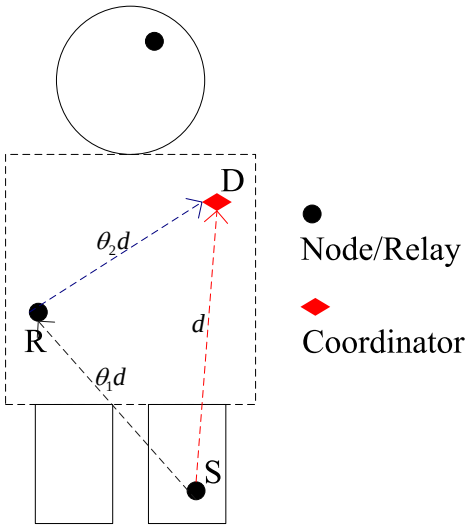

Figure 3.1: A simplified network model for WBANs.

D. This protocol can achieve a maximum degree of broadcasting and exhibits no receive collision [104]. For relay transmission techniques, there are two strategies are commonly used: AF relay transmission and decode and forward (DF) relay transmission. The AF relay applies linear transformation to amplify the received signal. The DF relay, on the other hand, decodes the received signal to remove the noise and then re-encodes it for forward transmission. It is noted that in practice the AF relay, when compared with the DF relay, requires significantly lower implementation complexity. Thus we only consider the AF relay in UWB based WBANs.

In the following, we will describe the UWB based WBAN channel models, spectral efficiency, and the energy consumption model, respectively.

3.2.1 Channel Model

The body surface to body surface (CM3) path loss model released by IEEE 802.15 working group is considered in this Chapter [46, 63]. Table. 3.1 below summarizes the corresponding parameters. Please note that, the impact of multipath fading and shadow-

ing is ignored since we mainly focus on the effect of relay location on the energy-saving performance of cooperative transmission in the Chapter. In the following Chapters, the multipath fading and shadowing will be taken into account in the system model for a more accurate and comprehensive study.

Table 3.1: UWB based WBAN CM3 Channel Model

Channel model	$PL(d) = P_0(d) + 10n\log_{10}(\frac{d}{d_0})$	
Location of S	Around the torso	Along the torso
Antenna separation from body surface	5 mm	5 mm
P_0[dB]	48.4	44.6
d_0[m]	0.1	0.1
n	5.9	3.1

As shown in Table. 3.1, two different channel models are discussed in this Chapter corresponding to different relative locations of S. With fixed D, "around the torso" refers to the condition that S and D are on the different sides of the human body and "along the torso" refers to the condition that S and D are on the same side of the human body. Due to diffraction around the body, the path loss exponent around the torso is much higher than that along the torso.

With the channel model, the relationship between the transmit UWB pulse power P_t and the receive pulse power P_r can be given by

$$\frac{P_t}{P_r} = MG_0d^n, \tag{3.1}$$

where $M = 10^{(P_0/10)}$ and $G_0 = (1/d_0)^n$. For analysis simplicity, we assume that links among S, R and D have the same channel model in UWB based WBANs when the relative location of S and D is known.

3.2.2 System Metric

To evaluate the energy saving performance of cooperative transmission and make a fair comparison with direct transmission counterpart, the condition that direct transmission and cooperative transmission can achieve the same desired SE performance [bits/s/Hz] is assumed in this Chapter.

For direct transmission from S to D, SE is given by

$$\beta_{SD} = \log_2(1 + \rho_{SD}) \approx \log_2(\rho_{SD}), \tag{3.2}$$

where we assume $\rho_{SD} = \frac{P_r^{SD}}{B \cdot N_0} \gg 1$ is the received SNR of the link between S and D, and P_r^{SD} is the received power at D. B is the bandwidth and N_0 is the single-sided PSD of additive white Gaussian noise (AWGN).

Similarly, for the AF cooperative transmission with the given protocol, the average SE is approximately given by [105]

$$\beta_{SRD} \approx \frac{1}{2}\log_2(1 + \theta_1^n \rho_{SR}) + \frac{1}{2}\log_2(1 + \frac{\rho_{SR}\rho_{RD}}{\rho_{SR} + \rho_{RD} + 1}) \approx \frac{1}{2}\log_2(\frac{\theta_1^n \rho_{SR}^2 \rho_{RD}}{\rho_{SR} + \rho_{RD}}), \tag{3.3}$$

where $\rho_{SR} = \frac{P_r^{SR}}{B \cdot N_0} \gg 1$ is the received SNR of the link between S and R, and P_r^{SR} is the received power at R. $\rho_{RD} = \frac{P_r^{RD}}{B \cdot N_0} \gg 1$ is the received SNR of the link between R and D, and P_r^{RD} is the received power at D from R. $\theta_1^n \rho_{SR}$ and $\frac{\rho_{SR}\rho_{RD}}{\rho_{SR}+\rho_{RD}}$ are the received SNR at D in the first and second time slot, respectively.

To satisfy $\beta_{SD} = \beta_{SRD}$, with (3.2) and (3.3), the SNR relationship between direct transmission and cooperative transmission follows

$$Z^2 = \rho_{SD}^2 \approx \frac{\theta_1^n \rho_{SR}^2 \rho_{RD}}{\rho_{SR} + \rho_{RD}}, \tag{3.4}$$

where Z is defined as the equivalent desired SNR for the desired SE. For analytical simplicity, we will employ Z as the performance metric instead of SE to evaluate the energy-saving performance of cooperative transmission in the sequel.

3.2.3 Energy Consumption Model

In this Chapter, a realistic nonlinear pulse-based energy consumption model [103] is applied. The total energy consumption for direct transmission can be expressed approximately as a function of the received SNR ρ_{SD}:

$$\xi_{SD} = \frac{M^2 {G_0}^2 B^2 N_0^2 {T_p}^2 \omega \gamma_p (1+\alpha)^2}{V\eta^2} {\rho_{SD}}^2 d^{2n} + \frac{M G_0 B N_0 T_p (1+\alpha)}{\eta} \rho_{SD} d^n + \frac{P_{ct} T_p + P_{cr} T_d}{\eta}, \tag{3.5}$$

where T_p is the UWB pulse waveform duration, $\gamma_p = \frac{1}{T_p}$ and T_d is the pulse frame duration. ω is the battery efficiency factor, α is the extra power loss factor of the power amplifier, V is the battery voltage, η is the transfer efficiency of the DC/DC converter and P_{ct} and P_{cr} are the transmitter and receiver circuit power consumption, respectively. Please note that antenna related parameters are beyond the scope of our thesis, although specific antenna patterns may effect the results in (3.5).

As given in (3.5), the total energy consumption includes three parts, where the first term refers to the excess energy loss due to the nonlinear battery discharge, the second term refers to the energy carried by the transmitted pulse and the third term represents the transceiver circuit energy consumption, which is a constant. It is shown that the second and third terms dominate the total energy consumption [106].

Substituting (3.4) into (3.5), we can rewrite the energy consumption of direct transmission with the desired Z as

$$\xi_{SD} = \frac{C_2}{\overline{Z}^2} d^{2n} + \frac{C_1}{\overline{Z}} d^n + C_0, \tag{3.6}$$

where $\overline{Z} = 1/Z$. $C_2 = \frac{M^2 {G_0}^2 {T_p}^2 B^2 \omega \gamma_p (1+\alpha)^2}{V\eta^2} {N_0}^2$, $C_1 = \frac{M G_0 T_p B (1+\alpha)}{\eta} N_0$ and $C_0 = \frac{P_{ct} T_p + P_{cr} T_d}{\eta}$.

In the next section, the energy consumption of cooperative transmission is presented with the desired Z and the minimization for energy consumption is derived accordingly.

3.3 Minimized Energy Consumption for Cooperative Transmission

In this section, we firstly establish the average total energy consumption of cooperative transmission in each time slot. Then the optimal power allocation is derived accordingly with the desired Z to minimize the total energy consumption of cooperative transmission.

3.3.1 Energy Consumption of Cooperative Transmission

In cooperative transmission, with the assumed AF cooperative protocol, D and R first receive the signal from the transmitter S in the first time slot, and then R, as a transmitter, forwards its received signal to D in the second time slot. Thus, it is concluded that the total energy consumption of cooperative transmission can be separated into three parts: 1) direct transmission energy consumption from S to R; 2) direct transmission energy consumption from R to D. 3) the receiver circuit energy consumption at D. As a result, the average energy consumption in each time slot can be expressed as

$$\xi_{SRD} = \frac{1}{2}C_2({\rho_{SR}}^2 d_1^{2n} + {\rho_{RD}}^2 d_2^{2n}) + \frac{1}{2}\left(C_1(\rho_{RD} d_1^n + \rho_{RD} d_2^n) + 2C_0 + \frac{P_{cr}T_d}{\eta}\right). \quad (3.7)$$

With (3.4), we have

$$\theta_1^n \overline{Z}^2 = \overline{\rho_{SR}} \cdot \overline{\rho_{RD}} + \overline{\rho_{SR}}^2, \quad (3.8)$$

where $\overline{\rho_{SR}} = 1/\rho_{SR}$ and $\overline{\rho_{RD}} = 1/\rho_{RD}$. Therefore, $\overline{\rho_{RD}}$ can be expressed as

$$\overline{\rho_{RD}} = \frac{\theta_1^n \overline{Z}^2 - \overline{\rho_{SR}}^2}{\overline{\rho_{SR}}}. \quad (3.9)$$

Substituting (3.9) into (3.7), with the desired Z, ξ_{SRD} can be rewritten in terms of $\overline{\rho_{SR}}$ as

$$\begin{aligned}\xi_{SRD}(\overline{\rho_{SR}}) = {} & \frac{1}{2}C_2\left(\frac{d_1^{2n}}{\overline{\rho_{SR}}^2} + \frac{\overline{\rho_{SR}}^2 d_2^{2n}}{(\theta_1^n \overline{Z}^2 - \overline{\rho_{SR}}^2)^2}\right) + \frac{1}{2}C_1\left(\frac{d_1^n}{\overline{\rho_{SR}}} + \frac{\overline{\rho_{SR}} d_2^n}{\theta_1^n \overline{Z}^2 - \overline{\rho_{SR}}^2}\right) \\ & + C_0 + \frac{1}{2}\frac{P_{cr}T_d}{\eta}. \end{aligned} \quad (3.10)$$

3.3.2 Optimal Power Allocation for Cooperative Transmission

With d_1, d_2 and the desired Z, we can derive the optimal $\overline{\rho_{SR}^o}$ to minimize ξ_{SRD} based on (3.10). Since $\overline{\rho_{SR}} = 1/\rho_{SR}$ is related to the power, the optimization problem can be considered as the optimal PA problem for minimizing the energy consumption of cooperative transmission.

As (3.10) is a convex function, the optimal $\overline{\rho_{SR}^o}$ can be achieved by setting the first order derivative of $\xi_{SRD}(\overline{\rho_{SR}})$ to zero. However, the computational complexity would be high since $\xi_{SRD}(\overline{\rho_{SR}})$ is a quartic formula of $\overline{\rho_{SR}}$. For this reason, an approximate solution with low-complexity is considered herein. As mentioned in Section 3.2.3, the energy carried by the transmitted pulse corresponding to the second term in (3.10) and the transceiver circuit energy consumption corresponding to the third term in (3.10) dominate the total energy consumption. Thus we can rewrite $\xi_{SRD}(\overline{\rho_{SR}})$ by ignoring the first term in (3.10) as

$$\xi_{SRD}(\overline{\rho_{SR}}) \approx \frac{1}{2}C_1\left(\frac{d_1^n}{\overline{\rho_{SR}}} + \frac{\overline{\rho_{SR}}d_2^n}{\theta_1^n\overline{Z}^2 - \overline{\rho_{SR}}^2}\right) + \left(C_0 + \frac{1}{2}\frac{P_{cr}T_d}{\eta}\right). \tag{3.11}$$

Setting the the first order derivative of (3.11) to zero, we have

$$\left(\frac{d_2^n}{d_1^n} - 1\right)\overline{\rho_{SR}}^4 + \left(\frac{d_2^n}{d_1^n} + 2\right)\theta_1^n\overline{Z}^2\overline{\rho_{SR}}^2 - (\theta_1^n\overline{Z}^2)^2 = 0, \tag{3.12}$$

since $\overline{\rho_{SR}} = 1/\rho_{SR} \ll 1$, we can assume $\overline{\rho_{SR}}^4 \approx 0$. Keeping in mind that $d_1 = \theta_1 d$ and $d_2 = \theta_2 d$, then the optimal $\overline{\rho_{SR}^o}$ can be approximately given by

$$\overline{\rho_{SR}^o} \approx \sqrt{\frac{\theta_1^n\overline{Z}^2}{d_2^n/d_1^n + 2}} = \frac{\theta_1^n\overline{Z}}{\sqrt{\theta_2^n + 2\theta_1^n}}. \tag{3.13}$$

With the optimal $\overline{\rho_{SR}^o}$, the minimized energy consumption ξ_{SRD}^o can be obtained by substituting (3.13) into (3.10)

$$\begin{aligned}\xi_{SRD}^o = {} & \frac{C_2 d^{2n}}{2\overline{Z}^2}\left((\theta_2^n + 2\theta_1^n)\left(1 + \frac{\theta_2^{2n}}{(\theta_2^n + \theta_1^n)^2}\right)\right) + \frac{C_1 d^n}{2\overline{Z}}\left(\sqrt{\theta_2^n + 2\theta_1^n}\left(1 + \frac{\theta_2^n}{\theta_2^n + \theta_1^n}\right)\right) \\ & + C_0 + \frac{P_{cr}T_d}{2\eta}.\end{aligned} \tag{3.14}$$

From (3.14), we can see that ξ_{SRD}^{o} is a function of θ_1 and θ_2. Different θ_1 and θ_2 may make the value of ξ_{SRD}^{o} different. In other words, the relay location has an impact on the energy-saving performance of cooperative transmission. Thus, a natural question arises: what are the conditions under which cooperative transmission is more energy efficient than direct transmission with the desired Z? To answer this question, an energy-saving relay selection criterion is investigated considering the energy consumption difference between ξ_{SD} and ξ_{SRD}^{o} in the next section.

3.4 Energy-Saving Relay Selection

We denote $\Delta\xi$ as the energy consumption difference between ξ_{SD} and ξ_{SRD}^{o}, which is given by

$$\begin{aligned}\Delta\xi &= \frac{C_2 d^{2n}}{2\overline{Z}^2}\left(2-(\theta_2^n+2\theta_1^n)(1+\frac{\theta_2^{2n}}{(\theta_2^n+\theta_1^n)^2})\right)+\frac{C_1 d^n}{2\overline{Z}}\left(2-\sqrt{\theta_2^n+2\theta_1^n}(1+\frac{\theta_2^n}{\theta_2^n+\theta_1^n})\right)\\ &\quad-\frac{P_{cr}T_d}{2\eta}\\ &= A(d^n)^2+B(d^n)+C, \end{aligned} \tag{3.15}$$

where

$$A=\frac{C_2}{2\overline{Z}^2}\left(2-(\theta_2^n+2\theta_1^n)(1+\frac{\theta_2^{2n}}{(\theta_2^n+\theta_1^n)^2})\right),$$

$$B=\frac{C_1}{2\overline{Z}}\left(2-\sqrt{\theta_2^n+2\theta_1^n}(1+\frac{\theta_2^n}{\theta_2^n+\theta_1^n})\right),$$

and

$$C=-\frac{P_{cr}T_d}{2\eta}<0.$$

As shown in (3.15), $\Delta\xi$ is a quadratic function of d^n and A, B and C are coefficients of the function. When $\Delta\xi > 0$, it means that cooperative transmission is more energy

efficient than direct transmission and vice verse. Thus the energy-saving relay selection criterion with the desired Z can be described as the following four rules:

1. If $A > 0$, then cooperative transmission is more energy efficient than direct transmission as long as the distance d is larger than the critical distance d_c, where $d_c^n = (-B + \sqrt{B^2 - 4AC})/(2A)$.

2. If $A \leq 0$ and $B \leq 0$, then direct transmission is always more energy efficient than cooperative transmission.

3. If $A \leq 0$, $B > 0$ and $B^2 - 4AC \leq 0$, then direct transmission is always more energy efficient than cooperative transmission.

4. If $A \leq 0$, $B > 0$ and $B^2 - 4AC > 0$, then cooperative transmission is more energy efficient than direct transmission as long as the distance d is in the range of d_{c1} to d_{c2}, where $d_{c1}^n = (-B + \sqrt{B^2 - 4AC})/(2A)$ and $d_{c2}^n = (-B - \sqrt{B^2 - 4AC})/(2A)$.

Obviously, the establishment of the relay selection criterion relies on coefficients A, B, C and distance d. Actually, with a given relay location, coefficients A and B are only related to the path loss exponent n corresponding to the WBAN channel property and distance d, and coefficient $|C|$ is the extra consumed circuit energy by cooperative transmission compared with direct transmission. Therefore, whether the given relay is selected or not depends on the channel property, distance d and the consumed circuit energy. To analyze the effect of these system parameters on the relay selection criterion more directly, relay regions corresponding to different rules of the criterion are given in Fig. 3.2 and Fig. 3.3.

In Fig. 3.2 and Fig. 3.3, three curves are plotted to divide the relay location into three valid regions, namely R1, R2 and R3. The black solid curve represents the function $\theta_1 + \theta_2 = 1$ over the default domain that $0 < \theta_1, \theta_2 < 1$. The blue dashed curve refers

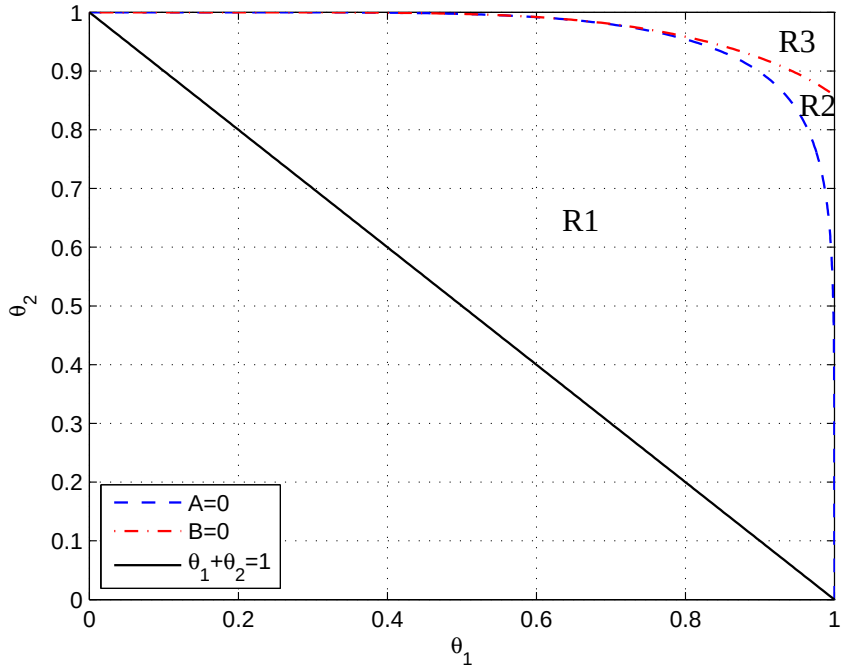

Figure 3.2: Relay regions corresponding to different criterion rules when S and D are on the different sides of the human body (around the torso).

to the function $A(\theta_1, \theta_2) = 0$ and the region below the dashed curve meets $A(\theta_1, \theta_2) > 0$. The red dash-dot curve refers to the function $B(\theta_1, \theta_2) = 0$ and the region below this curve meets $B(\theta_1, \theta_2) > 0$. Since θ_1 and θ_2 need to meet the requirement that $\theta_1 + \theta_2 \geq 1$, the black solid curve can be seen as the low bound for valid relay regions.

Based on conditions of the four rules, it is shown that when the relay is located in region R1, the first rule of the criterion is employed for the relay selection and the relay can be selected as long as $d \geq d_c$, where the value of critical distance d_c is dominated by C. It means that the energy consumed due to the path loss is not significant when the distance d is at a short range within region R1, and the coefficient C dominates the sign of $\Delta\xi$. In other words, cooperative transmission is not beneficial to improving the energy efficiency for short distance since the circuit energy consumption would dominates the total cooperative energy consumption. When the relay is located in region R2, the third

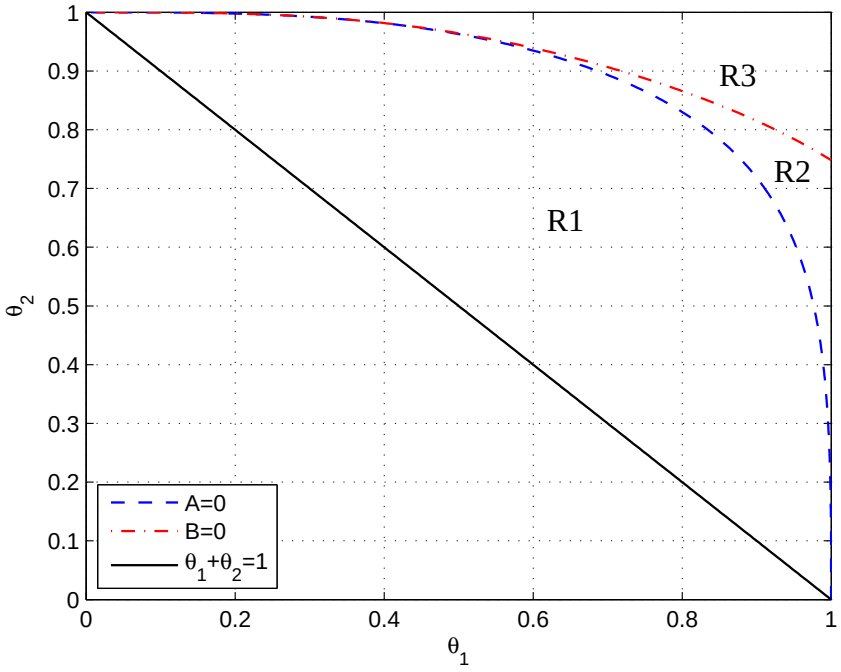

Figure 3.3: Relay regions corresponding to different criterion rules when S and D are on the same side of the human body (along the torso).

or fourth rule of the criterion could be employed for the relay selection and whether the relay is selected or not depends on the sign of $B^2 - 4AC$ and d. For the relay located in region R3, the second rule of the criterion is employed and it indicates that the relay in this region cannot be selected since the cooperative transmission is always less energy efficient. This is reasonable as the relay in region R3 is located far away from S and D so that the distances d_1 and d_2 are close to the distance d, the relaying transmission may experience a higher path loss compared with direct transmission. Thus more energy needs to be consumed by cooperative transmission to achieve the desired Z. Besides, comparing these two figures, we can see that the areas of regions R3 and R2 are larger when S is "along the torso". It reveals that when S and D are located on the same side of the human body and the path loss exponent n is smaller, the relaying transmission may offer less advantage in alleviating path loss and the circuit energy consumption may

impact more on the the total energy consumption. Thus it is more likely that the direct transmission is preferable for UWB based WBANs when S and D are located on the same side of the human body.

In the next section, the energy efficient performance of cooperative transmission is assessed by simulations in UWB based WBANs, and the above analysis for the proposed criterion is also confirmed.

3.5 Simulation Results

To assess the energy-saving performance of cooperative transmission and verify our proposed relay selection criterion in UWB based WBANs, numerical results are presented in this section. Simulation parameters for UWB based WBANs are given in Table. 3.2 [13, 103, 107]. According to the scale of the human body, transmission distance d is very limited. In this paper, we consider the case that $0 < d \leq 1.2$m.

Table 3.2: Simulation Parameters

$V = 1.2$V	$\alpha = 0.33$	$\omega = 0.05$
$\eta = 0.8$	$T_p = 16.026$ns	$T_d = 512.82$ns
$N_0/2 = -174$dBm/Hz	$P_{ct} = 0.2$mW	$P_{cr} = 3$mW

In Fig. 3.4, $\Delta\xi$ versus d with three different relay locations is presented when S is "around the torso" and $Z = 10$dB. From Fig. 3.2, we know that the first two relay locations are in region R1 and the third relay location is in region R3. (The relay located in region R2 is negligible since R2 only takes a small edge part of the whole relay regions) As shown in this figure, the first two relay locations, $\theta_1 = 0.4$ and $\theta_2 = 0.7$, $\theta_1 = 0.8$ and $\theta_2 = 0.9$, yield increasing $\Delta\xi$ along with the distance d, and we can see that when d is at a short range, $\Delta\xi$ is negative which means that direct transmission is more energy efficient than cooperative transmission. However, as d gets greater than a certain value,

$\Delta\xi$ changes to positive and goes up rapidly as d increases. This phenomenon confirms the existence of specific critical transmission distance d_c as stated in the first rule of the relay selection criterion. In contrast, $\Delta\xi$ for the third relay location is strictly negative which means that this relay would never be selected. This verifies the second rule of the proposed relay selection criterion. Since it is a decreasing curve along with d, it illustrates that the relaying transmission experiences a stronger path loss compared with direct transmission in this case, and thus more energy is consumed by cooperative transmission. This phenomenon matches our analysis well.

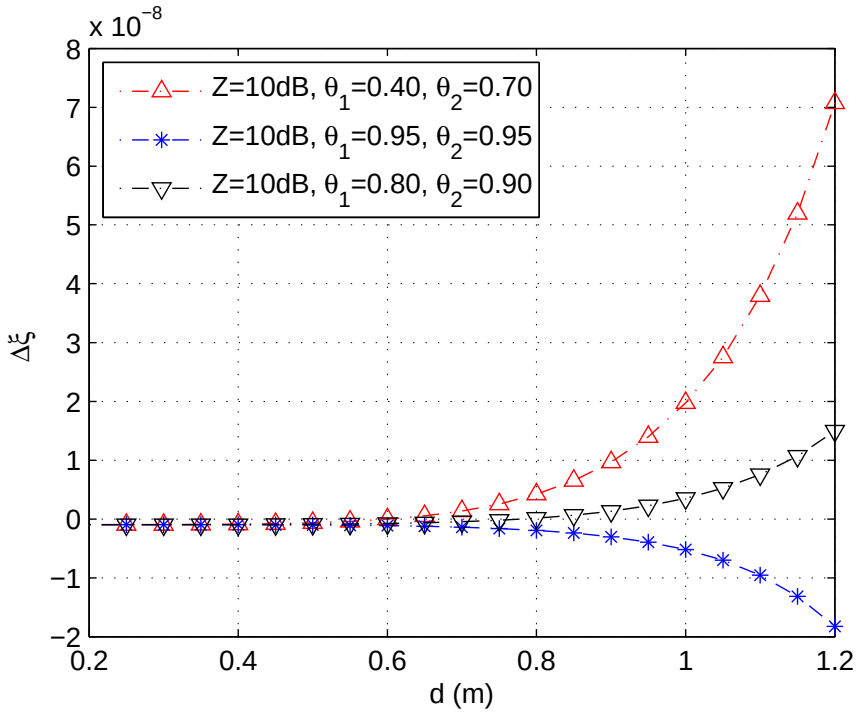

Figure 3.4: $\Delta\xi$ versus d with various relay locations when S and D are on the different sides of the human body (around the torso) and $Z = 10$dB.

In Fig. 3.5, $\Delta\xi$ versus d with three different relay locations is presented when S is "along the torso" and $Z = 10$dB. The relay locations are the same as in Fig. 3.4. Compared with the results in Fig. 3.4, it is interesting to find out that $\Delta\xi$ is always negative for these three relay locations. That is to say, direct transmission is preferable

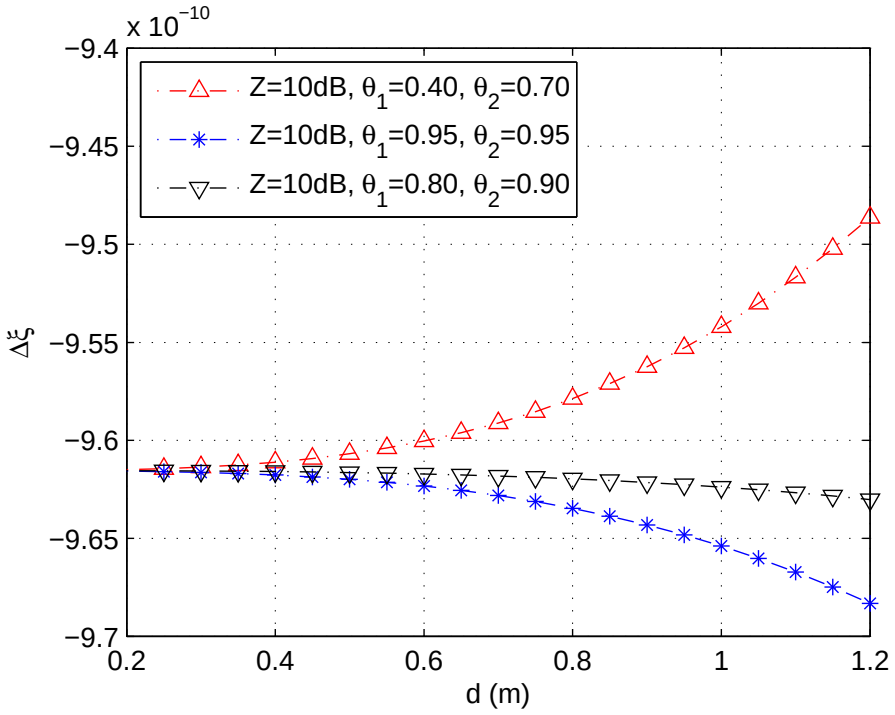

Figure 3.5: $\Delta\xi$ versus d with various relay locations when S and D are on the same side of the human body (along the torso) and $Z = 10$dB.

when S and D are located on the same side of the human body. As mentioned in the last section, when the path loss exponent n is small, circuit energy consumption makes a critical impact on the total energy consumption. Since it costs more circuit energy consumption, cooperative transmission would never take advantage in this case.

In Fig. 3.6, cooperation energy-gain versus desired Z is given when S is "around the torso" and $d = 0.8$, where cooperation energy-gain is defined as the percentage of the energy saving achieved by cooperative transmission compared with direct transmission. Since cooperative transmission has the advantage of enhancing SE, we can see that the cooperation energy-gain grows as Z increases. It is also illustrated that when the relay is far away from S and D, the cooperation energy-gain may be strictly negative for a range of Z. However, with the location $\theta_1 = 0.4$ and $\theta_2 = 0.7$, it shows that cooperative transmission has a significant improvement on energy-saving performance, i.e., around 45%

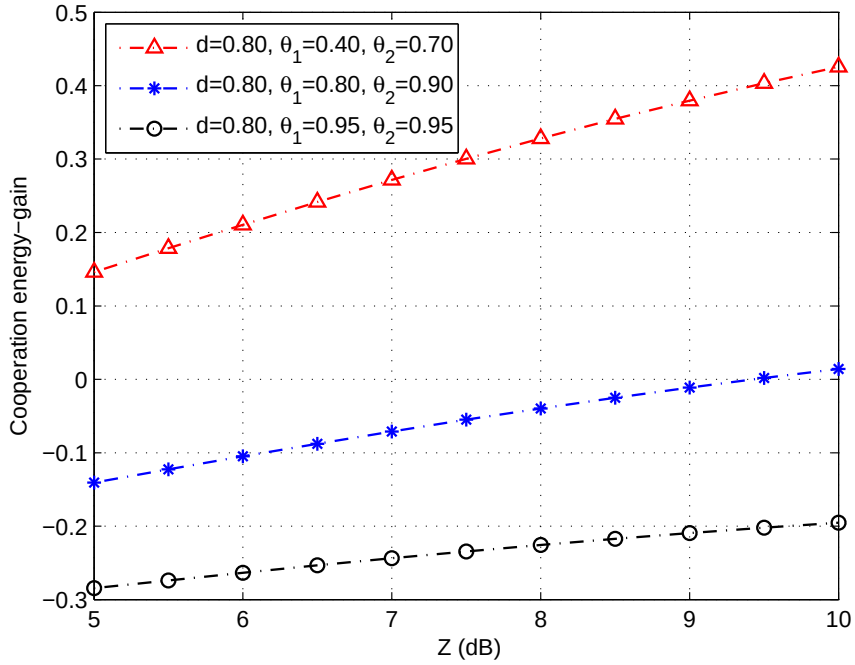

Figure 3.6: Cooperation energy-gain versus desired Z when S and D are on the different sides of the human body (around the torso) and $d = 0.8$.

energy is saved at $Z = 10$dB compared with direct transmission. A conclusion therefore can be made that, with proper relay location (close to S and D) and transmission distance $d > d_c$, cooperative transmission would be very beneficial to energy saving compared with direct transmission when S and D are located on the different sides of the human body.

In conclusion, cooperative transmission does not necessarily enhance EE when S and D are on the same side of the human body since a LoS is available. In contrast, with proper relay location and transmission distance when S and D are on the different sides of the human body, EE could be improved by around 45% compared with direct transmission. In addition, it is observed that the energy-saving performance of cooperative transmission has a notable difference with different relay location. The importance of relay location in WBANs therefore should not be ignored.

3.6 Summary

In this Chapter, an energy-saving relay-location based selection criterion is developed for UWB based WBANs with a realistic nonlinear energy consumption model. The optimal power allocation with a given relay location is derived for single-relay cooperative transmission to minimize the total energy consumption. Considering the energy consumption difference between direct transmission and cooperative transmission, the energy-saving relay selection criterion is proposed and analyzed afterwards. Without loss of generality, we divide the relay area in WBANs into three valid regions and then four selection rules are setup according to the different relay regions. From theoretical derivations and numerical results, it is clear that the relay location in different regions makes a big difference on the energy-saving performance of cooperative transmission. The relay location, therefore, plays a critical role in designing an efficient UWB based WBANs. Hence, deploying a relay node optimally in terms of the relay location in UWB based WBANs is of paramount importance (The related research work in this Chapter won the "Merit of Certificate" of IEEE ICUWB 2013). Since we only study the power allocation optimization with a given relay location in this work, a further research on the joint power allocation and relay location optimization for cooperative transmission is necessary and interesting.

In the following Chapters, the optimal power allocation and optimal relay location are jointly investigated for the spectral efficiency and energy efficiency optimization problems. With the joint optimal power allocation and relay location, we are able to provide an insight into the design of UWB based WBANs with respect to the proper placement of the wearable relay node along with the optimal transmit power level.

Chapter 4

Spectral Efficiency Optimization in Single-Relay UWB based WBANs

4.1 Introduction

As described in Section 2.4.2, spectral efficiency is a major challenge in UWB based WBANs that needs to be tackled. In this Chapter, we aim to solve the joint optimal relay location and power allocation problem to optimize spectral efficiency in single-relay assisted UWB based WBANs. Three practical transmission scenarios are investigated herein, which are along-torso scenario, around-torso scenario and in-body scenario, respectively. Each scenario refers to a specific physical location between the source and destination nodes in relation to each other. For each scenario, we seek the relay with the optimal location to achieve the maximum SE, together with the corresponding optimal power allocation. More precisely, generic relay-location based network models are firstly proposed for UWB based WBANs. Taking into account realistic power considerations for each scenario, the spectral efficiency optimization problem is then mathematically formulated and the optimal relay location and power allocation are jointly derived to achieve the maximum spectral efficiency. The analysis of the optimal relay location and

power allocation is given accordingly. Numerical results match those in Chapter 3 to some extent. Due to the presence of the LoS in the along-torso scenario, we show that direct transmission is preferable to the cooperative transmission, even though the optimal relay location is selected and the optimal power allocation is achieved in cooperative transmission. However, by utilizing an on-body relay node with the joint optimal relay location and power allocation in the around-torso and in-body scenarios, it is shown that spectral efficiency can be remarkably improved compared to other transmission schemes. Moreover, the transmission range in WBANs can be extended effectively and the power consumption can be transferred from the sensor node to the relay node, in which the lifetime of the sensor node can be prolonged significantly.

The Chapter is organized as follows. In Section 4.2, the system model is described, where the system scenario and considered channel models are presented, respectively. In Section 4.3, relay-location based network models are developed first, the spectral efficiency optimization problem in cooperative transmission for each transmission scenario is then formulated and the joint relay location and power allocation for each transmission scenario is derived accordingly. Simulation results are illustrated in Section 4.4. Summary is given in Section 4.5.

4.2 System Model

4.2.1 System Scenarios

Similar to Chapter 3, we consider a basic WBAN which is composed of three types of nodes: wearable or implant node S, one body network coordinator D, and one relay node R. As mentioned in Section 2.3, the node is used to monitor the physiological states of a person periodically, e.g., measuring heartbeat or recording body activities, and it is connected to the coordinator directly or through the relay node. Normally, the

coordinator is attached on the front side of the human body. Note that the application type of the node and its location in a WBAN depend on the requirement of the patient.

For cooperative transmission, the two-slot AF cooperative protocol in Chapter 3 is adopted herein. In this work, three typical scenarios in WBANs are investigated, namely, along-torso scenario, around-torso scenario, and in-body scenario. The three considered scenarios are described in detail in the following:

- Along-torso scenario: S, R and D are all on the same side of the human body. Since all signals are transmitted over the along-torso links, only the along-torso channel model is used for the theoretical formulation of the SE optimization in this scenario.

- Around-torso scenario: with a given location of D, S and D are on the different sides of the human body and R is assumed located on the same side with S. Since signals are transmitted over the along-torso channel for the S-R link and over the around-torso channels for the other two links, the along-torso and around-torso channel models are used for the theoretical formulation of the SE optimization in this scenario.

- In-body scenario: with a given location of D, R and D are on the same side of the human body and S is assumed located inside the human body. Since signals are transmitted over the along-torso channel for the R-D link and over the in-body channels for the other two links, the along-torso and in-body channel models are used for the theoretical formulation of the SE optimization in this scenario.

In the following, the mentioned three types of channel models in UWB based WBANs are presented mathematically, respectively. The corresponding path loss (including shadowing) and small scale fading are taken into account for each link.

4.2.2 Channel Models

In our work, the along-torso channel model and around-torso channel model are based on IEEE P802.15 realistic channel models. The IEEE P802.15 channel models (including narrowband channel models and UWB channel models) are developed by the IEEE 802.15.6 group based on real field measurements, which have been widely used for evaluating the performance of WBANs via computer simulation. For the in-body channel model, as mentioned in Section 2.4.1, there are currently few models describing the UWB radio propagation inside the human body. Thus, the state-of-the-art channel model in [69] is adopted, which is a statistical model developed by using a heterogeneous anatomical model that includes the frequency-dependent dielectric properties of different human tissues.

The effect of the body motion and the scattering inside the human body is also taken into account. Since we assume that all on-body nodes are only located on the front side of the human body or on the back side of the human body rather than the limbs, the impact of the body motion can be ignored in the along-torso and in-body scenarios based on the observations in the existing literature [60, 97]. However, a walking motion produces measurable fluctuations in the around-torso scenario, which cannot be ignored [60]. Therefore, the shadowing (variations) from the body motion, modeled as a Lognormal distribution, is included into the around-torso path loss model. On the other hand, the scattering inside the human body is caused by the different material dielectric properties along the propagation path, which is also necessary to be considered in the in-body channel model [69]. Table 4.1 summarizes the corresponding parameters for the path loss (including shadowing) models [46, 69, 60]. Notice that, H_0 represents the shadowing from the body motion, which is a Gaussian distributed random variable with mean 0.27 and standard deviation 1.5 [60]. H_1 represents the scattering inside the human body, which is a Gaussian distributed random variable with zero mean and standard deviation 7.84 [69].

Table 4.1: UWB based WBAN path loss (including shadowing) models

along-torso model	$PL_0^{dB}(d) = L_0 + 10n_0 \log_{10}(\frac{d}{d_0})$
L_0 [dB]	44.6
n_0	3.1
$d_0[m]$	0.1
around-torso model	$PL_1^{dB}(d) = L_1 + 10n_1 \log_{10}(\frac{d}{d_1}) + H_0$
L_1 [dB]	48.4
n_1	5.9
$d_1[m]$	0.1
in-body model	$PL_2^{dB}(d) = L_2 + a(d/d_2)^{n_2} + H_1$
L_2 [dB]	10
a	0.987
n_2	0.85
$d_2[m]$	0.001

[1] L_i is the path loss at the reference distance, for i=0,1,2.

[2] d_i is the reference distance, for i=0,1,2.

[3] n_i is the path loss exponent, for i=0,1,2.

[4] a is a fitting constant.

[5] H_i is Gaussian distributed random variable, for i=0,1.

For all the links considered, the energy-normalized channel impulse response (CIR) can be generally written as

$$h_k(t) = \sum_{l=0}^{L_k-1} \alpha_{l,k}\delta(t - \tau_{l,k}), \tag{4.1}$$

where $k \in \{SD, SR, RD\}$ denotes the links from S to D, S to R and R to D respectively. L_k is the number of multipaths, $\tau_{l,k}$ is the delay of the lth path, and $\alpha_{l,k}$ is the gain of the lth path. Since real signals are employed in UWB systems, each path gain is real also. Note that, the characteristics of L_k, $\tau_{l,k}$ and $\alpha_{l,k}$ are different in different scenarios. Further details on the delay profile for along-torso and around-torso links can be found in [46]. For the in-body link, the corresponding delay profile can be found in [69].

4.3 Spectral Efficiency Optimization

With the channel models, we first present the SE of direct transmission in this section. The SE optimization problem for each scenario is then described and solved by using the optimization theory. Specifically, to evaluate the impact of relay location in WBANs and find out the optimal relay location for the corresponding optimal SE in each considered scenario, two relay-location based cooperative network models are developed for on-body transmissions and in-body transmissions, respectively. In the proposed network model for on-body transmissions, we show that the along-torso scenario can be considered as a special case in the around-torso scenario. Since there is no extra challenges in the along-torso scenario for solving the SE optimization problem apart form the different channel parameters and the location of nodes in relation to each other, we only detail the SE optimization in the around-torso scenario and only give the solution of the considered problem in the around-torso scenario. For the around-torso scenario, the SE optimization problem in terms of RL and PA is mathematically formulated with the proposed model and globally optimal solutions are proven to exist and are derived, respectively. Similarly, the optimal RL and PA are also jointly obtained in the in-body scenario based on the proposed network model for in-body transmissions.

4.3.1 Spectral Efficiency of Direct Transmission

For analytical simplicity, we present the IR-UWB signal transmission with BPSK in WBANs (the transmission scheme is easily extended to other modulations, such as PPM or OOK). The random TH or DS codes are omitted herein.

At S, every transmitted BPSK symbol duration T_s consists of N_f consecutive frames each with duration T_f, where $T_s = N_f T_f$. The symbol information is conveyed by an ultrashort pulse waveform in each frame. Thus the transmitted symbol waveform can be

expressed as

$$s(t) = b\sqrt{P_s}\sum_{j=0}^{N_f-1}\omega(t - jT_f),\ b = \pm 1 \tag{4.2}$$

where b is the transmitted symbol and P_s is the transmit power of S and the value of P_s depends on the battery power limit of S. In on-body transmissions, we assume that $P_s \leq P^o_{max}$, where P^o_{max} is the maximum transmit power for the on-body node, which is constrained by FCC PSD emission limit for IR-UWB signals. Similarly, we assume that $P_s \leq P^i_{max}$ in the in-body scenario. $\omega(t)$ denotes the ultrashort pulse waveform with T_w duration, which has the unit energy $\int_{t=0}^{T_w}\omega^2(t) = 1$.

For all the links, it is assumed that channel $h_k(t)$ remains invariant over a symbol duration, but it changes from symbol to symbol. Thus, the received signal at D is given by

$$r_{SD}(t) = b\sqrt{\frac{P_s}{PL_{SD}(d_{SD})}}\sum_{j=0}^{N_f-1} g_{SD}(t - jT_f) + n_{SD}(t),\ b = \pm 1, \tag{4.3}$$

where

$$g_{SD}(t) = \omega(t) * h_{SD}(t) = \sum_{l=0}^{L_{SD}-1}\alpha_{l,SD}\omega(t - \tau_{l,SD}), \tag{4.4}$$

and $n_{SD}(t)$ is the additive white Gaussian noise with zero mean and variance σ_n^2. $*$ represents convolution. T_f is set to be large enough to avoid the inter-symbol interference (ISI).

At D, a received pulse waveform matched filter is employed. After summing up all the outputs over N_f frames, the decision statistic b at D can be written as

$$b_{SD} = bN_f\sqrt{\frac{P_s}{PL_{SD}(d_{SD})}}\bar{\xi}_{SD} + \hat{n}_{SD}, \tag{4.5}$$

where $\bar{\xi}_{SD}$ is the captured multipath energy during T_f at D in direct transmission and $\hat{n}_{SD}$ is a white Gaussian noise with zero mean and variance $N_f\bar{\xi}_{SD}\sigma_n^2$.

With (4.5), the SE (unit:bits/s/Hz) for direct transmission can be given by

$$SE_{SD} = \frac{1}{N_f}\log_2(1+\gamma_{SD}), \tag{4.6}$$

where $\gamma_{SD} = \frac{N_f P_s \bar{\xi}_{SD}}{PL_{SD}(d_{SD})\sigma_n^2}$ is the received SNR. Note that, $PL_{SD}(d_{SD})$ is different in the different scenarios. In the around-torso scenario, $PL_{SD}(d_{SD}) = 10^{PL_1^{dB}(d_{SD})/10}$. In the along-torso scenario, $PL_{SD}(d_{SD}) = 10^{PL_0^{dB}(d_{SD})/10}$. In the in-body scenario, $PL_{SD}(d_{SD}) = 10^{PL_2^{dB}(d_{SD})/10}$.

In the next section, the SE optimization for on-body cooperative transmissions and in-body cooperative transmissions are presented in detail, respectively.

4.3.2 Spectral Efficiency Optimization for On-Body Transmissions

Proposed Network Model for On-Body Transmissions

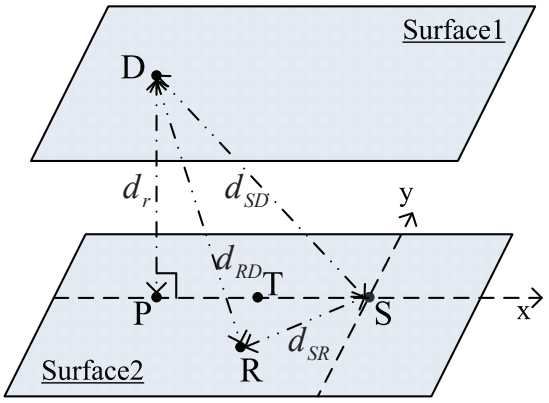

Figure 4.1: Proposed cooperative model for on-body transmissions in WBANs.

In Fig. 4.1, the cooperative network model for on-body transmissions is developed, where the around-torso scenario is considered. In this scenario, we only study the case that all nodes are only located on the front side of the human body or on the back

side of the human body rather than the limbs. Thus, a two-surface system model can be established under the reasonable assumption that each side of the human body is approximately treated as a level surface, as shown in Fig. 4.1. Without loss of generality, we assume that D is located on the front side of the human body (Surface1) and S and R are located on the back side of the human body (Surface2). The distance between these two surfaces is d_r ($d_r \geq 0$). d_{SD}, d_{SR}, and d_{RD} denote the distances from S to D, S to R, and R to D, respectively. We denote the projection of D on Surface2 by point P and point T is located in the middle between P and S. To represent the location of R, we construct a xy-plane on Surface2, where S is set to be the origin point and the x-axis is along P to S. It is worth noting that this equivalent cooperative model will be simplified to the one for the along-torso scenario when $d_r = 0$. In this case, D is located on the same surface with S. Thus, we can consider the along-torso scenario as a special case in the around-torso scenario.

Due to the similarity in structures, the around-torso scenario and along-torso scenario can be analytically similar for solving the SE optimization problem. In the sequel of this section, we focus on the SE optimization in the around-torso scenario and only detail the solution for the around-torso scenario. As a special case in the around-torso scenario, the corresponding solution in the along-torso scenario is not repeated in this work.

In the around-torso scenario, with given coordinates $\{x_r, y_r\}$ for R, we have

$$d_{SR}(x_r, y_r) = \sqrt{x_r^2 + y_r^2}, \tag{4.7}$$

and

$$d_{RD}(x_r, y_r) = \sqrt{(x_r + d_{SD}\sin\theta)^2 + y_r^2 + d_r^2}, \tag{4.8}$$

where $\theta = \arccos(d_r/d_{SD})$.

Formulation for the SE Optimization

Similar to D, R is also equipped with a matched filter. With the considered AF cooperative protocol, after summing up all the outputs over N_f frames, the decision statistic b in the first time slot at R and D can be given by

$$b_{SR} = bN_f\sqrt{\frac{P_1}{PL_{SR}(d_{SR})}}\xi_{SR} + \hat{n}_{SR}, \tag{4.9}$$

and

$$b_{SD,1} = bN_f\sqrt{\frac{P_1}{PL_{SD}(d_{SD})}}\xi_{SD} + \hat{n}_{SD}, \tag{4.10}$$

respectively, where P_1 is the transmit power at S in cooperative transmission. In the around-torso scenario, we have

$$PL_{SD}(d_{SD}) = 10^{PL_1^{dB}(d_{SD})/10} = M_1 d_{SD}^{n_1},$$

and

$$PL_{SR}(d_{SR}) = 10^{PL_0^{dB}(d_{SR})/10} = M_0 d_{SR}^{n_0},$$

where $M_0 = (1/d_0)^{n_0}10^{L_0/10}$ and $M_1 = (1/d_1)^{n_1}10^{L_1/10}10^{H_0/10}$ are constant. ξ_{SR} and ξ_{SD} are the captured multipath energy during T_f over the links S-R and S-D in the around-torso scenario, respectively. $\hat{n}_{SR}$ is a white Gaussian noise with zero mean and variance $N_f\xi_{SR}\sigma_n^2$. $\hat{n}_{SD}$ is a white Gaussian noise with zero mean and variance $N_f\xi_{SD}\sigma_n^2$.

In the second time slot, R forwards its received signals to D and the the forwarded symbol waveform at R can be expressed as

$$s_{RD}(t) = b_{SR}\sqrt{\frac{P_2}{|b_{SR}|}}\sum_{j=0}^{N_f-1}\omega(t - 2jT_f), \tag{4.11}$$

where P_2 is the transmit power at R and $|b_{SR}| = \frac{N_f^2 P_1 \xi_{SR}^2}{PL_{SR}(d_{SR})} + N_f\xi_{SR}\sigma_n^2$.

Accordingly, the decision statistic b in the second time slot at D can be given by

$$b_{RD,2} = b_{SR} N_f \sqrt{\frac{P_2}{|b_{SR}| PL_{RD}(d_{RD})}} \xi_{RD} + \hat{n}_{RD}, \tag{4.12}$$

where

$$PL_{RD}(d_{RD}) = 10^{PL_1^{dB}(d_{RD})/10} = M_1 d_{RD}^{n_1}.$$

ξ_{RD} are the captured multipath energy during T_f over the links R-D and $\hat{n}_{RD}$ is a white Gaussian noise with zero mean and variance $N_f \xi_{RD} \sigma_n^2$.

After maximum-ratio combining (MRC) [108] with $b_{RD,1}$ and $b_{RD,2}$ at D, the SE of the single-relay cooperative transmission in the around-torso scenario can be given by

$$SE_{SRD} = \frac{1}{2N_f} \log_2(1 + \gamma_1 + \gamma_2), \tag{4.13}$$

where γ_1 is the received SNR at D in the first time slot and

$$\gamma_2 = \frac{\gamma_{SR}\gamma_{RD}}{\gamma_{SR} + \gamma_{RD} + 1} \approx \frac{\gamma_{SR}\gamma_{RD}}{\gamma_{SR} + \gamma_{RD}}, \tag{4.14}$$

is the received SNR at D in the second time slot. γ_{SR} and γ_{RD} are the received SNRs for the links S-R and R-D, respectively.

The expressions of γ_1, γ_{SR} and γ_{RD} are given by

$$\gamma_1 = \frac{N_f P_1 \xi_{SD}}{PL_{SD}(d_{SD}) \sigma_n^2}, \tag{4.15}$$

$$\gamma_{SR} = \frac{N_f P_1 \xi_{SR}}{PL_{SR}(d_{SR}) \sigma_n^2}, \tag{4.16}$$

$$\gamma_{RD} = \frac{N_f P_2 \xi_{RD}}{PL_{RD}(d_{RD}) \sigma_n^2}. \tag{4.17}$$

In this work, to make a fair comparison with direct transmission, we assume that the total transmit power resource in cooperative transmission is not more than that in direct transmission, i.e., $P_1 + P_2 \leq P_s$.

Substituting (4.7), (4.8), and (4.14)-(4.17) into (4.13), we have

$$SE_{SRD}(x_r, y_r, P_1, P_2) = \frac{1}{2N_f}\log_2\left(1 + \underbrace{\frac{N_f P_1 \xi_{SD}}{PL_{SD}(d_{SD})\sigma_n^2}}_{\gamma_1(P_1)} + \underbrace{\frac{1}{\frac{PL_{SR}(d_{SR}(x_r,y_r))\sigma_n^2}{N_f P_1 \xi_{SR}} + \frac{PL_{RD}(d_{RD}(x_r,y_r))\sigma_n^2}{N_f P_2 \xi_{RD}}}}_{\gamma_2(x_r,y_r,P_1,P_2)}\right). \tag{4.18}$$

Obviously, SE_{SRD} is the function of variables $\{x_r, y_r, P_1, P_2\}$. To obtain the maximum SE_{SRD} in the around-torso scenario, we must find the optimal set $\{x_r^{se}, y_r^{se}, P_1^{se}, P_2^{se}\}$ to maximize $SE_{SRD}(x_r, y_r, P_1, P_2)$. Thus, the joint optimal RL and PA problem for the SE optimization in the around-torso scenario can be mathematically formulated as

$$\begin{aligned} \underset{x_r,y_r,P_1,P_2}{\text{maximize}} \quad & SE_{SRD}(x_r, y_r, P_1, P_2) \\ \text{subject to} \quad & \text{C1}: \left(x_r + \frac{d_{SD}\sin\theta}{2}\right)^2 + y_r^2 \le \left(\frac{d_{SD}\sin\theta}{2}\right)^2, \\ & \text{C2}: x_r \le \epsilon, \\ & \text{C3}: P_1 + P_2 \le P_s, \end{aligned} \tag{4.19}$$

where C1 is imposed to guarantee that R is only located in the circle centered at T with radius $\frac{d_{SD}\sin\theta}{2}$. This special circle for R is considered based on the fact that we can always find a corresponding relay location within the circle which can provide a better performance than those beyond the circle. C2 is imposed to guarantee that $\{x_r = 0, y_r = 0\}$ has to be beyond C1 since R cannot coincide with S, where $|\epsilon|$ is a very small constant and we set $-10^{-6} < \epsilon < 0$. With C1 and C2, we have $d_{SR}, d_{RD} < d_{SD}$.

As the along-torso scenario is considered as a special case of the around-torso scenario in the proposed network model, the SE expression in (4.18) and the problem formulation in (4.19) can also be applied to the along-torso scenario with $d_r = 0$. However, due to different channel parameters, the path loss models in the along-torso scenario from S to

D , S to R, and R to D should be expressed as,

$$PL_{SD}(d_{SD}) = 10^{PL_0^{dB}(d_{SD})/10} = M_0 d_{SD}^{n_0},$$

$$PL_{SR}(d_{SR}) = 10^{PL_0^{dB}(d_{SR})/10} = M_0 d_{SR}^{n_0},$$

and

$$PL_{RD}(d_{RD}) = 10^{PL_0^{dB}(d_{RD})/10} = M_0 d_{RD}^{n_0},$$

respectively.

In the next part, we detail the derivation and solution of the optimal RL and PA problem for the SE optimization in the around-torso scenario. For the along-torso scenario, the related optimal RL and PA can also be achieved with similar derivations and it is not repeated in this work.

Joint Optimal RL and PA in Cooperative Transmission

Since $\log_2(1+x)$ is a monotonically increasing function of x, we can rewrite the optimization problem as

$$\begin{aligned} &\underset{x_r, y_r, P_1, P_2}{\text{maximize}} \quad \gamma_1(P_1) + \gamma_2(x_r, y_r, P_1, P_2) \\ &\text{subject to} \quad \text{C1, C2, C3.} \end{aligned} \tag{4.20}$$

From (4.15), we can see that $\gamma_1(P_1)$ is a linear function of P_1, which indicates that $\gamma_1(P_1)$ is concave. To prove that $\gamma_2(x_r, y_r, P_1, P_2)$ is a concave function, we introduce the following Proposition and Theorem.

Proposition 4.1. *$\frac{PL_{SR}(d_{SR}(x_r,y_r))\sigma_n^2}{N_f P_1 \xi_{SR}}$ and $\frac{PL_{RD}(d_{RD}(x_r,y_r))\sigma_n^2}{N_f P_2 \xi_{RD}}$ in the around-torso scenario are both convex for $P_1, P_2 > 0$.*

Proof. For notational simplicity, we define

$$f_1(x_r, y_r, P_1) = \frac{PL_{SR}(d_{SR}(x_r, y_r))\sigma_n^2}{N_f P_1 \xi_{SR}} = \frac{(x_r^2 + y_r^2)^{\frac{n_0}{2}} M_0 \sigma_n^2}{N_f P_1 \xi_{SR}}, \tag{4.21}$$

and

$$f_2(x_r, y_r, P_2) = \frac{PL_{RD}(d_{RD}(x_r, y_r))\sigma_n^2}{N_f P_2 \xi_{RD}} = \frac{((x_r + d_{SD}\sin\theta)^2 + y_r^2 + d_r^2)^{\frac{n_1}{2}} M_1 \sigma_n^2}{N_f P_2 \xi_{RD}}. \tag{4.22}$$

Then, we denote $\mathbf{H}(f_1(x_r, y_r, P_1))$ and $\mathbf{H}(f_2(x_r, y_r, P_2))$ as the Hessian matrices of functions $f_1(x_r, y_r, P_1)$ and $f_2(x_r, y_r, P_2)$, respectively. The determinants of $\mathbf{H}(f_1(x_r, y_r, P_1))$ and $\mathbf{H}(f_2(x_r, y_r, P_2))$ are given by

$$|\mathbf{H}(f_1(x_r, y_r, P_1))| = \frac{M_0^3 \sigma_n^6 (n_0^3 - 2n_0^2)(x_r^2 + y_r^2)^{\frac{3n_0 - 4}{2}}}{P_1^5 N_f^3 \xi_{SR}^3}, \tag{4.23}$$

and

$$|\mathbf{H}(f_2(x_r, y_r, P_2))| = \frac{M_1^3 \sigma_n^6}{N_f^3 \xi_{RD}^3} \frac{(n_1^3 - 2n_1^2)((x_r + d_{SD}\sin\theta)^2 + y_r^2) + 2n_1^2 d_r^2}{P_2^5((x_r + d_{SD}\sin\theta)^2 + y_r^2 + d_r^2)^{\frac{6-3n_1}{2}}}, \tag{4.24}$$

respectively.

Since $n_0^3 - 2n_0^2 > 0$ and $n_1^3 - 2n_1^2 > 0$, $\mathbf{H}(f_1(x_r, y_r, P_1))$ and $\mathbf{H}(f_2(x_r, y_r, P_2))$ are both positive definite matrixes with $P_1, P_2 > 0$. In other words, $f_1(x_r, y_r, P_1)$ is jointly convex w.r.t. x_r, y_r, and P_1. $f_2(x_r, y_r, P_2)$ is jointly convex w.r.t. x_r, y_r, and P_2. □

Theorem 4.1. *Given that $f(x)$ and $g(y)$ are both convex, $\phi(x, y) = f(x) + g(y)$ is convex.*

Proof. Since $f(x)$ and $g(y)$ are convex, we have

$$f(tx_1 + (1-t)x_2) \leq tf(x_1) + (1-t)f(x_2), \tag{4.25}$$

and

$$g(ty_1 + (1-t)y_2) \leq tg(y_1) + (1-t)g(y_2), \tag{4.26}$$

where x_1 and x_2 are any two points for function $f(x)$ and y_1 and y_2 are any two points for function $g(y)$. $0 < t < 1$. We define that $z_1 = \{x_1, y_1\}$ and $z_2 = \{x_2, y_2\}$. Then we can write

$$\begin{aligned}\phi(tz_1 + (1-t)z_2) &= \phi(tx_1 + (1-t)x_2, ty_1 + (1-t)y_2) \\ &= f(tx_1 + (1-t)x_2) + g(ty_1 + (1-t)y_2) \\ &\leq tf(x_1) + (1-t)f(x_2) + tg(y_1) + (1-t)g(y_2) \\ &= t\phi(z_1) + (1-t)\phi(z_2) \end{aligned} \tag{4.27}$$

Thus, $\phi(x, y)$ is convex. □

By Proposition 4.1 and Theorem 4.1, we can see that $1/\gamma_2(x_r, y_r, P_1, P_2)$ is a convex function and $1/\gamma_2(x_r, y_r, P_1, P_2) > 0$. Hence, $\gamma_2(x_r, y_r, P_1, P_2)$ is concave w.r.t. C1-C3. As a result, the objective function in (4.20) is concave. Thus, it is concluded that the joint RL and PA problem for the around-torso scenario is a nonlinear convex optimization problem, which can be solved by using the Lagrange multiplier method with Karush-Kuhn-Tucker (KKT) conditions [109].

The Lagrangian of (4.20) can be given by

$$\begin{aligned}&\mathcal{L}(x_r, y_r, P_1, P_2, \mu_1, \mu_2, \mu_3) \\ &= \gamma_1(P_1) + \gamma_2(x_r, y_r, P_1, P_2) - \mu_1 \left(\left(x_r + \frac{d_{SD}\sin\theta}{2} \right)^2 + y_r^2 - \left(\frac{d_{SD}\sin\theta}{2} \right)^2 \right) \\ &- \mu_2(x_r - \epsilon) - \mu_3(P_1 + P_2 - P_s), \end{aligned} \tag{4.28}$$

where $\mu_1, \mu_2, \mu_3 \geq 0$ are the Lagrange multipliers connected to C1-C3.

Taking the stationarity condition of y_r and x_r, we get

$$\frac{\partial \mathcal{L}}{\partial y_r} = y_r \frac{n_0 M_0 A_1(x_r, y_r)}{N_f P_1 \xi_{SR}} + y_r \frac{n_1 M_1 A_2(x_r, y_r)}{N_f P_2 \xi_{RD}} + y_r \frac{2\mu_1}{\lambda_2^2(x_r, y_r, P_1, P_2)} = 0, \tag{4.29}$$

and

$$\frac{\partial \mathcal{L}}{\partial x_r} = \frac{x_r n_0 M_0 A_1(x_r, y_r)}{N_f P_1 \xi_{SR}} + \frac{(x_r + d_{SD}\sin\theta) n_1 M_1 A_2(x_r, y_r)}{N_f P_2 \xi_{RD}} + \frac{2(x_r + \frac{d_{SD}\sin\theta}{2})\mu_1 + \mu_2}{\lambda_2^2(x_r, y_r, P_1, P_2)} = 0. \tag{4.30}$$

Since $A_1(x_r, y_r) = (x_r^2 + y_r^2)^{\frac{n_0-2}{2}}$ and $A_2(x_r, y_r) = ((x_r + d_{SD}\sin\theta)^2 + y_r^2 + d_r^2)^{\frac{n_1-2}{2}}$ are both positive. Consequently, the optimal $y_r^{se} = 0$.

Considering the case $\mu_1 \neq 0$, we can set $(\tilde{x_r}^o + \frac{d_{SD}\sin\theta}{2})^2 + (y_r^o)^2 = (\frac{d_{SD}\sin\theta}{2})^2$ and $\mu_2 = 0$ based on the KKT conditions. With $y_r^o = 0$, $\tilde{x_r}^o = -d_{SD}\sin\theta$, and substituting $\tilde{x_r}^o$ into (4.30), we can see that $\frac{\partial \mathcal{L}}{\partial x_r}|_{\tilde{x_r}^o} < 0$. Hence, we can force $\mu_1 = 0$. Similarly, it is easy to prove that $\mu_2 = 0$.

Taking the stationarity condition of P_1 and P_2, we get

$$\frac{\partial \mathcal{L}}{\partial P_1} = \frac{\xi_{SD} N_f}{M_1 d_{SD}^{n_1} \sigma_n^2} + \frac{N_f \xi_{SR} \xi_{RD} P_2^2 A_3(x_r, 0)}{\sigma_n^2 \big(P_2 A_3(x_r, 0) + P_1 A_4(x_r, 0)\big)^2} - \mu_3 = 0, \tag{4.31}$$

and

$$\frac{\partial \mathcal{L}}{\partial P_2} = \frac{N_f \xi_{SR} \xi_{RD} P_1^2 A_4(x_r, 0)}{\sigma_n^2 \big(P_2 A_3(x_r, 0) + P_1 A_4(x_r, 0)\big)^2} - \mu_3 = 0, \tag{4.32}$$

where $A_3(x_r, y_r) = \xi_{RD} M_0 (x_r^2 + y_r^2)^{\frac{n_0}{2}} > 0$ and $A_4(x_r, y_r) = \xi_{SR} M_1 ((x_r + d_{SD}\sin\theta)^2 + y_r^2 + d_r^2)^{\frac{n_1}{2}} > 0$. To make sure that $\frac{\partial \mathcal{L}}{\partial P_1} = 0$ and $\frac{\partial \mathcal{L}}{\partial P_2} = 0$, μ_3 should be positive. Based on the KKT conditions, we thus have $P_1^{se} + P_2^{se} = P_s$.

In conclusion, $\{x_r^{se}, y_r^{se}, P_1^{se}, P_2^{se}\}$ satisfies (4.33)-(4.36):

$$y_r^{se} = 0, \tag{4.33}$$

$$\frac{x_r^{se} n_0 M_0 P_2^{se} \xi_{RD}}{n_1 M_1 P_1^{se} \xi_{SR}} A_1(x_r^{se}, 0) + (x_r^{se} + d_{SD}\sin\theta) A_2(x_r^{se}, 0) = 0, \tag{4.34}$$

$$\frac{\xi_{SD}}{M_1 d_{SD}^{n_1}} + \frac{\xi_{SR}\xi_{RD}(P_2^{se})^2 A_3(x_r^{se}, 0)}{(P_2^{se} A_3(x_r^{se}, 0) + P_1^o A_4(x_r^{se}, 0))^2} = \frac{\xi_{SR}\xi_{RD}(P_1^{se})^2 A_4(x_r^{se}, 0)}{(P_2^o A_3(x_r^{se}, 0) + P_1^{se} A_4(x_r^{se}, 0))^2}, \tag{4.35}$$

and

$$P_1^{se} + P_2^{se} = P_s, \tag{4.36}$$

Based on (4.33)-(4.36), the optimal solution $\{x_r^{se}, y_r^{se}, P_1^{se}, P_2^{se}\}$ is achieved for the SE maximization problem in the around-torso scenario. For the along-torso scenario, similar proofs and derivations are not repeated herein.

4.3.3 Spectral Efficiency Optimization for In-Body Transmissions

Proposed Network Model for In-Body Transmissions

In Fig. 4.2, the cooperative network model for in-body scenario is considered, where S is located inside the human body (e.g., chest), and R and D are located on the same side of the human body. The penetration depth from S to the body surface is d_r ($d_r > 0$). Similar to the on-body cooperative model, we denote the projection of S on the body surface by point P. On the body surface, we can construct a xy-plane to present the location of R, where P is set to be the origin point and the x-axis is along P to D.

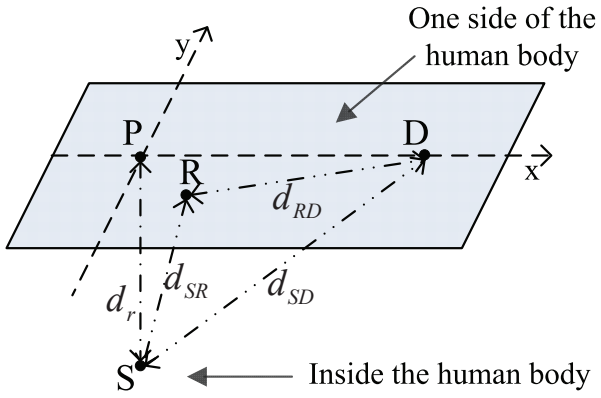

Figure 4.2: Proposed cooperative model for in-body transmissions in WBANs.

With given coordinates $\{x_r, y_r\}$ for R, we have

$$d_{SR} = \sqrt{x_r^2 + y_r^2 + d_r^2}, \tag{4.37}$$

and

$$d_{RD} = \sqrt{(x_r - d_{SD}\sin\theta)^2 + y_r^2}, \tag{4.38}$$

Formulation for the SE Optimization

In the in-body scenario, the along-torso channel model for on-body to on-body links and the in-body channel model for in-body to on-body links are used for the formulation of SE optimization. Based on Table 4.1, the path losses in the linear scale from S to D, S to R, and R to D in the in-body scenario can be obtained as,

$$PL_{SD}(d_{SD}) = 10^{PL_2^{dB}(d_{SD})/10}, \tag{4.39}$$

$$PL_{SR}(d_{SR}) = 10^{PL_2^{dB}(d_{SR})/10}, \tag{4.40}$$

and

$$PL_{RD}(d_{RD}) = 10^{PL_0^{dB}(d_{RD})/10}, \tag{4.41}$$

respectively.

With (4.37)-(4.41), the SE in the in-body scenario can also be written as a function of relay location $\{x_r, y_r\}$ and power allocation $\{P_1, P_2\}$:

$$\begin{aligned} SE_{SRD}(x_r, y_r, P_1, P_2) =& \frac{1}{2N_f}\log_2\left(1 + \underbrace{\frac{N_f P_1 \xi_{SD}}{PL_{SD}(d_{SD})\sigma_n^2}}_{\gamma_1(P_1)}\right. \\ &\left. + \underbrace{\frac{1}{\frac{PL_{SR}(d_{SR}(x_r,y_r))\sigma_n^2}{N_f P_1 \xi_{SR}} + \frac{PL_{RD}(d_{RD}(x_r,y_r))\sigma_n^2}{N_f P_2 \xi_{RD}}}}_{\gamma_2(x_r,y_r,P_1,P_2)}\right). \end{aligned} \tag{4.42}$$

Thus, the corresponding SE optimization problem in the in-body scenario can be mathematically formulated as

$$\begin{aligned} \underset{x_r,y_r,P_1,P_2}{\text{maximize}} \quad & SE_{SRD}(x_r, y_r, P_1, P_2) \\ \text{subject to} \quad & \text{C1} : x_r^2 + y_r^2 \leq (d_{SD}\sin\theta)^2, \\ & \text{C2} : x_r \leq d_{SD}\sin\theta + \hat{\delta}, \\ & \text{C3} : P_1 + P_2 \leq P_s, \\ & \text{C4} : P_2 \leq P_{max}^o, \end{aligned} \tag{4.43}$$

where C1 is imposed to guarantee that R is only located in the circle centered at P with radius $d_{SD}\sin\theta$. C2 is imposed to guarantee that $\{x_r = d_{SD}\sin\theta, y_r = 0\}$ has to be beyond C1 since R cannot coincide with D. $|\hat{\delta}|$ is an extremely small constant and we set $-10^{-6} < \hat{\delta} < 0$. C4 is imposed to guarantee that P_2 meets the requirement of the FCC PSD emission limit for IR-UWB signals since R is an on-body node.

Joint Optimal RL and PA in Cooperative Transmission

Similar to Section 4.3.2, we can rewrite the SE optimization problem as

$$\begin{aligned} \underset{x_r,y_r,P_1,P_2}{\text{maximize}} \quad & \gamma_1(P_1) + \gamma_2(x_r, y_r, P_1, P_2) \\ \text{subject to} \quad & \text{C1}, \text{C2}, \text{C3}, \text{C4}. \end{aligned} \tag{4.44}$$

Since $\gamma_1(P_1)$ is a linear function of P_1, $\gamma_1(P_1)$ is concave. To prove that $\gamma_2(x_r, y_r, P_1, P_2)$ is a concave function, we introduce the following Proposition.

Proposition 4.2. *$\frac{PL_{SR}(d_{SR}(x_r,y_r))\sigma_n^2}{N_f P_1 \xi_{SR}}$ and $\frac{PL_{RD}(d_{RD}(x_r,y_r))\sigma_n^2}{N_f P_2 \xi_{RD}}$ in the in-body scenario are both convex for $P_1, P_2 > 0$.*

Proof. For notational simplicity, we define

$$f_1(x_r, y_r, P_1) = \frac{PL_{SR}(d_{SR}(x_r, y_r))\sigma_n^2}{N_f P_1 \xi_{SR}} = \frac{M_3 h \sigma_n^2 10^{M_4 (x_r^2 + y_r^2 + d_r^2)^{\frac{n_2}{2}}}}{N_f P_1 \xi_{SR}}, \tag{4.45}$$

and

$$f_2(x_r, y_r, P_2) = \frac{PL_{RD}(d_{RD}(x_r, y_r))\sigma_n^2}{N_f P_2 \xi_{RD}} = \frac{((x_r - d_{SD}\sin\theta)^2 + y_r^2)^{\frac{n_0}{2}} M_0 \sigma_n^2}{N_f P_2 \xi_{RD}}, \tag{4.46}$$

where $M_3 = 10^{L_2/10}$, $h = 10^{H_1/10}$, $M_4 = \frac{a}{10 d_2^{n_2}}$.

Then, we denote $\mathbf{H}(f_1)$ and $\mathbf{H}(f_2)$ as the Hessian matrices of functions $f_1(x_r, y_r, P_1)$ and $f_2(x_r, y_r, P_2)$, respectively. The determinants of $\mathbf{H}(f_1)$ and $\mathbf{H}(f_2)$ are given by

$$|\mathbf{H}(f_1)| = \frac{\ln 10^2 M_3^3 M_4^2 n_2^2 h^3 \sigma_n^6 10^{3M_4(x_r^2+y_r^2+d_r^2)^{\frac{n_2}{2}}} f_3(x_r, y_r)}{N_f^3 P_1^5 \xi_{SR}^3 (x_r^2 + y_r^2 + d_r^2)^{(3-n_2)}}, \tag{4.47}$$

where

$$\begin{aligned} f_3(x_r, y_r) &= 2d_r^2 + 2n_2 x_r^2 + 2n_1 y_r^2 - 2x_r^2 - 2y_r^2 \\ &\quad + \ln 10 M_4 n_2 (y_r^2 + x_r^2)(x_r^2 + y_r^2 + d_r^2)^{\frac{n_2}{2}} \end{aligned} \tag{4.48}$$

and

$$|\mathbf{H}(f_2)| = \frac{M_0^3 \sigma_n^6 (n_0^3 - 2n_0^2)((x_r - d_{SD}\sin\theta)^2 + y_r^2)^{\frac{3n_0-4}{2}}}{P_2^5 N_f^3 \xi_{RD}^3}. \tag{4.49}$$

Since $f_3(x_r, y_r) > 0$ and $n_0^3 - 2n_0^2 > 0$, $\mathbf{H}(f_1)$ and $\mathbf{H}(f_2)$ are both positive definite matrices with $P_1, P_2 > 0$. In other words, $f_1(x_r, y_r, P_1)$ is jointly convex w.r.t. x_r, y_r, and P_1. $f_2(x_r, y_r, P_2)$ is jointly convex w.r.t. x_r, y_r, and P_2. □

By Proposition 4.2, $1/\gamma_2(x_r, y_r, P_1, P_2)$ is a convex function and $1/\gamma_2(x_r, y_r, P_1, P_2) > 0$. Hence, $\gamma_2(x_r, y_r, P_1, P_2)$ is concave w.r.t. C1-C4. As a result, the objective function in (4.44) is concave. Thus, the SE optimization problem in this case is also a nonlinear convex optimization problem. It is therefore solved by using the Lagrange multiplier method with the KKT conditions.

The Lagrangian of (4.44) can be given by

$$\begin{aligned} &\mathcal{L}(x_r, y_r, P_1, P_2, \mu_1, \mu_2, \mu_3, \mu_4) \\ =&\gamma_1(P_1) + \gamma_2(x_r, y_r, P_1, P_2) - \mu_1\left(x_r^2 + y_r^2 - (d_{SD}\sin\theta)^2\right) - \mu_2(x_r - d_{SD}\sin\theta - \hat{\delta}) \\ &- \mu_3(P_1 + P_2 - P_s) - \mu_4(P_2 - P_{max}^o), \end{aligned} \tag{4.50}$$

where $\mu_1, \mu_2, \mu_3, \mu_4 \geq 0$ are the Lagrange multipliers connected to C1-C4. Considering the KKT conditions and taking the stationarity condition of each variable, we can prove that $\mu_1 = \mu_2 = 0$ and the globally optimal solution $\{x_r^{se}, y_r^{se}, P_1^{se}, P_2^{se}\}$ satisfies (4.51)-(4.55):

$$y_r^{se} = 0, \tag{4.51}$$

$$x_r^{se} PL_{SR}\big(d_{SR}(x_r^{se}, 0)\big)\big((x_r^{se})^2 + d_r^2\big)^{\frac{n_2-2}{2}} = \frac{P_1^{se}\xi_{SR}M_0 n_0 (d_{SD}\sin\theta - x_r^{se})^{n_0-1}}{P_2^{se}\xi_{RD}\ln 10 M_4 n_2}, \tag{4.52}$$

$$P_1^{se} + P_2^{se} = P_s, \tag{4.53}$$

and

$$P_2^{se} = \min\{P_{max}^o, \tilde{P}_2\}, \tag{4.54}$$

where $\tilde{P}_2$ satisfies

$$\begin{aligned} &\frac{\xi_{SD}}{PL_{SD}(d_{SD})} + \frac{\xi_{SR}\xi_{RD}A_5(x_r^{se}, 0)\tilde{P}_2^2}{\big(\tilde{P}_2 A_5(x_r^{se}, 0) + (P_s - \tilde{P}_2)A_6(x_r^{se}, 0)\big)^2} \\ &= \frac{\xi_{SR}\xi_{RD}A_6(x_r^{se}, 0)(P_s - \tilde{P}_2)^2}{\big(\tilde{P}_2 A_5(x_r^{se}, 0) + (P_s - \tilde{P}_2)A_6(x_r^{se}, 0)\big)^2} \end{aligned} \tag{4.55}$$

and $A_5(x_r^{se}, 0) = PL_{SR}\big(d_{SR}(x_r^{se}, 0)\big)\xi_{RD}$ and $A_6(x_r^{se}, 0) = PL_{RD}\big(d_{RD}(x_r^{se}, 0)\big)\xi_{SR}$.

4.3.4 Discussions

1. A typical application for the around-torso scenario in a WBAN is the post-neck surgery tracking for the patient, where a sensor node is placed on the neck of the patient to measure the angular motion of the neck and send the updated status of recovery to the coordinator in the front pocket.

2. A typical application for the in-body scenario in a WBAN is the pacemaker inside the chest. Normally, the pacemaker system, which consists of a battery pack (pulse

generator) and either one of two wires (leads), is surgically implanted under the skin in the chest. It can continuously monitor (sense) the patient heart's natural rhythm and feedback the patient health status to the coordinator. If it is necessary, the pacemaker will stimulate the heart to beat when it senses that the patient heart's rhythm is too slow.

3. In a WBAN, the number of nodes and their application types depend on the requirement of the patient. Based on the 802.15.6 standard [13], a multiple access mode known as "improvised access" is supported in the WBAN standard, whereby the coordinator can inform nodes that they have been granted one-off exclusive time slots to transmit or receive information. Thus, in a particular time slot, only one node is active and other nodes are inactive (in a sleep mode or act as relays). Without loss of generality, an ideal MAC layer is assumed.

4. The proposed joint optimal RL and PA scheme provides an insight into the spectral-efficient design of healthcare applications with respect to the proper placement of the wearable relay node along with the optimal transmit power level in WBANs. When the number of nodes in a WBAN is small (e.g., only one or two nodes are attached on or in the human body), relays can be added to the WBAN with the optimal placements based on the proposed scheme, which would not cause the comfort issue to the patient. When the node density in a WBAN is high, it is inappropriate to add additional relays for nodes. In fact, inactive nodes can be selected as relays to cooperate in forwarding the data from the active node towards the coordinator. Thus, the proposed scheme can be also considered as a source of inspiration for the relay selection in this case. For instance, the coordinator can adopt the proposed scheme for the current active node. Based on the information about the corresponding optimal relay location, the inactive node, whose location

is closest to the optimum, can be selected as a relay candidate.

4.4 Simulation Results

To evaluate SE of the proposed single-relay assisted transmission scheme in UWB based WBANs, numerical simulations are conducted in this section, which consist of two parts: the SE evaluation for on-body transmissions and the SE evaluation for in-body transmissions. The simulations are performed in MATLAB with Monte Carlo method. MATLAB's optimization toolbox is used for solving the convex programming in the simulations. All the simulation results are averaged over 5000 channel realizations.

In simulations, T_w and T_f are chosen to be 2ns and 150ns, respectively. N_f is set to be 4 and the noise power density is set to be -174dBm/Hz and the system bandwidth B is 500MHz [13]. Since the average FCC PSD emission limit for on-body UWB transmissions is -41.3dBm/MHz [6], the maximum average transmit power P_{ave} is -14.3dBm. With the duty cycle T_w/T_f, $P^o_{max} = P_{ave} * T_f/T_w = 4$dBm [56]. For the in-body transmissions, we set $P^i_{max} \leq 10$dBm considering the emission limit and safety inside the human body [56]. According to the scale of the human body, d_{SD} is very limited in UWB based WBANs. Without loss of generality, we consider the case that 0.5m$\leq d_{SD} \leq$ 0.8m for on-body transmissions and 0.2m$\leq d_{SD} \leq$ 0.3m for in-body transmissions. At R and D, we assume that all of the dispersive energies are captured without considering the ISI.

4.4.1 Spectral Efficiency Evaluation for On-Body Transmissions

In this part, the SE performance for on-body transmissions is evaluated. We first analyze the features of the optimal RL and PA in each scenario. Then, the comparison between the proposed scheme and other transmission schemes is presented.

Analysis of Optimal Relay location and Power Allocation

Table 4.2: Averaged optimal set $\left\{\mathrm{E}\{x_r^{se}\}, \mathrm{E}\{y_r^{se}\}, \mathrm{E}\{P_1^{se}\}, \mathrm{E}\{P_2^{se}\}\right\}$ for on-body transmissions

Along-torso scenario ($d_r = 0$)				
d_{SD}	0.5m	0.6m	0.7m	0.8m
$\mathrm{E}\{x_r^{se}\}$	-0.30	-0.36	-0.42	-0.48
$\mathrm{E}\{y_r^{se}\}$	0	0	0	0
$\mathrm{E}\{P_1^{se}\}$	$0.70P_s$	$0.70P_s$	$0.70P_s$	$0.70P_s$
$\mathrm{E}\{P_2^{se}\}$	$0.30P_s$	$0.30P_s$	$0.30P_s$	$0.30P_s$
Around-torso scenario with $d_r = 0.2$m				
d_{SD}	0.5m	0.6m	0.7m	0.8m
$\mathrm{E}\{x_r^{se}\}$	-0.41	-0.51	-0.61	-0.70
$\mathrm{E}\{y_r^{se}\}$	0	0	0	0
$\mathrm{E}\{P_1^{se}\}$	$0.40P_s$	$0.48P_s$	$0.54P_s$	$0.59P_s$
$\mathrm{E}\{P_2^{se}\}$	$0.60P_s$	$0.52P_s$	$0.46P_s$	$0.41P_s$

Table 4.2 presents the averaged joint optimal set $\left\{\mathrm{E}\{x_r^{se}\}, \mathrm{E}\{y_r^{se}\}, \mathrm{E}\{P_1^{se}\}, \mathrm{E}\{P_2^{se}\}\right\}$ with various values of d_{SD} for the along-torso scenario and the around-torso scenario, respectively. It is shown that the simulation results match the theoretical derivation in Section 4.3.2. The optimal relay is always located on the negative x-axis for both scenarios and we can see that the averaged optimal relay location is very close to the point P in the around-torso scenario. With $P_1^{se} + P_2^{se} = P_s$, it is evident that the optimal SE based scheme always uses the maximum power for capacity maximization. For the along-torso scenario, we can see that the optimal power allocation ratio $\frac{P_1^{ee}}{P_2^{ee}}$ is invariant with different d_{SD}. This is due to the fact that, since in the along-torso scenario, all signals are transmitted over the along-torso channels, the optimal relay location relative to S and D is unchanged when d_{SD} varies. Thus $\frac{P_1^{se}}{P_2^{se}}$ does not vary. As opposed to the along-torso scenario, $\frac{P_1^{se}}{P_2^{se}}$ varies with d_{SD} in the around-torso scenario. This can be explained by the fact that signals are transmitted over the along-torso channel only for the S-R link and over the around-torso channels for the other two links. The change of d_{SD} has an impact

on the optimal relay location relative to S and D and therefore $\frac{P_1^{se}}{P_2^{se}}$. Moreover, with a fixed d_r and larger d_{SD}, it can be observed that more power is allocated to S to make sure that the maximum SE can be achieved in the around-torso scenario.

Effect of Body Motion

As mentioned in Section 4.2.2, the shadowing for on-body transmissions results from the body motion and a walking motion only produces measurable fluctuations in the around-torso scenario. Thus, we only study the impact of the body motion on the proposed scheme in the around-torso scenario.

Table 4.3 shows $\left\{\mathrm{E}\{x_r^{se}\}, \mathrm{E}\{y_r^{se}\}, \mathrm{E}\{P_1^{se}\}, \mathrm{E}\{P_2^{se}\}\right\}$ in the around-torso scenario without body motion when $d_r = 0.2$m. By comparing the optimal RL and PA in Table 4.2 and Table 4.3, we can observe the impact of shadowing due to the body motion on the proposed scheme and it is clear that the proposed scheme is able to adjust the optimal RL and PA readily when external circumstances vary. To overcome the shadow fading, the optimal RL in the proposed scheme moves towards point S slightly and accordingly more power is allocated to R. In this manner, γ_{SR} and γ_{RD} are balanced adaptably under the condition that the body motion is present, and thus SE is optimized in this circumstance.

Table 4.3: Averaged optimal set $\left\{\mathrm{E}\{x_r^{se}\}, \mathrm{E}\{y_r^{se}\}, \mathrm{E}\{P_1^{se}\}, \mathrm{E}\{P_2^{se}\}\right\}$ in the around-torso scenario without body motion

$d_r = 0.2$m				
d_{SD}	0.5m	0.6m	0.7m	0.8m
$\mathrm{E}\{x_r^{se}\}$	-0.42	-0.52	-0.62	-0.72
$\mathrm{E}\{y_r^{se}\}$	0	0	0	0
$\mathrm{E}\{P_1^{se}\}$	$0.42P_s$	$0.50P_s$	$0.56P_s$	$0.61P_s$
$\mathrm{E}\{P_2^{se}\}$	$0.58P_s$	$0.50P_s$	$0.44P_s$	$0.39P_s$

In Fig. 4.3, the SE performance of the proposed scheme with and without body motion in the around-torso scenario is illustrated. Undoubtedly, the case without considering the

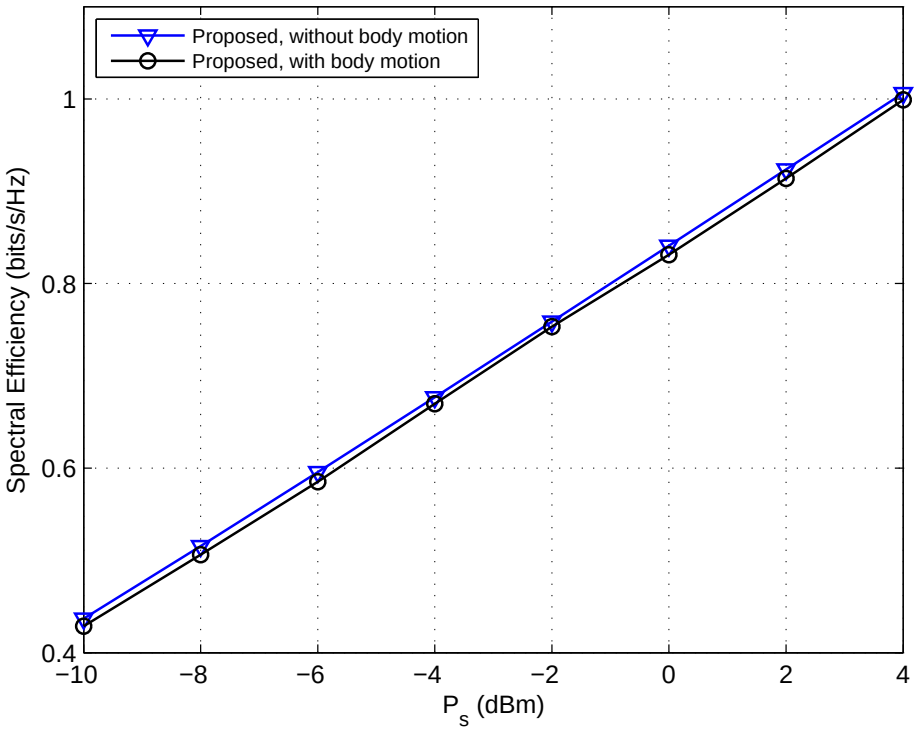

Figure 4.3: SE performance of the proposed scheme with and without body motion in the around-torso scenario when $d_{SD} = 0.6$m and $d_r = 0.2$m.

body motion is ideal since the shadow fading is neglected and thus the optimal SE in this case can be treated as an up-bound that can be achieved by the proposed scheme. Evidently, the proposed scheme can achieve a close to up-bound performance when the shadowing is considered, which means that the proposed scheme is capable of overcoming the effect of the shadowing by adjusting its optimal RL and PA adaptably, as shown in Table 4.3.

In the following, with the features of the optimal RL and PA presented in Table 4.2 and Table 4.3, some intended comparisons are also made in the around-torso scenario to further verify the effectiveness of our proposed scheme.

Spectral Efficiency Performance Comparison

In Fig. 4.4, the average SE is compared between direct transmission and the proposed scheme in the along-torso scenario ($d_r = 0$). As shown in this figure, direct transmission is much more spectral efficient than the proposed scheme and the performance gap between the two schemes increases significantly as P_s increases. This is because when a line-of-sight (LoS) between S and D is present in UWB based WBANs, the path loss exponent is small and a high SNR can be achieved by direct transmission. However, the pre-log factor $\frac{1}{2}$ in (4.13) causes a substantial loss for cooperative transmission in SE in this case and this loss is especially more significant in the higher SNR regime. Thus, we can see that the proposed scheme is not beneficial to the spectral efficiency in the along-torso scenario. In other words, when the source and destination are on the same side of the human body, the source prefers to transmit its signals to the destination directly.

Fig. 4.5 depicts the average SE versus P_s with $d_{SD} = 0.6$m and $d_r = 0.2$m in the around-torso scenario. To evaluate the performance of the proposed scheme, comparisons are made with: 1) the optimal PA scheme at point P, 2) the optimal PA scheme at point T, 3) selection amplify-and-forward (S-AF) scheme [73], and 4) direct transmission. In the optimal PA schemes at points P and T, the optimal P_1 and P_2 are exploited to maximize SE when R is fixed at points P and T, respectively. In the S-AF scheme, we assume that 6 relays are randomly located in the circle defined in C1 and each relay has the same power as S, i.e., $\frac{P_s}{2}$. The relay that can achieve the maximum SE is selected. From this figure, it can be observed that the proposed scheme can achieve the best SE among all the schemes and all the cooperative transmission schemes outperform direct transmission. Moreover, SE with the optimal PA at P is very close to the optimum in the proposed scheme, which indicates that the location of P is a good choice to place the relay node in this case. Compared to direct transmission, we can see that the proposed scheme can provide a remarkable performance improvement and up to 17 times improvement can be

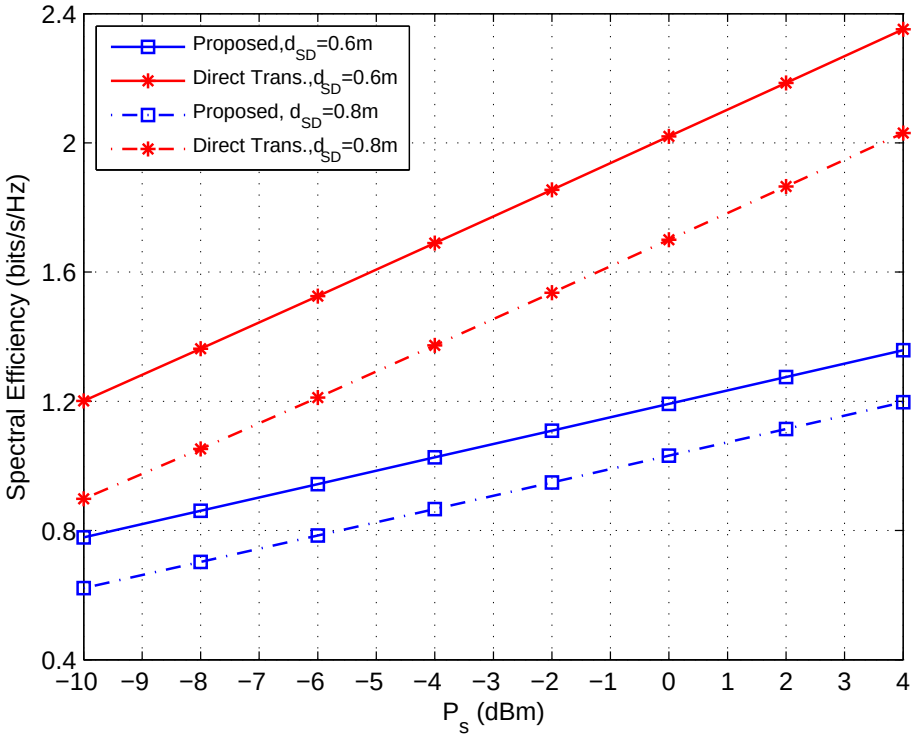

Figure 4.4: Average SE versus P_s for the along-torso scenario.

achieved when the battery of the sensor node is very limited (e.g., $P_s \leq -8$dBm). From the perspective of power consumption, we notice that the transmit power at S by using the proposed scheme can be much less (more than 14dB) compared to that by direct transmission when the same SE is achieved. This evidence indicates that the lifetime of the sensor node can be prolonged considerably with the assistance of the relay, which demonstrates that the proposed scheme is an effective way to enhance SE and prolong the lifetime of the sensor node.

Fig. 4.6 illustrates the average SE versus d_{SD} with different d_r and fixed $P_s = 4$dBm in the around-torso scenario. Comparisons are made with: 1) the optimal PA scheme at point P, 2) the equal PA scheme at point T, 3) S-AF scheme, and 4) direct transmission. Similar to Fig. 4.5, it is shown that the the proposed scheme is the most spectral efficient

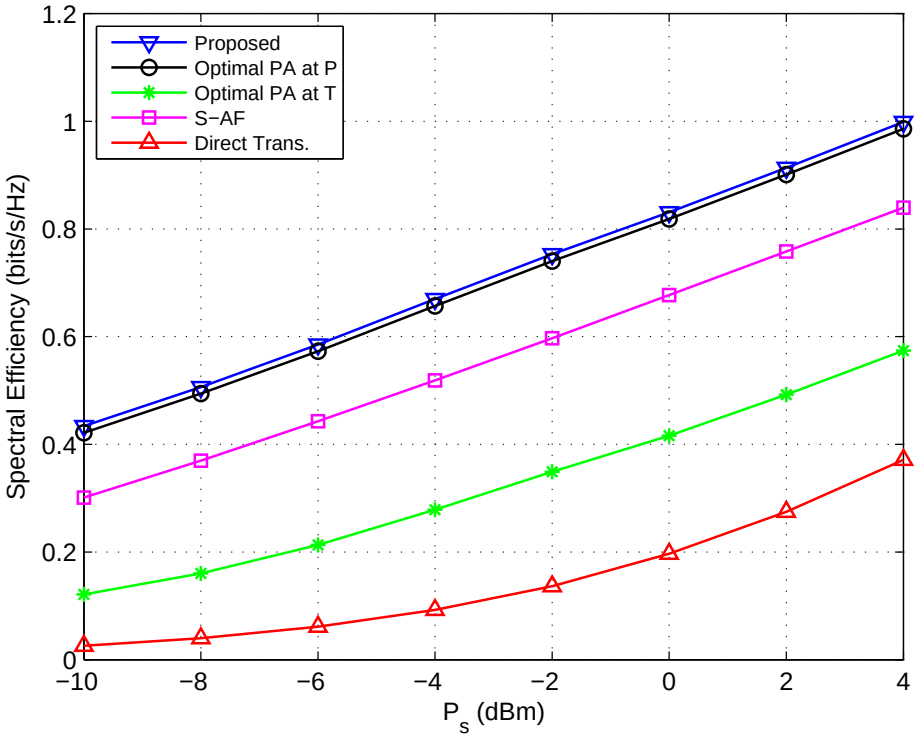

Figure 4.5: Average SE versus P_s in the around-torso scenario when $d_{SD} = 0.6$m and $d_r = 0.2$m.

among all the schemes. We also notice that direct transmission is very sensitive to d_{SD}. That is to say, without the LoS between S and D, the significant propagation loss in the around-torso scenario would affect the performance of direct transmission adversely. In contrast, the proposed scheme exhibits a weak dependence upon d_{SD}, which reveals that the proposed scheme can extend the transmission range effectively in the around-torso scenario.

4.4.2 Spectral Efficiency Evaluation for In-Body Transmissions

In this part, the SE performance of the proposed scheme in the in-body scenario is evaluated. Similar to the on-body transmissions, we firstly present the corresponding optimal RL and PA for in-body transmissions. With the presented features of the optimal

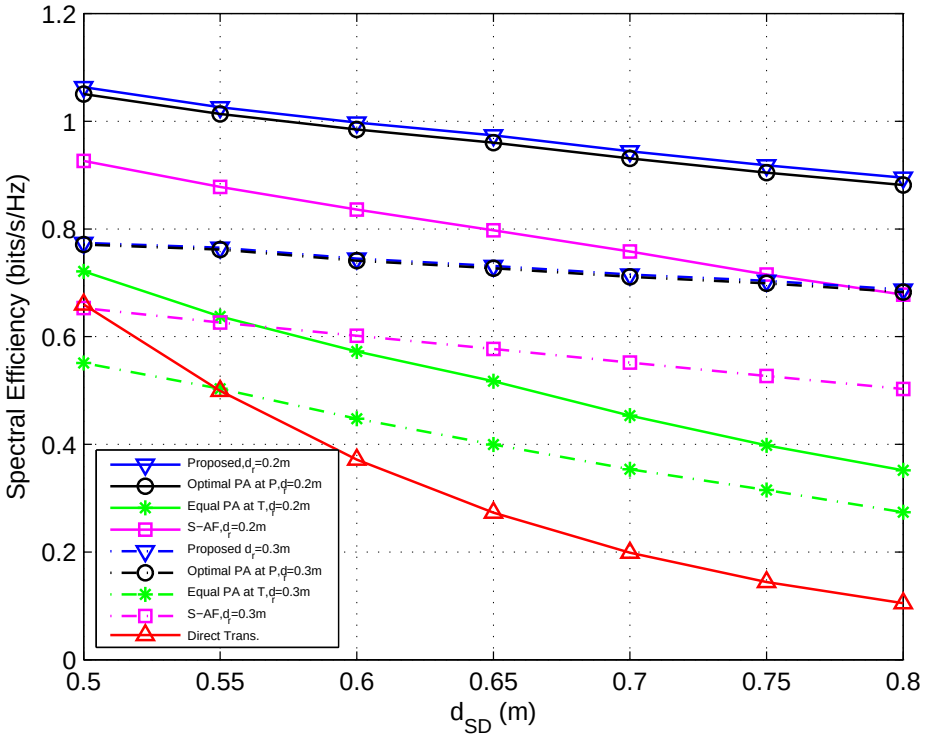

Figure 4.6: Average SE versus d_{SD} in the around-torso scenario with different d_r and $P_s = 4$dBm.

RL and PA, some intended comparisons are then made to verify the effectiveness of the proposed scheme in the in-body scenario. Note that, the shadowing for in-body transmissions results from scattering inside the human body. In practice, the scattering inside the human body is not avoidable in WBANs. Thus, there is no need to study the effect of the scattering inside the human body on the proposed scheme separately.

Analysis of Optimal Relay location and Power Allocation

Table 4.4 shows the averaged joint optimal set $\left\{\mathrm{E}\{x_r^{se}\}, \mathrm{E}\{y_r^{se}\}, \mathrm{E}\{P_1^{se}\}, \mathrm{E}\{P_2^{se}\}\right\}$ with various values of P_s for the in-body scenario. Since the on-body transmit power P_2 cannot exceed the FCC PSD limit, i.e., P_{max}^o, we can see that P_2^{se} is limited to be equal to P_{max}^o in the high total transmit power regimes, i.e., $P_s \geq 6$dBm. This result indicates that the SE

Table 4.4: Averaged optimal set $\left\{\mathrm{E}\{x_r^{se}\}, \mathrm{E}\{y_r^{se}\}, \mathrm{E}\{P_1^{se}\}, \mathrm{E}\{P_2^{se}\}\right\}$ for in-body transmissions

In-body scenario with $d_r = 5$cm and $d_{SD} = 0.2$m						
P_s	-10dBm	-6dBm	-2dBm	2dBm	6dBm	10dBm
$\mathrm{E}\{x_r^{se}\}$	0.033	0.033	0.033	0.033	0.038	0.055
$\mathrm{E}\{y_r^{se}\}$	0	0	0	0	0	0
$\mathrm{E}\{P_1^{se}\}$	$0.28P_s$	$0.28P_s$	$0.28P_s$	$0.28P_s$	$P_s - P_{max}^o$	$P_s - P_{max}^o$
$\mathrm{E}\{P_2^{se}\}$	$0.72P_s$	$0.72P_s$	$0.72P_s$	$0.72P_s$	P_{max}^o	P_{max}^o
In-body scenario with $d_r = 5$cm and $d_{SD} = 0.3$m						
P_s	-10dBm	-6dBm	-2dBm	2dBm	6dBm	10dBm
$\mathrm{E}\{x_r^{se}\}$	0.038	0.038	0.038	0.038	0.050	0.67
$\mathrm{E}\{y_r^{se}\}$	0	0	0	0	0	0
$\mathrm{E}\{P_1^{se}\}$	$0.18P_s$	$0.18P_s$	$0.18P_s$	$0.18P_s$	$P_s - P_{max}^o$	$P_s - P_{max}^o$
$\mathrm{E}\{P_2^{se}\}$	$0.82P_s$	$0.82P_s$	$0.82P_s$	$0.82P_s$	P_{max}^o	P_{max}^o

of the proposed scheme may increase gradually over the high total transmit power regimes since P_2^{se} is constrained by the transmit power allowance P_{max}^o and P_2^{se} plays a critical role on the SE performance considering the *R-D* link transmission takes the advantage of experiencing a much lower path loss compared to the *S-R* link in the in-body scenario. Moreover, with the optimal PA in the proposed scheme, it turns out that S only needs to transmit a small amount of P_s in the low-to-moderate regimes so that the optimal SE can be achieved. This evidence reveals that the proposed scheme can transfer the most power consumption from the implant node to the on-body relay. In this way, the lifetime of the implant node can be prolonged, which is very beneficial to the implant node considering its battery cannot be easily replaced.

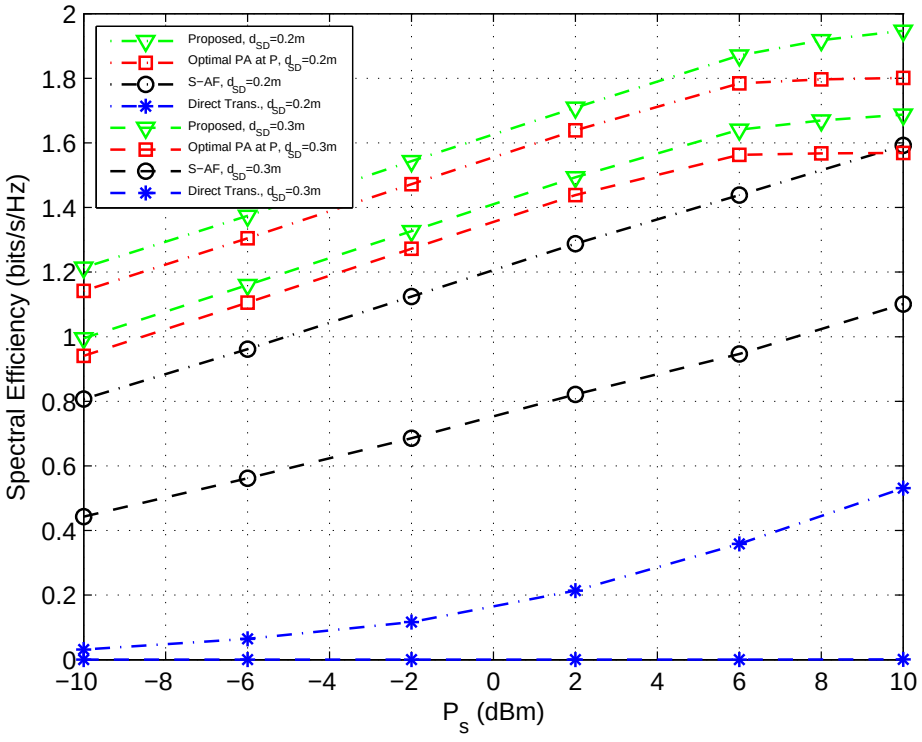

Figure 4.7: Average SE versus P_s for the in-body scenario with different d_{SD} and d_r = 5cm.

Spectral Efficiency Performance Comparison

Fig. 4.7 presents the average SE versus P_s with different d_{SD} and fixed $d_r = 5$cm in the in-body scenario. As expected, we can see that the proposed scheme can provide a significant improvement in term of SE compared to direct transmission. Moreover, it can be noticed that the SE of the proposed scheme ascends in a gradual way and the SE with optimal PA at point P approaches a constant over the high total transmit power regimes. This result verifies the accuracy of our analysis based on Table 4.4 well. In addition, it is observed that the SE of direct transmission deteriorates drastically when $d_{SD} = 0.3$m, which indicates that direct transmission cannot provide a satisfactory transmission performance in this scenario due to the severe propagation conditions within the human body. Thus, the deployment of a relay node is essential for in-body transmissions.

In conclusion, direct transmission may not be able to provide an acceptable transmission performance in UWB based WBANs except in the along-torso scenario. In contrast, the proposed scheme is an effective approach for the spectral-efficient transmission, particularly in the around-torso and in-body scenarios. By utilizing an on-body relay node with the joint optimal RL and PA, the proposed scheme can achieve a better performance in terms of SE than other transmission schemes. It is also shown that the proposed scheme is capable of overcoming the effect of the shadowing and achieving a SE performance close to that without considering the shadowing. Furthermore, with the joint optimal RL and PA scheme, the transmission range in WBANs can be extended effectively and the power consumption can be transferred from the sensor node to the relay node, in which the lifetime of the sensor node can be prolonged significantly compared to direct transmission.

4.5 Summary

In UWB based WBANs, ultra-low power transmissions with strong propagation blockage around or inside the human body may lead to unsatisfactory spectral efficiency. Hence, enhancing spectral efficiency is a major task in UWB based WBANs that needs to be tackled.

In this Chapter, we consider using relay networks to enhance spectral efficiency performance and extend coverage in UWB based WBANs, where an on-body wearable relay is employed to assist a WBAN node in communicating with a WBAN coordinator. The basic idea of this work is to exploit the optimal relay location along with the optimal power allocation for the spectral efficiency optimization in UWB based WBANs. Defined in the IEEE 802.15.6 standard, three practical transmission scenarios in WBANs were taken into account, namely, the along-torso scenario, the around-torso scenario and the

in-body scenario. Each scenario refers to the different relative physical locations between source and destination nodes. In each scenario, realistic wireless propagation channel models are adapted to provide a comprehensive and accurate analysis.

Specifically, the relay-location based network models for on-body transmissions and in-body transmissions are firstly developed, respectively. Due to the similarity in structure, the along-torso scenario can be treated as a special case in the around-torso scenario. We therefore only detail the solution of the spectral efficiency optimization problem in the around-torso scenario and in-body scenario. For each scenario, the relationship between the relay location and link distances is then setup based on the proposed network model. Accordingly, the spectral efficiency optimization problem in terms of relay location and power allocation is mathematically formulated. Considering the realistic power constraints, we prove that globally optimal solutions exist for each optimization problem and provide the derived closed-form expressions. Numerical results show the necessity of utilization of a relay node for the spectral-efficient transmission in UWB based WBANs and demonstrate the effectiveness of the proposed scheme in particular for the around-torso and in-body scenarios. With the joint optimal relay location and power allocation, the proposed scheme is capable of overcoming the effect of shadowing. Moreover, it is able to prolong the lifetime of a sensor node and extend the transmission range in WBANs significantly compared to direct transmission. In practice, the proposed scheme can be considered as a source of inspiration for the relay selection in WBANs, which provides an insight into the spectral-efficient design of WBANs with respect to selection of the proper placement of the wearable relay node along with the optimal transmit power level. The related research work in this Chapter is published in IEEE WCNC 2014 and EURASIP Journal on Wireless Communications and Networking 2015.

In the next Chapter, the objective of achieving optimal energy efficiency in single-relay UWB based WBANs will be further investigated, where algorithm for the optimal

solutions is proposed.

Chapter 5

Energy Efficiency Optimization in Single-Relay UWB based WBANs

5.1 Introduction

Besides spectral efficiency, energy efficiency is also an important metric in UWB based WBANs. In this Chapter, the energy efficiency optimization in terms of relay location and power allocation is investigated in single-relay UWB based WBANs. As mentioned in Section 2.4.3, considerable related research has focused on the intelligent MAC protocol design (i.e., by turning off the radio whenever data transmission and receiving are not expected) or transmission power control to enhance energy efficiency. Yet, the influence of relay location has been rarely studied from an energy efficiency point of view in UWB based WBANs. Thus, similar to the spectral efficiency optimization in Chapter 4, a truly joint optimization scheme for the energy efficiency optimization problem is proposed, in which relay location and power allocation are optimized jointly.

Since system scenarios and channel models are assumed as exactly the same as those in Chapter 4, they are not repeated in this Chapter. Without loss of generality, on-body transmissions and in-body transmissions in WBANs are also both considered in this work.

The relay-location based network models developed in Section 4.3 are adapted to setup the energy efficiency optimization formulations mathematically. Based on the formulations, the energy efficiency optimization problem can be categorized into a nonlinear concave fractional programming problem. To solve this problem, an iterative algorithm known as the Dinkelbach method is proposed. As demonstrated by simulations, relay location also has a notable impact on energy efficiency. With the joint optimal relay location and power allocation, the proposed scheme outperforms other single-relay transmission schemes. Moreover, up to 30 times improvement on energy efficiency can be achieved compared to direct transmission in particular for the around-torso scenario and in-body scenario when the battery of the sensor node is very limited, which indicates that the proposed scheme is able to prolong the network lifetime in WBANs significantly.

The Chapter is organized as follows. In Section 5.2, the energy efficiency optimization problems for on-body transmissions and in-body transmissions are formulated and solved, respectively. Simulation results are illustrated in Section 5.3. A summary is given in Section 5.4.

5.2 Energy Efficiency Optimization

In this section, the analysis of the EE optimization in single-relay UWB based WBANs is detailed. To solve the EE optimization problem effectively, an iterative algorithm is proposed to guarantee that the optimal EE for each scenario can be achieved. With the proposed algorithm, closed-form expressions of the optimal RL and PA are derived accordingly.

5.2.1 Energy Efficiency Optimization for On-Body Transmissions

Problem Formulation

In this part, the EE optimization for on-body transmissions in UWB based WBANs is studied, where the around-torso scenario and along-torso scenario are taken into account. As presented in Section 4.3.2, the along-torso scenario is treated as a special case in the around-torso scenario. We therefore only detail the solution of the energy efficiency optimization problem in the around-torso scenario in this section.

In this thesis, we define the EE as the ratio of SE over the total power dissipation [unit:bits/Joule/Hz] [110]. Based on the SE formulation in Section 4.3.2, the SE expression in the around-torso scenario can be written as

$$SE_{SRD}(x_r, y_r, P_1, P_2) = \frac{1}{2N_f}\log_2\left(1+\underbrace{\frac{N_f P_1 \xi_{SD}}{PL_{SD}(d_{SD})\sigma_n^2}}_{\gamma_1(P_1)} + \underbrace{\frac{1}{\frac{PL_{SR}(d_{SR}(x_r,y_r))\sigma_n^2}{N_f P_1 \xi_{SR}} + \frac{PL_{RD}(d_{RD}(x_r,y_r))\sigma_n^2}{N_f P_2 \xi_{RD}}}}_{\gamma_2(x_r,y_r,P_1,P_2)}\right), \tag{5.1}$$

where

$$PL_{SD}(d_{SD}) = 10^{PL_1^{dB}(d_{SD})/10} = M_1 d_{SD}^{n_1},$$

$$PL_{SR}(d_{SR}) = 10^{PL_0^{dB}(d_{SR})/10} = M_0 d_{SR}^{n_0},$$

and

$$PL_{RD}(d_{RD}) = 10^{PL_1^{dB}(d_{RD})/10} = M_1 d_{RD}^{n_1}.$$

On the other hand, the average power dissipation per frame in cooperative transmission can be written as

$$P_{SRD} = \frac{1}{2}\big(\varepsilon(P_1+P_2) + 2P_{ct} + 3P_{cr}\big), \tag{5.2}$$

where ε is a constant which accounts for the inefficiency of the power amplifier. P_{ct} is the power dissipation for transmitter circuit per frame and P_{cr} is the power dissipation for receiver circuit per frame.

Using (5.1) and (5.2), the EE of cooperative transmission in the around-torso scenario can be given by

$$EE_{SRD} = \frac{SE_{SRD}}{P_{SRD}} = \frac{\log_2\left(1+\gamma_1(P_1)+\gamma_2(x_r,y_r,P_1,P_2)\right)}{N_f\left(\varepsilon(P_1+P_2)+2P_{ct}+3P_{cr}\right)}. \tag{5.3}$$

Obviously, EE_{SRD} is the function of variables $\{x_r, y_r, P_1, P_2\}$. To obtain the maximum EE_{SRD} for cooperative transmission, we must find the optimal set $\{x_r^{ee}, y_r^{ee}, P_1^{ee}, P_2^{ee}\}$ that makes $EE_{SRD}(x_r, y_r, P_1, P_2)$ achieve its maximum. Thus, the joint optimal RL and PA problem for the energy efficiency optimization in the around-torso scenario can be mathematically formulated as

$$\begin{aligned} \underset{x_r,y_r,P_1,P_2}{\text{maximize}} \quad & EE_{SRD}(x_r,y_r,P_1,P_2) \\ \text{subject to} \quad & \text{C1}: \left(x_r+\frac{d_{SD}\sin\theta}{2}\right)^2+y_r^2 \le \left(\frac{d_{SD}\sin\theta}{2}\right)^2, \\ & \text{C2}: x_r \le \epsilon, \\ & \text{C3}: P_1+P_2 \le P_s. \end{aligned} \tag{5.4}$$

Joint Optimal Relay Location and Power Allocation

As we can see, the EE optimization problem in (5.4) is a nonlinear concave fractional programming problem [111]. Thus, we introduce the following Theorem.

Theorem 5.1. *The joint optimal relay location and power allocation* $\{x_r^{ee}, y_r^{ee}, P_1^{ee}, P_2^{ee}\}$ *achieves the maximum energy efficiency* EE_{max} *if and only if*

$$\begin{aligned} &\max_{x_r,y_r,P_1,P_2} SE_{SRD}(x_r,y_r,P_1,P_2) - EE_{max}P_{SRD}(P_1,P_2) \\ =&SE_{SRD}(x_r^{ee},y_r^{ee},P_1^{ee},P_2^{ee}) - EE_{max}P_{SRD}(P_1^{ee},P_2^{ee}) = 0 \end{aligned}$$

Proof. Proof of Forward Implication:

With $\{x_r^{ee}, y_r^{ee}, P_1^{ee}, P_2^{ee}\}$ and EE_{max}, we have

$$\begin{aligned} EE_{max} &= \frac{SE_{SRD}(x_r^{ee}, y_r^{ee}, P_1^{ee}, P_2^{ee})}{P_{SRD}(P_1^{ee}, P_2^{ee})} \geq \frac{SE_{SRD}(x_r, y_r, P_1, P_2)}{P_{SRD}(P_1, P_2)}. \\ \Longrightarrow\ & SE_{SRD}(x_r, y_r, P_1, P_2) - EE_{max} P_{SRD}(P_1, P_2) \leq 0, \\ & SE_{SRD}(x_r^{ee}, y_r^{ee}, P_1^{ee}, P_2^{ee}) = EE_{max} P_{SRD}(P_1^{ee}, P_2^{ee}). \end{aligned}$$

Therefore, we can see that

$$\max_{x_r, y_r, P_1, P_2} SE_{SRD}(x_r, y_r, P_1, P_2) - EE_{max} P_{SRD}(P_1, P_2) = 0,$$

and $\{x_r^{ee}, y_r^{ee}, P_1^{ee}, P_2^{ee}\}$ is the corresponding optimal solution for achieving the maximum.

Proof of Reverse Implication:

Suppose that $\{x_r^*, y_r^*, P_1^*, P_2^*\}$ is the optimal solution that makes $SE_{SRD}(x_r^*, y_r^*, P_1^*, P_2^*) - EE_{max} P_{SRD}(P_1^*, P_2^*) = 0$. Then, we have

$$\begin{aligned} & SE_{SRD}(x_r, y_r, P_1, P_2) - EE_{max} P_{SRD}(P_1, P_2) \\ \leq\ & SE_{SRD}(x_r^*, y_r^*, P_1^*, P_2^*) - EE_{max} P_{SRD}(P_1^*, P_2^*) = 0, \end{aligned}$$

which implies that

$$\begin{aligned} & \frac{SE_{SRD}(x_r, y_r, P_1, P_2)}{P_{SRD}(P_1, P_2)} \leq \frac{SE_{SRD}(x_r^*, y_r^*, P_1^*, P_2^*)}{P_{SRD}(P_1^*, P_2^*)} \\ \text{and } & \frac{SE_{SRD}(x_r^*, y_r^*, P_1^*, P_2^*)}{P_{SRD}(P_1^*, P_2^*)} = EE_{max}. \end{aligned}$$

Thus, it proves that $\{x_r^*, y_r^*, P_1^*, P_2^*\}$ is also the optimal solution for the original EE optimization problem. □

Based on Theorem 5.1, for the considered nonlinear fractional programming problem in (5.4), there exists an equivalent problem with an objective function in a subtractive form, e.g., $SE_{SRD}(x_r, y_r, P_1, P_2) - EE_{max} P_{SRD}(P_1, P_2)$, which has the same optimal solution. Therefore, with the transformed problem, an iterative algorithm known as the Dinkelbach method can be proposed for solving the EE optimization problem in (5.4) equivalently,

which guarantees the convergence to EE_{max} [112]. Table 5.1 summarizes the proposed iterative algorithm. In each iteration, the problem in (5.5) with a given q has to be solved.

$$\begin{aligned} &\underset{x_r,y_r,P_1,P_2}{\text{maximize}} \quad SE_{SRD}(x_r,y_r,P_1,P_2) - qP_{SRD}(P_1,P_2) \\ &\text{subject to} \quad \text{C1, C2, C3.} \end{aligned} \tag{5.5}$$

Table 5.1: The proposed iterative algorithm

Initialization:

1) Set the maximum number of iterations L_{max} and maximum error tolerance η.

2) Set the iterative index $k = 0$ and the initial value $q^{\{k=0\}} = 0$.

Iterations:

WHILE $k \leq L_{max}$

Solve the optimization problem in (4.38) with the updated q^k and denote the corresponding optimal solution $\{x_r^k, y_r^k, P_1^k, P_2^k\}$;

IF $SE_{SRD}(x_r^k, y_r^k, P_1^k, P_2^k) - q^k P_{SRD}(P_1^k, P_2^k) < \eta$ **THEN**

BREAK;

ELSE

Set $q^{k+1} = \frac{SE_{SRD}(x_r^k, y_r^k, P_1^k, P_2^k)}{P_{SRD}(P_1^k, P_2^k)}$ and $k = k + 1$;

END IF

END WHILE

Output:

RETURN $\{x_r^{ee}, y_r^{ee}, P_1^{ee}, P_2^{ee}\} = \{x_r^k, y_r^k, P_1^k, P_2^k\}$ and $EE_{max} = \frac{SE_{SRD}(x_r^k, y_r^k, P_1^k, P_2^k)}{P_{SRD}(P_1^k, P_2^k)}$.

Since the problem in (5.5) is a strictly quasi-concave optimization problem, we can solve it by using the Lagrange multiplier method with the KKT conditions. The La-

grangian of (5.5) can be given by

$$\begin{aligned}
&\mathcal{L}(x_r, y_r, P_1, P_2, \mu_1, \mu_2, \mu_3) \\
=&SE_{SRD}(x_r, y_r, P_1, P_2) - qP_{SRD}(P_1, P_2) - \mu_1(P_1 + P_2 - P_s) \\
&- \mu_2 \left(\left(x_r + \frac{d_{SD}\sin\theta}{2} \right)^2 + y_r^2 - \left(\frac{d_{SD}\sin\theta}{2} \right)^2 \right) - \mu_3(x_r - \epsilon),
\end{aligned} \tag{5.6}$$

where $\mu_1, \mu_2, \mu_3 \geq 0$ are the Lagrange multipliers connected to C1-C3.

We define $\{\tilde{x}_r, \tilde{y}_r, \tilde{P}_1, \tilde{P}_2\}$ as the solution of the problem (5.5). Considering the KKT conditions and taking the stationarity condition of each variable, we can prove that $\mu_2 = \mu_3 = 0$ and the solution $\{\tilde{x}_r, \tilde{y}_r, \tilde{P}_1, \tilde{P}_2\}$ meets (5.7)-(5.10) with a given q, e.g.,

$$\tilde{y}_r = 0, \tag{5.7}$$

$$\frac{\tilde{x}_r n_0 M_0 \tilde{P}_2 \xi_{RD}}{n_1 M_1 \tilde{P}_1 \xi_{SR}} A_1(\tilde{x}_r, 0) + (\tilde{x}_r + d_{SD}\sin\theta) A_2(\tilde{x}_r, 0) = 0, \tag{5.8}$$

$$A_3 + \frac{\xi_{SR}\xi_{RD} A_4(\tilde{x}_r, 0)\tilde{P}_2^2}{(\tilde{P}_2 A_4(\tilde{x}_r, 0) + \tilde{P}_1 A_5(\tilde{x}_r, 0))^2} = \frac{\xi_{SR}\xi_{RD} A_5(\tilde{x}_r, 0)\tilde{P}_1^2}{(\tilde{P}_2 A_4(\tilde{x}_r, 0) + \tilde{P}_1 A_5(\tilde{x}_r, 0))^2}, \tag{5.9}$$

and

$$\frac{\frac{1}{2\sigma_n^2} \frac{\xi_{SR}\xi_{RD} A_5(\tilde{x}_r,0)\tilde{P}_1^2}{(\tilde{P}_2 A_4(\tilde{x}_r,0) + \tilde{P}_1 A_5(\tilde{x}_r,0))^2}}{1 + \frac{N_f}{\sigma_n^2}\tilde{P}_1 A_3 + \frac{N_f}{\sigma_n^2} \frac{\xi_{SR}\xi_{RD}\tilde{P}_1\tilde{P}_2}{\tilde{P}_2 A_4(\tilde{x}_r,0) + \tilde{P}_1 A_5(\tilde{x}_r,0)}} = \ln(2)\left(\frac{\varepsilon q}{2} + \mu_1\right), \tag{5.10}$$

where $A_1(x_r, y_r) = (x_r^2 + y_r^2)^{\frac{n_0-2}{2}}$ and $A_2(x_r, y_r) = ((x_r + d_{SD}\sin\theta)^2 + y_r^2 + d_r^2)^{\frac{n_1-2}{2}}$. $A_3 = \frac{\xi_{SD}}{M_1 d_{SD}^{n_1}}$ is constant. $A_4(x_r, y_r) = \xi_{RD} M_0 (x_r^2 + y_r^2)^{\frac{n_0}{2}}$ and $A_5(x_r, y_r) = \xi_{SR} M_1 ((x_r + d_{SD}\sin\theta)^2 + y_r^2 + d_r^2)^{\frac{n_1}{2}}$.

Discussion

With (5.7)-(5.10), we can see that the optimal relay location is always located on the x-axis in the proposed model. Besides, it is revealed that the value of x_r^{ee} and $\alpha = P_1^{ee}/P_2^{ee}$

are determined by the given d_{SD} and d_r and they are independent of q and P_s. In (5.10), it is noted that whether the value of μ_1 is equal to 0 or not depends on the values of P_s and q. Based on the KKT conditions, $\tilde{P}_1 + \tilde{P}_2 < P_s$ when $\mu_1 = 0$ and $\tilde{P}_1 + \tilde{P}_2 = P_s$ when $\mu_1 > 0$.

For the along-torso scenario, the related problem can be also formulated and the corresponding joint optimal RL and PA can be achieved with the same iterative algorithm and a similar derivation.

Similar to the proposed SE optimization scheme in Section 4, the proposed EE optimization scheme can provide an insight into the energy-efficient design of WBANs with respect to the proper placement of the wearable relay node along with the optimal transmit power level.

5.2.2 Energy Efficiency Optimization for In-Body Transmissions

Similarly, the corresponding EE in the in-body scenario can be written as

$$EE_{SRD}(x_r, y_r, P_1, P_2) = \frac{SE_{SRD}(x_r, y_r, P_1, P_2)}{P_{SRD}(P_1, P_2)} \tag{5.11}$$

where

$$SE_{SRD}(x_r, y_r, P_1, P_2) = \frac{1}{2N_f} \log_2 \left(1 + \underbrace{\frac{N_f P_1 \xi_{SD}}{M_3 h 10^{M_4 d_{SD}^{n_2}} \sigma_n^2}}_{\gamma_1(P_1)} + \underbrace{\frac{1}{\frac{M_3 h 10^{M_4 d_{SR}^{n_2}(x_r, y_r)} \sigma_n^2}{N_f P_1 \xi_{SR}} + \frac{M_0 d_{RD}^{n_0}(x_r, y_r) \sigma_n^2}{N_f P_2 \xi_{RD}}}}_{\gamma_2(x_r, y_r, P_1, P_2)} \right).$$

Therefore, the EE optimization problem in the in-body scenario can be mathematically

formulated as

$$\begin{aligned} \underset{x_r,y_r,P_1,P_2}{\text{maximize}} \quad & EE_{SRD}(x_r, y_r, P_1, P_2) \\ \text{subject to} \quad & \text{C1} : x_r^2 + y_r^2 \leq (d_{SD}\sin\theta)^2, \\ & \text{C2} : x_r \leq d_{SD}\sin\theta + \hat{\delta}, \\ & \text{C3} : P_1 + P_2 \leq P_s, \\ & \text{C4} : P_2 \leq P_{max}^o. \end{aligned} \tag{5.12}$$

Since the problem in (5.12) is also a nonlinear concave fractional programming problem, the proposed iterative algorithm can be applied in this case. As the corresponding derivations for the optimal solution are similar to those in (5.4), we do not include them herein.

5.3 Simulation Results

To evaluate EE of the proposed scheme in UWB based WBANs, numerical simulations are conducted in this section. The simulations are also performed in MATLAB with Monte Carlo method. The MATLAB's optimization toolbox is used for solving the convex programming in the simulations. All the simulation results are averaged over 5000 channel realizations.

In the simulations, T_w and T_f are chosen to be 2ns and 150ns, respectively. N_f is set to be 4. The noise PSD is -174dBm/Hz and the system bandwidth is 500MHz. Since the average FCC PSD emission limit for UWB signals is -41.3dBm/MHz, the maximum average transmit power P_{ave} is -14.3dBm. With the duty cycle T_w/T_f, $P_{max}^o = P_{ave} * T_f/T_w = 4$dBm. In addition, ε is set to be 2. P_{ct} and P_{cr} are set to be 100μW and 150μW, respectively [107]. According to the scale of the human body, d_{SD} is very limited in UWB based WBANs. Without loss of generality, we consider the case that 0.5m$\leq d_{SD} \leq$ 0.8m

for on-body transmissions and 0.2m$\leq d_{SD} \leq$ 0.3m for in-body transmissions. At R and D, we assume that all of the dispersive energies are captured without considering the ISI.

5.3.1 Energy Efficiency Evaluation for On-Body Transmissions

Table 5.2: $\left\{\mathrm{E}\{x_r^{ee}\}, \mathrm{E}\{y_r^{ee}\}\right\}$ and $\alpha = \mathrm{E}\{P_1^{ee}/P_2^{ee}\}$ for both scenarios

Along-torso scenario ($d_r = 0$)				
d_{SD}	0.5m	0.6m	0.7m	0.8m
$\mathrm{E}\{x_r^{ee}\}$	-0.30	-0.36	-0.42	-0.48
$\mathrm{E}\{y_r^{ee}\}$	0	0	0	0
α	2.37	2.37	2.37	2.37
Around torso-scenario with $d_r = 0.2$m				
d_{SD}	0.5m	0.6m	0.7m	0.8m
$\mathrm{E}\{x_r^{ee}\}$	-0.41	-0.51	-0.61	-0.70
$\mathrm{E}\{y_r^{ee}\}$	0	0	0	0
α	0.74	1.02	1.32	1.64

Table 5.2 presents the averaged optimal relay location $\left\{\mathrm{E}\{x_r^{ee}\}, \mathrm{E}\{y_r^{ee}\}\right\}$ and power ratio $\alpha = \mathrm{E}\{P_1^{ee}/P_2^{ee}\}$ of the proposed scheme with various values of d_{SD} for both on-body scenarios. It is shown that the optimal relay is always located on the negative x-axis for both scenarios and it is very close to the point P in the around-torso scenario. For the along-torso scenario, we can see that the power ratio α is invariant with different d_{SD}. This is due to the fact that, since in the along-torso scenario, all signals are transmitted over the along torso channels, the optimal relay location relative to S and D is unchanged when d_{SD} varies. Thus α does not vary. Different from the along-torso scenario, α varies with d_{SD} in the around-torso scenario. This can be explained by the fact that signals are transmitted over the along-torso channel only for the S-R link and over the around-torso channels for the other two links. The change of d_{SD} has an impact on the optimal relay location relative to S and D and therefore α.

Fig. 5.1 depicts the average EE versus P_s in the around-torso scenario. Five transmis-

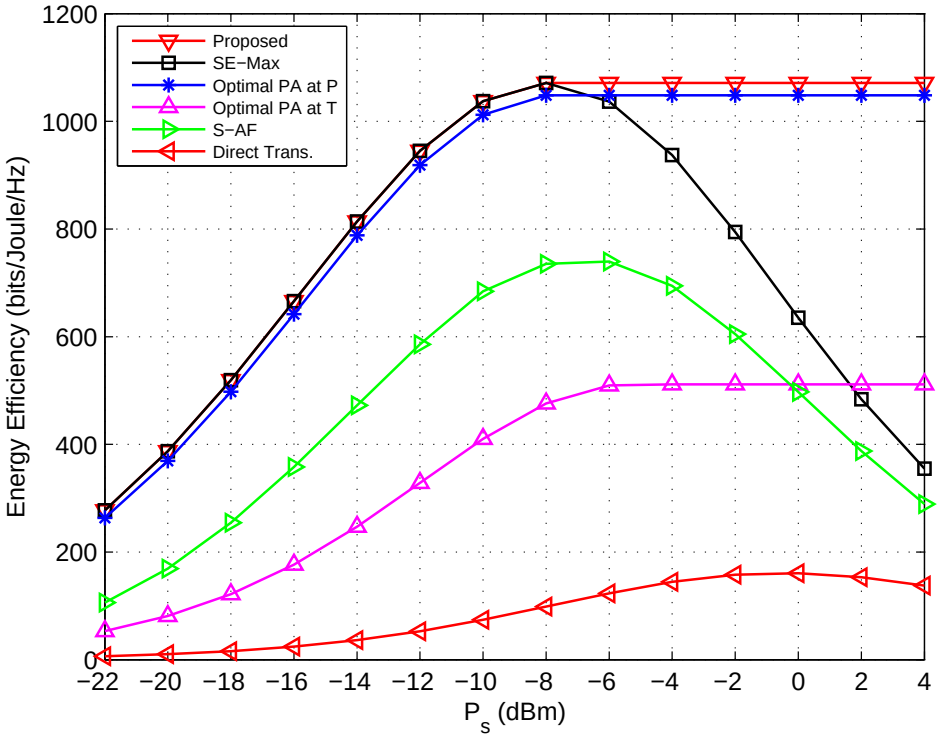

Figure 5.1: Average energy efficiency versus P_s in the around-torso scenario with $d_{SD} = 0.6$m and $d_r = 0.2$m.

sion schemes are illustrated in this figure to compare with the proposed joint optimal PA and RL scheme, which are the SE-maximizing (SE-Max) scheme, the optimal PA scheme at point P, the optimal PA scheme at point T, the S-AF scheme, and direct transmission, respectively. In the SE-Max scheme, SE with constraints C1-C3 is maximized. In the optimal PA schemes at points P and T, the optimal P_1 and P_2 are exploited to maximize EE when R is fixed at points P and T, respectively. In the S-AF scheme, we assume that 6 relays are randomly located in the circle defined in C1 and the relay that can achieve the maximum EE is selected. As shown in this figure, the proposed scheme outperforms all the other schemes. The optimal EE and SE can be achieved simultaneously by the proposed scheme when P_s is in the low-to-moderate regimes. As P_s increases in the moderate-to-high regimes, the energy efficiency of the SE-Max scheme decreases rapidly, which can

be explained by the fact that the SE-Max scheme always uses the maximum power for capacity maximization which is harmful for EE. Compared to direct transmission, we can see that the proposed scheme can provide a remarkable performance improvement and up to 30 times improvement can be achieved when the battery of the sensor node is very limited (e.g., $P_s \leq -20$dBm). This evidence indicates that the lifetime of WBANs can be prolonged considerably by using the proposed scheme. Furthermore, it is noticed that a large performance gap exists between the optimal PA schemes at points P and T and the EE of the optimal PA scheme at point P is very close to the optimum, which matches our analysis well in Table 5.2. Based on these observations, we can see that relay location is also an important factor for energy-efficient transmissions in WBANs and placing the relay close to P is a good option for achieving high EE.

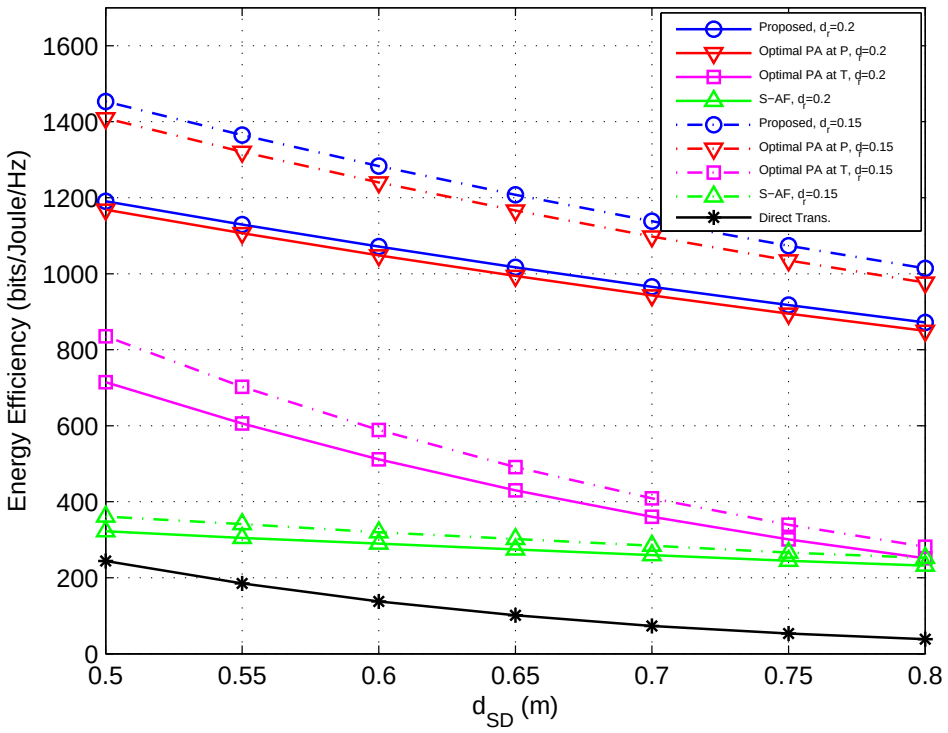

Figure 5.2: Average EE versus d_{SD} in the around-torso scenario with $P_s = 4$dBm.

Fig. 5.2 illustrates the average EE versus d_{SD} with fixed $P_s = 4$dBm in the around-torso scenario. Two cases with $d_r = 0.15$m and $d_r = 0.2$m are considered, respectively. It is shown that the EE of direct transmission is sensitive to d_{SD}. In contrast, the EE of the proposed scheme exhibits a weak dependence upon d_{SD}, which indicates that the proposed scheme can be an effective way for the extension of transmission range.

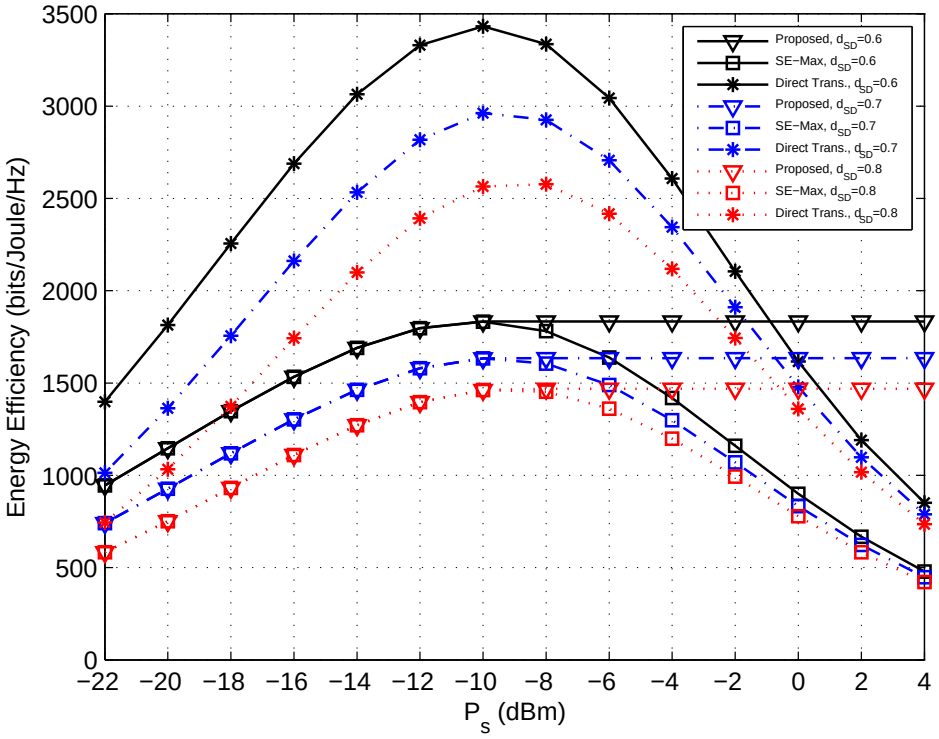

Figure 5.3: Energy efficiency versus P_s in the along-torso scenario.

In Fig. 5.3, the average EE versus P_s with different d_{SD} in the along-torso scenario ($d_r = 0$) is depicted. Different from the results in Fig. 5.1, direct transmission is more energy efficient than the proposed scheme when P_s is in the low-to-moderate regimes. This is because when a LoS between S and D is present, the path loss exponent is small, and thus the circuit power dissipation dominates the performance of EE. Since cooperative transmission costs more circuit power, it would not be of advantage in this case.

5.3.2 Energy Efficiency Evaluation for In-Body Transmissions

Table 5.3: Averaged optimal solution $\left\{\mathrm{E}\{x_r^{ee}\}, \mathrm{E}\{y_r^{ee}\}, \mathrm{E}\{P_1^{ee}\}, \mathrm{E}\{P_2^{ee}\}\right\}$

Parameters: $d_r = 5$cm and $d_{SD} = 0.3$m						
P_s	-14dBm	-10dBm	-6dBm	-2dBm	2dBm	6dBm
$\mathrm{E}\{x_r^{ee}\}$	0.038	0.038	0.038	0.038	0.038	0.038
$\mathrm{E}\{y_r^{ee}\}$	0	0	0	0	0	0
$\frac{\mathrm{E}\{P_1^{ee}\}}{P_s}$	0.1800	0.1800	0.0677	0.0269	0.0105	0.0042
$\frac{\mathrm{E}\{P_2^{ee}\}}{P_s}$	0.8200	0.8200	0.2926	0.1165	0.0464	0.0185

Table 5.3 shows the averaged optimal solution $\left\{\mathrm{E}\{x_r^{ee}\}, \mathrm{E}\{y_r^{ee}\}, \mathrm{E}\{P_1^{ee}\}, \mathrm{E}\{P_2^{ee}\}\right\}$ for the EE optimization when $d_r = 5$cm and $d_{SD} = 0.3$m. Similar to the results in the SE optimization, the optimal relay location for EE is always on the positive x-axis and the averaged optimal relay location is fixed for all the scenarios and close to P. Actually, the similarity of the optimal relay locations between SE and EE is based on the fact that the denominator in (5.11) is not related to $\{x_r, y_r\}$, consequently, the optimal EE and SE may share the same optimal relay location when P_s is in the low-to-moderate regimes. On the other hand, different from the results in the SE optimization, only a small amount of total power P_s is used for the optimal energy efficient transmission when $P_s \geq -10$dBm and P_1^{ee} and P_2^{ee} both remain unvaried as P_s increases, which provides the evidence that the system will get consistently saturated at the maximum EE after reaching it. Accordingly, the power allocated to S and R will remain unchanged as P_s varies.

In Fig. 5.4, the average EE versus P_s with $d_{SD} = 0.3$m and $d_r = 5$cm is illustrated. Undoubtedly, with the joint optimal relay location and power allocation, the proposed EE-maximizing scheme outperforms all the other schemes. Moreover, the EE of the proposed EE-maximizing scheme approaches a constant when P_s increases, which complies with the analysis in Table 5.3. By comparing the other schemes to the proposed EE-maximizing

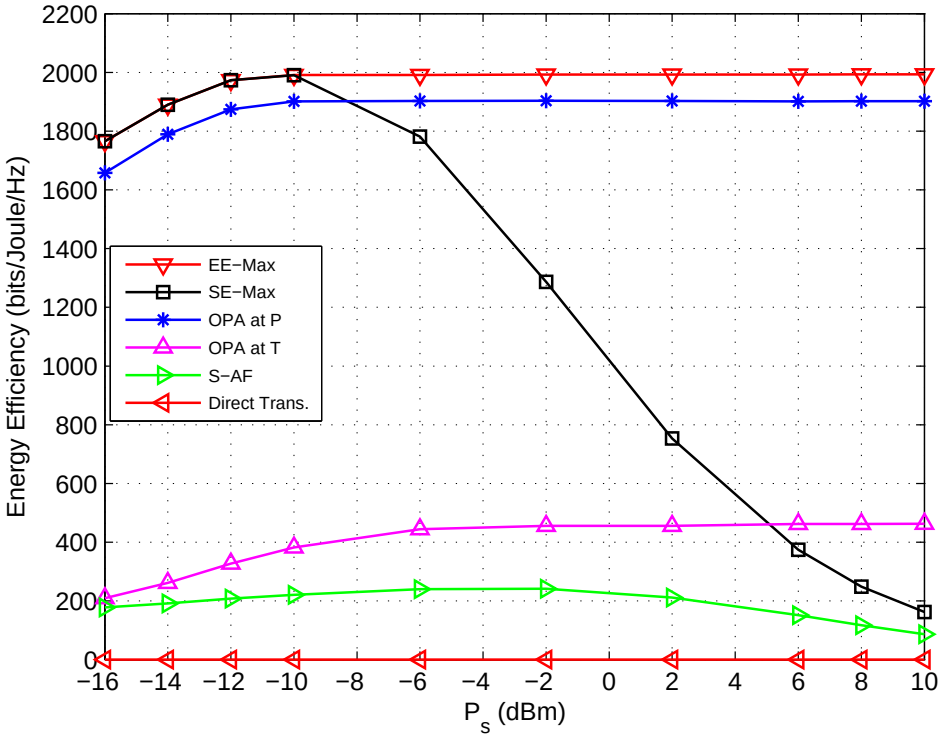

Figure 5.4: Average EE versus P_s in the in-body scenario with $d_{SD} = 0.3$m and $d_r = 5$cm.

scheme, the conclusion for the SE optimization can also be similarly reached for the EE optimization in this figure. Without the assistance of the relay, direct transmission is clearly impractical for energy efficient transmission in the in-body transmission scenario. Furthermore, we can see that the relay location also plays a critical role for the energy efficient transmission in the in-body scanrio. For the proposed SE-maximizing scheme, its EE coincides with the optimal EE when P_s is in the low regimes. As P_s increases, EE of the proposed SE-maximizing scheme decreases rapidly since the total transmit power is always fully used for capacity maximization which is detrimental to EE.

In Fig. 5.5, the average EE versus d_{SD} with $P_s = 10$dBm and $d_r = 5$cm is displayed. Similar to the results in Fig. 5.2, it is shown that the proposed EE-maximizing scheme also exhibits a weak dependence upon d_{SD} in the in-body scenario. Therefore, based on

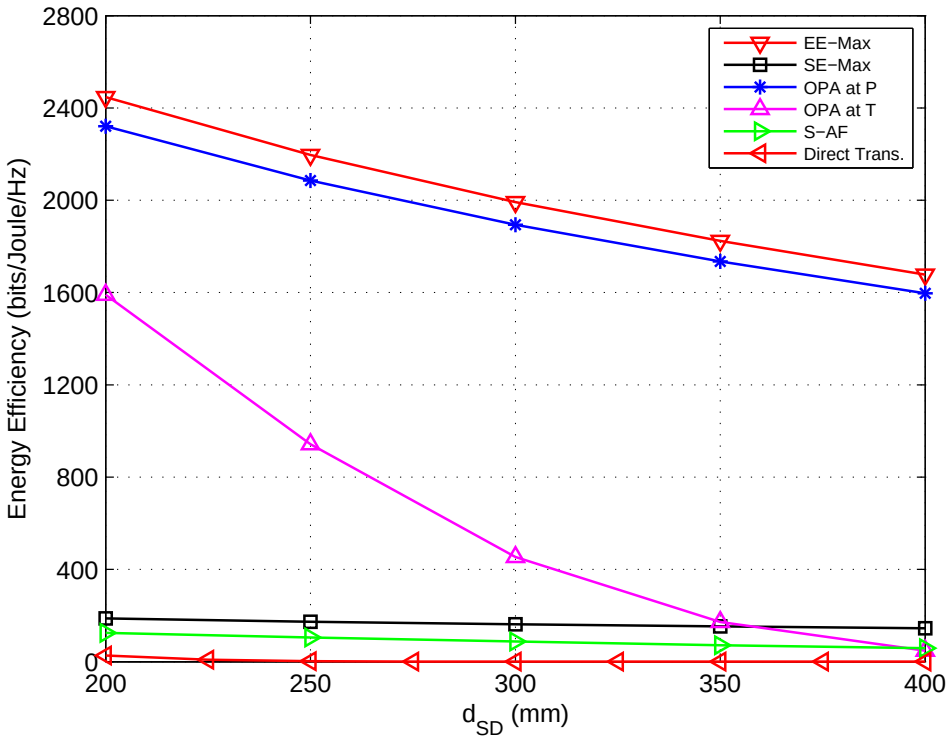

Figure 5.5: Average EE versus d_{SD} in the in-body scenario with $P_s = 10$dBm and $d_r = 5$cm.

the results in Fig. 5.2 and Fig. 5.5, it is demonstrated that the utilization of a single relay is very helpful to boost the energy-efficient transmission range in UWB based WBANs.

5.4 Summary

In this Chapter, we investigate energy efficiency of single-relay cooperative transmission in UWB based WBANs. Similar to the spectral efficiency optimization in the last Chapter, the joint optimal relay location and power allocation are derived and analyzed for the energy efficiency optimization. The related research work in this Chapter is published in IEEE ICC 2015.

Based on the observations in Section 5.3 along with the results in Section 4.4, it is

stated that the utilization of an on-body relay node is essential especially in the around-torso scenario and in-body scenario for the spectral and energy efficient transmission, and the impact of the relay location cannot be neglected. With the corresponding joint optimal relay location and power allocation, spectral efficiency and energy efficiency can be remarkably improved compared to direct transmission. Moreover, most of the power consumption can be transferred from the on-body/implant node to the on-body relay, which helps the node with lifetime increase.

Although the energy efficiency and spectral efficiency in UWB based WBANs are thoroughly studied in Chapter 4 and Chapter 5, it is noticed that the optimal energy efficiency and spectral efficiency coincide only when P_s is in low regimes. In fact, as shown in Fig. 5.1 and Fig. 5.4, the two metrics conflict in the moderate-to-high regimes of P_s, in which the optimal spectral efficiency leads to a comparably low energy efficiency and vice versa. As a result, balancing the performance between spectral efficiency and energy efficiency is important in UWB based WBANs. In the next Chapter, joint optimal energy efficiency and spectral efficiency is further investigated in single-relay UWB based WBANs.

Chapter 6

Joint Energy Efficiency and Spectral Efficiency Optimization in Single-Relay UWB based WBANs

6.1 Introduction

Although energy efficiency and spectral efficiency are two important metrics in UWB based WBANs, optimizing one metric may not result in the other one being optimized. As pointed out in Chapter 4 and Chapter 5, the optimal energy efficiency and spectral efficiency conflict when the battery resources of a node are in the moderate-to-high regimes. Thus, how to balance the tradeoff between energy efficiency and spectral efficiency is of prime significance in UWB based WBANs.

In this Chapter, a utility function is constructed for the tradeoff between energy efficiency and spectral efficiency by applying the Cobb-Douglas production function. Since the utility optimization problem is a non-concave fractional program, a numerical algorithm by combining sequential quadratic programming (SQP) algorithm and scatter search is firstly proposed to obtain the globally optimal solution. Then, a low complexity

algorithm based on linear approximation is proposed to obtain the suboptimal solution. In the simulations, we validate the efficacy of the proposed algorithms for achieving the optimal utility. We also compare the proposed suboptimal algorithm to the numerical algorithm and it is shown that the suboptimal algorithm has close-to-optimal performance. The proposed utility, as an effective metric for the energy-spectral efficiency tradeoff, is able to balance the performance between the spectral efficiency and energy efficiency with any desirable preference, which can be a guideline with regard to the relay placement and power allocation in designing energy-spectral efficient transmissions in UWB based WBANs.

The Chapter is organized as follows. In Section 6.2, the utility for the tradeoff between energy efficiency and spectral efficiency is proposed. In Section 6.3, the proposed algorithms for the tradeoff optimization are presented. Simulation results are given in Section 6.4. The Chapter is summarized in Section 6.5.

6.2 Utility for Tradeoff between Energy Efficiency and Spectral Efficiency

To balance performance between EE and SE and optimize the two metrics simultaneously with desirable preferences, the utility for the tradeoff between these two metrics is constructed firstly by the Cobb-Douglas production function [113]. In economics, the Cobb-Douglas production function is a popular functional form of the production function which has been widely used to represent the technological relationship between the amounts of two or more inputs, particularly physical capital and labor, and the amount of output that can be produced by those inputs. Accordingly, the simplest Cobb-Douglas model has the following form:

$$Y = AL^{\beta}K^{\alpha}, \tag{6.1}$$

where Y is the total production. A is the total factor productivity. L and K represents the label and capital, respectively. β and α are the output elasticities of capital and labor, respectively. Currently, this model has been applied to various aspects in wireless communications [114, 115, 116, 117]. Inspired by the Cobb-Douglas production function model, the utility function used in this thesis is obtained as follows:

$$U = \left(EE_{SRD}\right)^{w}\left(SE_{SRD}\right)^{1-w}, \tag{6.2}$$

where $w \in [0, 1]$. w and $1 - w$ are defined as the desirable preferences for EE and SE, respectively. When $w > 0.5$, it reveals that EE is more of a concern than SE for the WBAN node and vice versa.

Based on the definitions of SE and EE in Chapter 4 and Chapter 5, we have the following transformation:

$$U(x_r, y_r, P_1, P_2) = \frac{SE_{SRD}(x_r, y_r, P_1, P_2)}{\psi(P_1, P_2)}, \tag{6.3}$$

where $\psi(P_1, P_2) \triangleq P^{w}_{SRD}(P_1, P_2)$.

With (6.3), we can formulate the utility optimization problem for the considered three transmission scenarios. In the around-torso scenario, the utility optimization problem subject to the relay location and power allocation can be written as

$$\begin{aligned} \underset{x_r, y_r, P_1, P_2}{\text{maximize}} \quad & U(x_r, y_r, P_1, P_2) \\ \text{subject to} \quad & \text{C1} : \left(x_r + \frac{d_{SD}\sin\theta}{2}\right)^2 + y_r^2 \leq \left(\frac{d_{SD}\sin\theta}{2}\right)^2, \\ & \text{C2} : x_r \leq \epsilon, \\ & \text{C3} : P_1 + P_2 \leq P_s. \end{aligned} \tag{6.4}$$

Note that, the along-torso scenario is considered as a special case of the around-torso scenario in the proposed network model.

Similarly, the utility optimization problem in the in-body scenario subject to the relay

location and power allocation can be given by

$$\begin{aligned} \underset{x_r,y_r,P_1,P_2}{\text{maximize}} \quad & U(x_r, y_r, P_1, P_2) \\ \text{subject to} \quad & \text{C1} : x_r^2 + y_r^2 \leq (d_{SD} \sin\theta)^2, \\ & \text{C2} : x_r \leq d_{SD} \sin\theta + \hat{\delta}, \\ & \text{C3} : P_1 + P_2 \leq P_s, \\ & \text{C4} : P_2 \leq P_{max}^o. \end{aligned} \tag{6.5}$$

6.3 Proposed Algorithms for Tradeoff Optimization

In (6.4) or (6.5), $\{x_r^o, y_r^o, P_1^o, P_2^o\}$ denotes the optimal solution and U_{max} denotes the maximum utility. From (6.3), we can see that the optimization problems are non-concave fractional programs [111] since $SE_{SRD}(x_r, y_r, P_1, P_2)$ and $\psi(P_1, P_2)$ are both concave. In fact, there is no standard approach for solving this type of problem. In this section, we first use a numerical algorithm to find the optimal solution. Then, we propose a low-complexity algorithm to find a suboptimal solution.

6.3.1 Numerical Algorithm

To find the globally optimal solution, the SQP algorithm and scatter search are employed in this work.

The SQP algorithm [109] is a powerful iterative method for non-convex and nonlinear optimization. Schittkowski [118], for example, has implemented and tested a version that outperforms every other tested method in terms of efficiency, accuracy, and percentage of successful solutions, over a large number of test problems. In the SQP algorithm, the principal idea is the formulation of a QP subproblem based on a quadratic approximation

of the Lagrangian function, as shown in (6.6).

$$\mathcal{L}(\chi, \lambda) = U(\chi) + \sum_{i=1}^{r} \lambda_i g_i(\chi), \tag{6.6}$$

where $\chi = [x_r, y_r, P_1, P_2]$ and $\lambda = [\lambda_1 \dots \lambda_r]$. r denotes the number of inequality constraints in (6.4) or (6.5). g_i denotes the inequality equation in the ith constraint.

With (6.6), a QP subproblem can be generated as follows:

$$\begin{aligned} \underset{\rho}{\text{maximize}} \quad & \frac{1}{2}\rho^T H_k \rho + \nabla U(\chi_k)^T \rho \\ \text{subject to} \quad & \nabla g_i(\chi_k)^T \rho + g_i(\chi_k) \leq 0, \ i = 1, \dots, r. \end{aligned} \tag{6.7}$$

This subproblem can be solved using any QP algorithm and the solution is used to form a new iterate:

$$\chi_{k+1} = \chi_k + \alpha_k \rho, \tag{6.8}$$

where the step length parameter α_k is determined by an appropriate line search procedure so that a sufficient decrease in a merit function is obtained. The matrix H_k is a positive definite approximation of the Hessian matrix of the Lagrangian function in (6.6) and H_k can be updated by any of the quasi-Newton methods. Within finite iterations, the SQP algorithm will converge to a local optimum.

On the other hand, the scatter search is a global optimization algorithm, which can find the optimal solution effectively by calling the SQP algorithm several times with different initial points. In our simulations, Matlab's optimization toolbox is used to implement the the SQP method.

6.3.2 Sub-Optimal Algorithm

However, the computational complexity of the proposed numerical algorithm is unaffordable in practice. Consequently, we propose a computationally more affordable algorithm to obtain a suboptimal solution.

With a linear approximation, we firstly approximate $\psi(P_1, P_2)$ in a linear form, which is given by

$$\begin{aligned}\psi(P_1, P_2) &\approx \widetilde{\psi}(P_1, P_2) \\ &= \psi(\hat{P}_1, \hat{P}_2) + \frac{\partial \psi}{\partial P_1}(\hat{P}_1, \hat{P}_2)(P_1 - \hat{P}_1) + \frac{\partial \psi}{\partial P_2}(\hat{P}_1, \hat{P}_2)(P_2 - \hat{P}_2). \end{aligned} \tag{6.9}$$

$\psi(P_1, P_2)$ can be approached by $\widetilde{\psi}(P_1, P_2)$ when $\hat{P}_i$ is close to P_i for $i = 1, 2$.

Substituting (6.9) into (6.3), the maximization subject for the EE-SE tradeoff can then be modified as

$$\underset{x_r, y_r, P_1, P_2}{\text{maximize}} \quad \frac{SE_{SRD}(x_r, y_r, P_1, P_2)}{\widetilde{\psi}(P_1, P_2)}. \tag{6.10}$$

Since $\widetilde{\psi}(P_1, P_2)$ is a linear function of P_1 and P_2, the problem in (6.10) is transferred into a concave fractional program problem. Thus, the proposed method for the EE optimization in Chapter 5 is applicable here. On the other hand, we can see that the value of $\{\hat{P}_1, \hat{P}_2\}$ is important for approaching the optimal solution of (6.4) or (6.5). In fact, we can approach the optimal solution of (6.4) or (6.5) by a sequence solution of (6.10) with updating $\{\hat{P}_1, \hat{P}_2\}$. As a result, the proposed suboptimal algorithm to solve the problem in (6.4) or (6.5) can be summarized as the following sequence of steps:

1. Set $\{\tilde{x}_r^0, \tilde{y}_r^0, \tilde{P}_1^0, \tilde{P}_2^0\}$ as the initial value and $\{\hat{P}_1, \hat{P}_2\} = \{\tilde{P}_1^0, \tilde{P}_2^0\}$. Set the iterative index $k = 1$.

2. Solve the problem in (6.10) in the kth iteration and define the optimal solution as $\{\tilde{x}_r^k, \tilde{y}_r^k, \tilde{P}_1^k, \tilde{P}_2^k\}$.

3. If $U(\tilde{x}_r^k, \tilde{y}_r^k, \tilde{P}_1^k, \tilde{P}_2^k) - U(\tilde{x}_r^{k-1}, \tilde{y}_r^{k-1}, \tilde{P}_1^{k-1}, \tilde{P}_2^{k-1}) \leq \overline{\eta}$, then the algorithm ends and return $\{x_r^o, y_r^o, P_1^o, P_2^o\} = \{\tilde{x}_r^k, \tilde{y}_r^k, \tilde{P}_1^k, \tilde{P}_2^k\}$. Otherwise, $\{\hat{P}_1, \hat{P}_2\} = \{\tilde{P}_1^k, \tilde{P}_2^k\}$ and update $k = k + 1$, and return to Step 2 until L'_{max} is reached.

Here L'_{max} denotes the maximum number of iterations and $\overline{\eta}$ denotes the maximum error tolerance.

6.4 Simulation Results

In the simulations, all the simulation parameters are the same as those in Chapter 4 and Chapter 5. All the simulation results are averaged over 5000 channel realizations.

To make the proposed utility comparable with EE and SE, normalization is used in the simulations. The normalized utility, EE and SE can be defined as

$$\begin{aligned}&\overline{U}(x_r, y_r, P_1, P_2)\\ =&\left(\frac{EE_{SRD}(x_r, y_r, P_1, P_2)}{EE_{max}}\right)^{w}\left(\frac{SE_{SRD}(x_r, y_r, P_1, P_2)}{SE_{max}}\right)^{1-w}\end{aligned} \tag{6.11}$$

$$\overline{EE}_{SRD}(x_r, y_r, P_1, P_2) = \frac{EE_{SRD}(x_r, y_r, P_1, P_2)}{EE_{max}}, \tag{6.12}$$

and

$$\overline{SE}_{SRD}(x_r, y_r, P_1, P_2) = \frac{SE_{SRD}(x_r, y_r, P_1, P_2)}{SE_{max}}, \tag{6.13}$$

respectively. Note that, EE_{max} and SE_{max} are both constant.

Table 6.1: Averaged optimal solution $\left\{\mathrm{E}\{x_r^o\}, \mathrm{E}\{y_r^o\}, \mathrm{E}\{P_1^o\}, \mathrm{E}\{P_2^o\}\right\}$ for the utility optimization

Around-torso scenario: $d_r = 0.2$m, $d_{SD} = 0.6$m, and $P_s = 0$dBm						
w	0	0.2	0.4	0.6	0.8	1
$\mathrm{E}\{x_r^o\}$	-0.51	-0.51	-0.51	-0.51	-0.51	-0.51
$\mathrm{E}\{y_r^o\}$	0	0	0	0	0	0
$\frac{\mathrm{E}\{P_1^o\}}{P_s}$	0.4800	0.4676	0.2595	0.1449	0.1025	0.0802
$\frac{\mathrm{E}\{P_2^o\}}{P_s}$	0.5200	0.5324	0.2541	0.1420	0.1004	0.0786
In-body scenario: $d_r = 5$cm, $d_{SD} = 0.3$m, and $P_s = 0$dBm						
w	0	0.2	0.4	0.6	0.8	1
$\mathrm{E}\{x_r^o\}$	0.038	0.038	0.038	0.038	0.038	0.038
$\mathrm{E}\{y_r^o\}$	0	0	0	0	0	0
$\frac{\mathrm{E}\{P_1^o\}}{P_s}$	0.1800	0.1476	0.0476	0.0291	0.0210	0.0168
$\frac{\mathrm{E}\{P_2^o\}}{P_s}$	0.8200	0.6353	0.2064	0.1262	0.0925	0.0735

Table 6.1 illustrates the averaged optimal solution $\{\mathrm{E}\{x_r^o\}, \mathrm{E}\{y_r^o\}, \mathrm{E}\{P_1^o\}, \mathrm{E}\{P_2^o\}\}$ for the utility optimization with various values of w. As shown in this table, the averaged optimal relay location $\{x_r^o, y_r^o\}$ is independent of w when $P_s = 0$dBm. This is because that the optimal EE and SE share the same optimal relay location when $P_s = 0$dBm. At $w = 0$, the EE-SE tradeoff optimization is simplified to the SE optimization, thus $\{x_r^o, y_r^o, P_1^o, P_2^o\} = \{x_r^{se}, y_r^{se}, P_1^{se}, P_2^{se}\}$. As w becomes bigger, we can find out that there is a tendency for the usage of P_s to get smaller and when $w = 1$, only the EE optimization is considered, thus $\{x_r^o, y_r^o, P_1^o, P_2^o\} = \{x_r^{ee}, y_r^{ee}, P_1^{ee}, P_2^{ee}\}$. Intuitively, EE is more of a concern than the SE for the implant node when w is bigger, a less amount of the total transmit power P_s therefore will be allocated to S and R to optimize the desirable tradeoff.

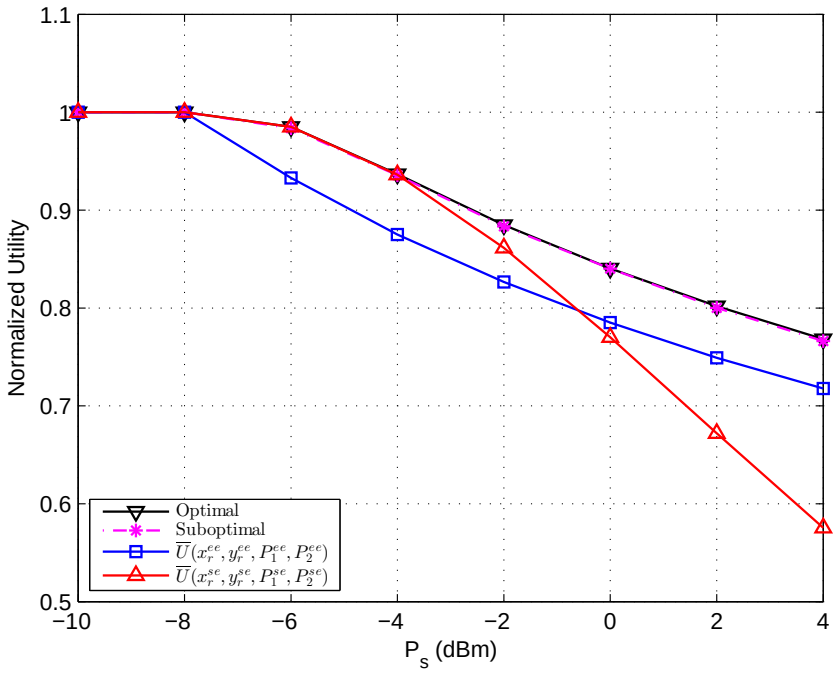

Figure 6.1: The normalized utility versus P_s with $w = 0.5$ in the around-torso scenario.

To verify the effectiveness of the proposed algorithms for the EE-SE tradeoff, the normalized utility versus P_s in the around-torso scenario and in-body scenario are shown

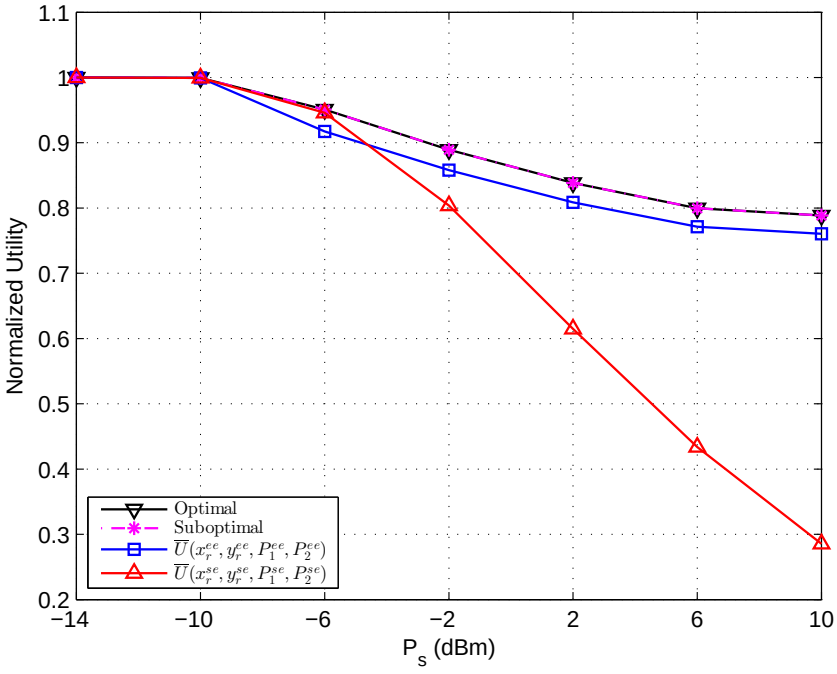

Figure 6.2: The normalized utility versus P_s with $w = 0.5$ in the in-body scenario.

in Fig. 6.1 and Fig. 6.2, respectively, where EE and SE have equally preference. In both figures, the proposed numerical algorithm (denoted as "Optimal") and the proposed suboptimal algorithm (denoted as "Suboptimal") are both displayed. For comparison, $\overline{U}\{x_r^{ee}, y_r^{ee}, P_1^{ee}, P_2^{ee}\}$ and $\overline{U}\{x_r^{se}, y_r^{se}, P_1^{se}, P_2^{se}\}$ are also considered. As expected, both proposed algorithms provide the best performance and the suboptimal algorithm has close-to-optimal performance.

In Fig. 6.3 and 6.4, the normalized utility, EE and SE achieved by $\{x_r^o, y_r^o, P_1^o, P_2^o\}$ with various values of w are presented for the around-torso scenario and in-body scenario, respectively. It can be seen that $\overline{EE}_{SRD}\{x_r^o, y_r^o, P_1^o, P_2^o\}$ is a non-decreasing function of w and $\overline{SE}_{SRD}\{x_r^o, y_r^o, P_1^o, P_2^o\}$ is a non-increasing function of w, these observations comply with the results and our analysis in Table 6.1. Furthermore, from this figure it can be determined that the proposed utility for the EE-SE tradeoff can effectively balance

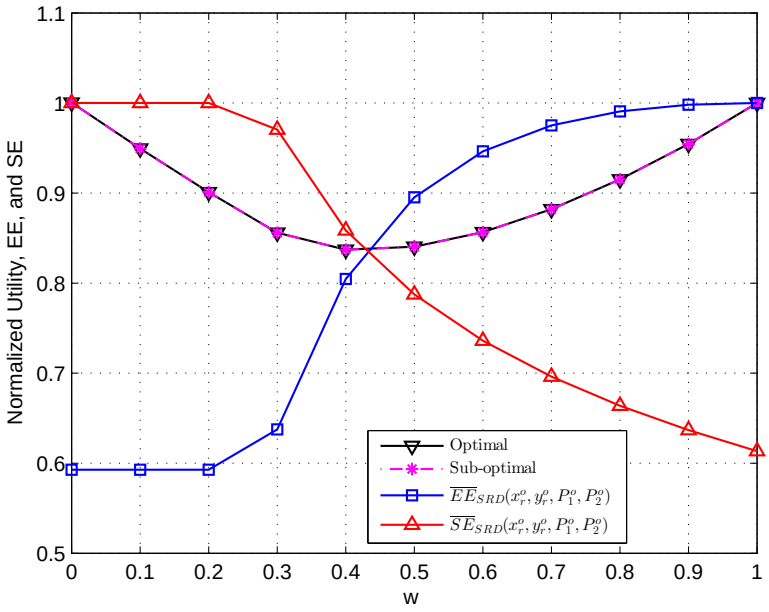

Figure 6.3: The normalized utility, EE, and SE with $\{x_r^o, y_r^o, P_1^o, P_2^o\}$ when $P_s = 0$dBm in the around-torso scenario.

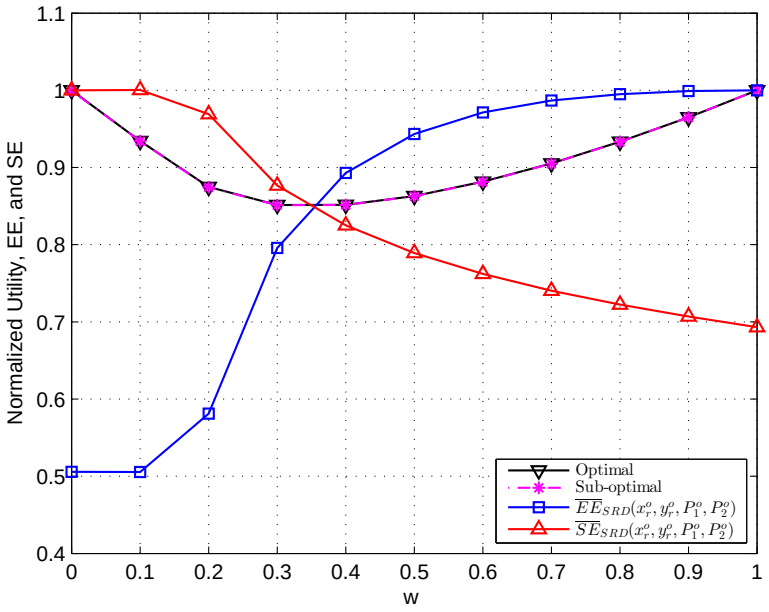

Figure 6.4: The normalized utility, EE, and SE with $\{x_r^o, y_r^o, P_1^o, P_2^o\}$ when $P_s = 0$dBm in the in-body scenario.

performance between EE and SE with any given preference w.

In conclusion, the observations from Fig. 6.1 to Fig. 6.4 validate the efficacy of the proposed algorithms for achieving the optimal utility and demonstrate that the proposed utility, as an effective metric for the EE-SE tradeoff, is able to balance the performance between EE and SE with any desirable preference, which can be a guideline in terms of the relay placement and power allocation in designing the energy-spectral efficient transmission in UWB based IBANs.

6.5 Summary

In this Chapter, the joint optimal energy efficiency and spectral efficiency is studied in single-relay UWB based WBANs. To design the energy-spectral efficient WBANs, we adopt a utility for the tradeoff between energy efficiency and spectral efficiency. Since the utility optimization problem is a non-concave fractional program, algorithms are proposed to obtain the globally optimal solution and a low complexity suboptimal solution, respectively. We prove the efficacy of the proposed algorithms and validate that the proposed utility, as an effective metric for the energy-spectral efficiency tradeoff, is able to balance the performance between energy efficiency and spectral efficiency with any desirable preference. The related research work in this Chapter is submitted to IEEE/ACM Transactions on Networking.

As described throughout Chapter 4 to Chapter 6, we mainly focused on the design and optimization in single-relay UWB based WBANs. In the next Chapter, we will extend the work from the single-relay case to a multiple-relay case. Spectral efficiency optimization and energy efficiency optimization will be studied from the point of view of distributed beamforming.

Chapter 7

Spectral Efficiency Optimization and Energy Efficiency Optimization in Multiple-Relay UWB based WBANs

7.1 Introduction

In this Chapter, spectral efficiency optimization and energy efficiency optimization are investigated in multiple-relay UWB based WBANs. To the best of knowledge, there is little work about optimizing spectral efficiency and energy efficiency in multiple-relay assisted WBANs. Since the basic idea and principle for solving the optimization problems are the same in the cases of in-body transmissions and on-body transmissions, we only present the work for in-body transmissions herein.

Explicitly, an implant WBAN, consisting of one implanted transmitter, several parallel wearable relays and one body network coordinator is considered in this Chapter. At the coordinator and at each relay, a Rake receiver and matched filter are employed to capture the multipath energy, respectively. To evaluate the impact of relay location in the multiple-relay case, a modified model based on the proposed one in Fig. 4.2 is

developed. With the modified model, the spectral efficiency optimization and energy efficiency optimization problems are mathematically formulated, respectively, under the assumption that the individual relay power is constrained due to the FCC regulations for UWB signals. After some transformations, both problems are equivalent to solving distributed network beamforming problems, where each relay properly adjusts its own power to make the system spectral efficiency and energy efficiency maximized.

In the spectral efficiency optimization, the network beamforming can be reduced to a quasi-convex optimization problem, which can be solved by using convex optimization. In the energy efficiency optimization, since the problem is a non-convex and nonlinear problem, the SQP algorithm combined with scatter search proposed in Section 6.3 are exploited to find the global optimum. Simulations results show that the proposed beamforming scheme is superior to other transmission schemes regarding spectral efficiency and energy efficiency. A considerable improvement can be achieved not only in spectral efficiency but also in energy efficiency compared to direct transmission. Moreover, our numerical examples reveal that the optimal relay location varies with the battery power of the implant node.

The Chapter is organized as follows. In Section 7.2, the system scenario and multiple-relay based cooperative model are presented. In Section 7.3, distributed beamforming transmissions are described. Optimal power allocation schemes are proposed for spectral efficiency optimization and energy efficiency optimization in 7.4 and 7.5, respectively. Simulation results are given in Section 7.6. The Chapter is summarized in Section 7.7.

7.2 System Scenarios and Proposed Cooperative Model

As shown in Fig. 7.1, a modified cooperative model based on the proposed one in Fig. 4.2 for implant WBANs is developed, where S is implanted in the human chest, and m wearable relay nodes (R_i, for i=1,...,m) and D are assumed to be on the same side of the body surface. In this work, a special parallel relay topology is considered, where m relays have the same x-coordinate x_0 [mm] ($x_0 \geq 0$) and are evenly distributed along y-axis. With a given y-coordinate y_i [mm] for relay i, we have

$$d_{SR_i} = \sqrt{x_0^2 + y_i^2 + d_r^2},$$

and

$$d_{R_iD} = \sqrt{(x_0 - d_{SD}\sin\theta)^2 + y_i^2},$$

where d_{SR_i} and d_{R_iD} are the distances from S to relay i and relay i to D, respectively. It is worth to note that we herein study a simplified two-step AF protocol. In the first step, S broadcasts its signal to relays, and during the second step, the relays forwards their received signals to D.

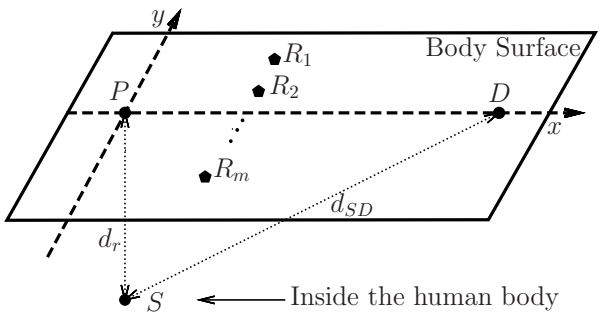

Figure 7.1: Modified cooperative model for implant WBANs.

7.3 Distributed Beamforming Transmission

For analytical simplicity, we present the IR-UWB signal model with BPSK. The random TH or DS codes are also not considered in this thesis.

As presented in Section 4.3, the transmitted symbol waveform at S can be expressed as

$$s(t) = b\sqrt{P_s}\sum_{j=0}^{N_f-1}\omega(t-jT_f),\ b=\pm 1 \tag{7.1}$$

With the assumptions that channel $h_k(t)$ remains invariant over a symbol duration but it changes from symbol to symbol, the received signal at relay i is given by

$$r_{SR_i}(t) = b\sqrt{\frac{P_s}{PL_{SR_i}(d_{SR_i})}}\sum_{j=0}^{N_f-1} g_{SR_i}(t-jT_f) + n_{SR_i}(t), \tag{7.2}$$

where

$$g_{SR_i}(t) = \omega(t) * h_{SR_i}(t) = \sum_{l=0}^{L_{SR_i}-1}\alpha_{l,SR_i}\omega(t-\tau_{l,SR_i}), \tag{7.3}$$

and $n_{SR_i}(t)$ is AWGN with zero mean and variance σ^2. T_f is set to be large enough to avoid the ISI.

At each relay, a received pulse waveform matched filter is employed. During each frame duration, the output of the matched filter at relay i is given by

$$\begin{aligned}\bar{r}_{SR_i}(j) &= \int_{jT_f}^{(j+1)T_f} r_{SR_i}(t)g_{SR_i}(t-jT_f)dt \\ &= b\sqrt{\frac{P_s}{PL_{SR_i}(d_{SR_i})}}\xi_{T_f}(h_{SR_i}) + \bar{n}_{SR_i}(j),\end{aligned} \tag{7.4}$$

where $j \in [0, N_f-1]$. $\xi_{T_f}(h_{SR_i})$ is the captured multipath energy during T_f at relay i and $\bar{n}_{SR_i}(j)$ is still AWGN with zero mean and variance $\xi_{T_f}(h_{SR_i})\sigma^2$.

After summing up all the outputs over N_f frames, the decision statistic b at relay i

can be written as

$$b_{R_i} = bN_f\sqrt{\frac{P_s}{PL_{SR_i}(d_{SR_i})}}\xi_{T_f}(h_{SR_i}) + \underbrace{\sum_{j=0}^{N_f-1}\bar{n}_{SR_i}(j)}_{\hat{n}_{SR_i}}. \tag{7.5}$$

With $\{b_{R_i}\}_{i=1}^{m}$, distributed space-time block coding (STBC) is applied at relays to achieve spatial diversity gain [119]. Let $\mathbf{B}$ be the STBC matrix with the dimension $m \times N_f'$, where N_f' is the block length. Examples of the STBC matrix are shown in Table 7.1. In this thesis, we assume that $N_f = QN_f'$ and Q is an integer. Thus, N_f frames are divided into Q frame blocks and the transmitted signal vector from relays in the second hop can be modeled as

$$\mathbf{t}_R(t) = \sqrt{P_{max}^o}\sum_{q=1}^{Q}\hat{\mathbf{b}}_R\hat{\mathbf{K}}_R\hat{\mathbf{W}}_R\mathbf{B}\boldsymbol{\omega}(t - N_fT_f, q), \tag{7.6}$$

where $\mathbf{t}_R(t) = [t_{R_1}(t), t_{R_2}(t), \ldots, t_{R_m}(t)]^T$ and the element $t_{R_i}(t)$ represents the transmitted signal at relay i. P_{max}^o is the maximum transmit power at each relay, which is constrained by the FCC regulations. $\hat{\mathbf{b}}_R \triangleq \text{diag}\{b_{R_1}, \ldots, b_{R_m}\}$. $\hat{\mathbf{K}}_R \triangleq \text{diag}\{|b_{R_1}|^{-1}, \ldots, |b_{R_m}|^{-1}\}$ and $|x|$ represents the absolute value of x. $|b_{R_i}| = (\frac{N_f^2P_s\xi_{T_f}^2(h_{SR_i})}{PL_{SR_i}(d_{SR_i})} + N_f\xi_{T_f}(h_{SR_i})\sigma^2)^{\frac{1}{2}}$. $\hat{\mathbf{W}}_R \triangleq \text{diag}\{w_1, \ldots, w_m\}$ is the diagonal matrix of the relay power allocation weights and $0 \leq w_i \leq 1$. Clearly, the transmit power of relay i is $w_i^2P_{max}^o$. We define $\boldsymbol{\omega}(t,q) \triangleq [\omega(t-N_f'(q-1)T_f), \omega(t-N_f'(q-1)T_f-T_f), \ldots, \omega(t-N_f'(q-1)T_f-(N_f'-1)T_f)]^T$ is the waveform vector with length N_f'.

After passing through the channels from the relays to D, the received signal at D can be represented by

$$\begin{aligned} r_D(t) =& \sqrt{P_{max}^o}\sum_{q=1}^{Q}\sum_{i=1}^{m}\frac{\mathbf{e}_i^T\hat{\mathbf{b}}_R\hat{\mathbf{K}}_R\hat{\mathbf{W}}_R\mathbf{B}\mathbf{g}_{R_iD}(t - N_fT_f, q)}{\sqrt{PL_{R_iD}(d_{R_iD})}} \\ &+ n_D(t), \end{aligned} \tag{7.7}$$

where $\mathbf{e}_i$ is the ith column of the identity matrix. $\mathbf{g}_{R_iD}(t,q) \triangleq [g_{R_iD}(t-N_f'(q-1)T_f), g_{R_iD}(t-$

Table 7.1: Examples of STBC matrix **B** for relays

m	N_f'	**B**
2	2	$\begin{pmatrix} 1 & -1 \\ 1 & 1 \end{pmatrix}$
3	4	$\begin{pmatrix} 1 & -1 & -1 & -1 \\ 1 & 1 & 1 & -1 \\ 1 & -1 & 1 & 1 \end{pmatrix}$
4	4	$\begin{pmatrix} 1 & -1 & -1 & -1 \\ 1 & 1 & 1 & -1 \\ 1 & -1 & 1 & 1 \\ 1 & 1 & -1 & 1 \end{pmatrix}$

$N_f'(q-1)T_f - T_f), \ldots, g_{R_iD}(t - N_f'(q-1)T_f - (N_f'-1)T_f)]^T$ and $g_{R_iD}(t) = \omega(t) * h_{R_iD}(t)$. $n_D(t)$ is the AWGN with zero mean and variance σ^2.

At D, a Rake receiver with L_r fingers is employed and the delayed reference waveforms $\{\omega(t - \tau(l_r))\}_{l_r=0}^{L_r-1}$ are used. After combining the Rake outputs over N_f' frames in each frame block, the output per frame block can be written as

$$\begin{aligned} z_D &= \sqrt{P_{max}^o} \sum_{l_r=0}^{L_r-1} \boldsymbol{\beta}_{RD}^T(l_r) \mathbf{B}\mathbf{B}^T \hat{\mathbf{K}}_R \hat{\mathbf{W}}_R \hat{\mathbf{P}\mathbf{L}}_{RD} \mathbf{b}_R + \bar{n}_D(t) \\ &= N_f' \sqrt{P_{max}^o} \boldsymbol{\xi}_{RD}^T \hat{\mathbf{K}}_R \hat{\mathbf{W}}_R \hat{\mathbf{P}\mathbf{L}}_{RD} \mathbf{b}_R + \bar{n}_D \end{aligned} \tag{7.8}$$

where $l_r \in [0, L_r - 1]$. $\mathbf{b}_R = [b_{R_1}, \ldots, b_{R_m}]^T$. $\boldsymbol{\beta}_{RD}(l_r) \triangleq [\beta_{R_1D}^2(l_r), \ldots, \beta_{R_mD}^2(l_r)]^T$ and $\beta_{R_iD}(l_r) = \int_0^{T_f} g_{R_iD}\omega(t - \tau(l_r))dt$. $\hat{\mathbf{P}\mathbf{L}}_{RD} \triangleq \text{diag}\{PL_{R_1D}^{-\frac{1}{2}}(d_{R_1D}), \ldots, PL_{R_mD}^{-\frac{1}{2}}(d_{R_mD})\}$. $\boldsymbol{\xi}_{RD} \triangleq [\xi_{R_1D}, \ldots, \xi_{R_mD}]^T$ and $\xi_{R_iD} = \sum_{l_r=0}^{L_r-1} \beta_{R_iD}^2(l_r)$. Notice that ξ_{R_iD} represents the captured multipath energy from link R_i to D. $\bar{n}_D$ is the AWGN with zero mean and variance $N_f' \sum_{i=1}^m \xi_{R_iD}\sigma^2$.

Summing up all outputs over Q frame blocks and substituting (7.5) into (7.8), the decision variable for b can be given by

$$\begin{aligned}\hat{z} &= N_f\sqrt{P^o_{max}}\boldsymbol{\xi}^T_{RD}\hat{\mathbf{K}}_R\hat{\mathbf{W}}_R\hat{\mathbf{PL}}_{RD}\mathbf{b}_R + \hat{n}_D \\ &= bN_f^2\sqrt{P^o_{max}P_s}\boldsymbol{\xi}^T_{RD}\hat{\mathbf{K}}_R\hat{\mathbf{W}}_R\hat{\mathbf{PL}}_{RD}\hat{\mathbf{PL}}_{SR}\boldsymbol{\xi}_{SR} \\ &+ N_f\sqrt{P^o_{max}}\boldsymbol{\xi}^T_{RD}\hat{\mathbf{K}}_R\hat{\mathbf{W}}_R\hat{\mathbf{PL}}_{RD}\hat{\mathbf{n}}_{SR} + \hat{n}_D, \end{aligned} \tag{7.9}$$

where $\hat{\mathbf{PL}}_{SR} \triangleq \text{diag}\{PL^{-\frac{1}{2}}_{SR_1}(d_{SR_1}), \ldots, PL^{-\frac{1}{2}}_{SR_m}(d_{SR_m})\}$ and $\boldsymbol{\xi}_{SR} \triangleq [\xi_{T_f}(h_{SR_1}), \ldots, \xi_{T_f}(h_{SR_m})]^T$. $\hat{\mathbf{n}}_{SR} \triangleq [\hat{n}_{SR_1}, \ldots, \hat{n}_{SR_m}]^T$. $\hat{n}_D$ is the AWGN with zero mean and variance $N_f\sum_{i=1}^m \xi_{R_iD}\sigma^2$.

In (7.9), we identify three components

$$\hat{z}_s = bN_f^2\sqrt{P^o_{max}P_s}\boldsymbol{\xi}^T_{RD}\hat{\mathbf{K}}_R\hat{\mathbf{W}}_R\hat{\mathbf{PL}}_{RD}\hat{\mathbf{PL}}_{SR}\boldsymbol{\xi}_{SR}, \tag{7.10}$$

$$\hat{z}_{n_{SR}} = N_f\sqrt{P^o_{max}}\boldsymbol{\xi}^T_{RD}\hat{\mathbf{K}}_R\hat{\mathbf{W}}_R\hat{\mathbf{PL}}_{RD}\hat{\mathbf{n}}_{SR}, \tag{7.11}$$

and

$$\hat{z}_{n_{RD}} = \hat{n}_D, \tag{7.12}$$

as the useful signal, noise from the first hop, and noise from the second hop, respectively.

Obviously, the SE/EE optimization based beamforming design is to find the optimal $\mathbf{w}_R = [w_1, \ldots, w_m]^T$ to maximize the received SE/EE, which is equivalent to the optimal relay power allocation.

7.4 Optimal Power Allocation for Spectral Efficiency Optimization

In this section, we analyze the optimal relay power allocation at the relays for SE optimization. Since SE is a monotonically increasing function of the received SNR, the received SNR is optimized accordingly.

Based on (7.9)-(7.12), the received SNR at D can be expressed as

$$\mathrm{SNR}_D(\mathbf{w}_R) = \frac{\mathrm{E}\{|\hat{z}_s|^2\}}{\mathrm{E}\{|\hat{z}_{n_{SR}}|^2\} + \mathrm{E}\{|\hat{z}_{n_{RD}}|^2\}}. \tag{7.13}$$

Using (7.10), we have

$$\mathrm{E}\{|\hat{z}_s|^2\} = \mathbf{w}_R^T \mathbf{O}_s \mathbf{w}_R, \tag{7.14}$$

where $\mathbf{O}_s = N_f^4 P_{max}^o P_s \mathbf{V}\mathbf{V}^T$ and $\mathbf{V} = \hat{\boldsymbol{\xi}}_{RD}\hat{\mathbf{K}}_R\hat{\mathbf{P}}\hat{\mathbf{L}}_{RD}\hat{\mathbf{P}}\hat{\mathbf{L}}_{SR}\boldsymbol{\xi}_{SR}$. $\hat{\boldsymbol{\xi}}_{RD} \triangleq \mathrm{diag}\{\xi_{R_1D}, \ldots, \xi_{R_mD}\}$.

Using (7.11), we have

$$\mathrm{E}\{|\hat{z}_{n_{SR}}|^2\} = \mathbf{w}_R^T \mathbf{O}_n \mathbf{w}_R, \tag{7.15}$$

where $\mathbf{O}_n = N_f^3 P_{max}^o \sigma^2 \hat{\boldsymbol{\xi}}_{RD}^2 \hat{\mathbf{K}}_R^2 \hat{\mathbf{P}}\hat{\mathbf{L}}_{RD}^{\,2} \hat{\boldsymbol{\xi}}_{SR}$ and $\hat{\boldsymbol{\xi}}_{SR} \triangleq$
$\mathrm{diag}\{\xi_{T_f}(h_{SR_1}), \ldots, \xi_{T_f}(h_{SR_m})\}$.

From (7.12), we obtain

$$\mathrm{E}\{|\hat{z}_{n_{RD}}|^2\} = N_f \sum_{i=1}^{m} \xi_{R_iD}\sigma^2. \tag{7.16}$$

Using (7.13)-(7.16), the distributed beamforming problem for the SE optimization can be written as

$$\begin{aligned} \underset{\mathbf{w}_R}{\text{maximize}} \quad & \frac{\mathbf{w}_R^T \mathbf{O}_s \mathbf{w}_R}{\mathbf{w}_R^T \mathbf{O}_n \mathbf{w}_R + N_f \sum_{i=1}^{m} \xi_{R_iD}\sigma^2} \\ \text{subject to} \quad & \mathbf{0}_m \preceq \mathbf{w}_R \preceq \mathbf{I}_m, \end{aligned} \tag{7.17}$$

where $\mathbf{0}_m$ is an m-dimensional vector with all zero entries and $\mathbf{I}_m$ is an m-dimensional vector with all one entries. With two m-dimensional vectors $\mathbf{a}$ and $\mathbf{c}$, $\mathbf{a} \preceq \mathbf{c}$ means $a_i \leq c_i$ for all $i \in [1, m]$.

With an auxiliary variable τ [109], (7.17) is equivalent to

$$\begin{aligned} \underset{\mathbf{w}_R, \tau}{\text{maximize}} \quad & \tau \\ \text{subject to} \quad & \frac{\mathbf{w}_R^T \mathbf{O}_s \mathbf{w}_R}{\mathbf{w}_R^T \mathbf{O}_n \mathbf{w}_R + N_f \sum_{i=1}^{m} \xi_{R_iD}\sigma^2} \geq \tau^2 \\ & \mathbf{0}_m \preceq \mathbf{w}_R \preceq \mathbf{I}_m. \end{aligned} \tag{7.18}$$

Introducing the following notations

$$\mathbf{U}^T\mathbf{U} \triangleq \begin{pmatrix} N_f \sum_{i=1}^{m} \xi_{R_iD}\sigma^2 & \mathbf{0}_m^T \\ \mathbf{0}_m & \mathbf{O}_n \end{pmatrix}, \tag{7.19}$$

$$\tilde{\mathbf{w}}_R \triangleq [1, \mathbf{w}_R^T]^T, \tag{7.20}$$

and

$$\tilde{\mathbf{V}} \triangleq [0, \mathbf{V}^T]^T, \tag{7.21}$$

(7.18) can be further written as

$$\begin{aligned} \underset{\tilde{\mathbf{w}}_R,\tau}{\text{maximize}} \quad & \tau \\ \text{subject to} \quad & N_f^2\sqrt{P_{max}P_s}\tilde{\mathbf{w}}_R^T\tilde{\mathbf{V}} \geq \tau\|\mathbf{U}\tilde{\mathbf{w}}_R\| \\ & \mathbf{0}_m \preceq \tilde{\mathbf{w}}_R \preceq \mathbf{I}_m \\ & \tilde{\mathbf{w}}_R^T\mathbf{e}_1 = 1. \end{aligned} \tag{7.22}$$

Since (7.22) is a quasi-convex problem, it can be reduced to the following second-order cone programming feasibility problem

$$\begin{aligned} \text{find} \quad & \tilde{\mathbf{w}}_R \\ \text{subject to} \quad & N_f^2\sqrt{P_{max}P_s}\tilde{\mathbf{w}}_R^T\tilde{\mathbf{V}} \geq \tau\|\mathbf{U}\tilde{\mathbf{w}}_R\| \\ & \mathbf{0}_m \preceq \tilde{\mathbf{w}}_R \preceq \mathbf{I}_m \\ & \tilde{\mathbf{w}}_R^T\mathbf{e}_1 = 1. \end{aligned} \tag{7.23}$$

Let τ^* be the optimal value of in (7.22). Then, for any $\tau > \tau^*$, (7.23) is infeasible. On the contrary, if (7.23) is feasible, then we conclude that $\tau \leq \tau^*$. Hence, the optimum τ^* and the optimal power allocation vector $\tilde{\mathbf{w}}_R^o$ can be found by using the bisection search method [109]. Assuming that τ^* lies in the interval $[\tau_{min}, \tau_{max}]$, the bisection search procedure to solve (7.22) can be concluded as the following sequence of steps:

1. $\tau = (\tau_{min} + \tau_{max})/2$.

2. Solve the convex feasibility problem (7.23). If (7.23) is feasible, then $\tau_{min} = \tau$, otherwise $\tau_{max} = \tau$.

3. If $\tau_{max} - \tau_{min} < \eta$, then stop. Otherwise, go to the first Step.

Here, η is the maximum error tolerance in τ.

After obtaining the optimal power allocation vector $\tilde{\mathbf{w}}_R^o$, the optimal SE can be given by $\frac{1}{2N_f}\log_2\left(1 + SNR_D(\mathbf{w}_R^o)\right)$.

7.5 Optimal Power Allocation for Energy Efficiency Optimization

For the EE optimization, we formulate the distributed beamforming problem in this section. Since the problem is nonconvex, a numerical algorithm is proposed to find the global optimum.

Based on the EE definition in Chapter 5, EE for the distributed beamforming transmission can be expressed as

$$EE_{SRD}(\mathbf{w}_R) \triangleq \frac{SE_{SRD}(\mathbf{w}_R)}{P_{SRD}(\mathbf{w}_R)}, \tag{7.24}$$

where

$$SE_{SRD}(\mathbf{w}_R) = \frac{1}{2N_f}\log_2(1 + \frac{\mathbf{w}_R^T\mathbf{O}_s\mathbf{w}_R}{\mathbf{w}_R^T\mathbf{O}_n\mathbf{w}_R + N_f\sum_{i=1}^{m}\xi_{R_iD}\sigma^2}), \tag{7.25}$$

and

$$P_{SRD} = \frac{1}{2}\left(P_s + \mathbf{w}_R^T\mathbf{w}_R P_{max} + (m+1)(P_{ct} + P_{cr})\right). \tag{7.26}$$

Consequently, the distributed beamforming problem for the EE optimization can be written as

$$\begin{aligned} \underset{\mathbf{w}_R}{\text{maximize}} \quad & \frac{SE_{SRD}(\mathbf{w}_R)}{P_{SRD}(\mathbf{w}_R)} \\ \text{subject to} \quad & \mathbf{0}_m \preceq \mathbf{w}_R \preceq \mathbf{I}_m. \end{aligned} \tag{7.27}$$

Using (7.25) and (7.26), we can see that the problem in (7.27) is a non-convex and nonlinear programming problem and the corresponding Karush-Kuhn-Tucker (KKT) equations are only necessary for the optimal solution. In this work, the SQP algorithm and the scatter search proposed in Section 6.3 are employed to find the global optimal solution $\mathbf{w}_R^o$. As mentioned in 6.3, the SQP algorithm is a powerful iterative method for nonconvex and nonlinear optimization. At each major iteration, an approximation is made of the Hessian of the Lagrangian function using a quasi-Newton updating method. This is then used to generate a QP subproblem whose solution is used to form a search direction for a line search. The procedure for the SQP algorithm combined with the scatter search is detailed in Section 6.3.1 and thus it is not repeated herein. Unfortunately, it is unable to provide the close-form expression of $\mathbf{w}_R^o$ since the optimal solution can only be found numerically.

7.6 Simulation Results

To evaluate performance of the proposed distributed beamforming scheme regarding SE and EE in UWB based WBANs, numerical results and examples are presented in this section. In the simulations, T_w and T_f are chosen to be 0.7ns and 100ns, respectively. N_f is set to be 4 and the system bandwidth is 1.4GHz. Since the average FCC PSD emission limit for UWB signals is -41.3dBm/MHz, the maximum average transmit power P_{ave} is -9.8dBm. With the duty cycle T_w/T_f, $P_{max}^o = P_{ave} * T_f/T_w \approx 12$dBm. For the transmit power of the implant node, we set $P_s \leq 10$dBm considering the emission limit and safety

inside the human body. d_{SD} and d_r are set to be 200mm and 50mm, respectively. At the relays, we assume that $\xi_{T_f}(h_{SR_i}) \approx 1$ for all $i \in [1, m]$ without considering the ISI. At D, a selective Rake receiver is employed to combine the L_r strongest multipath components.

7.6.1 Spectral Efficiency of Proposed Distributed Beamforming Scheme

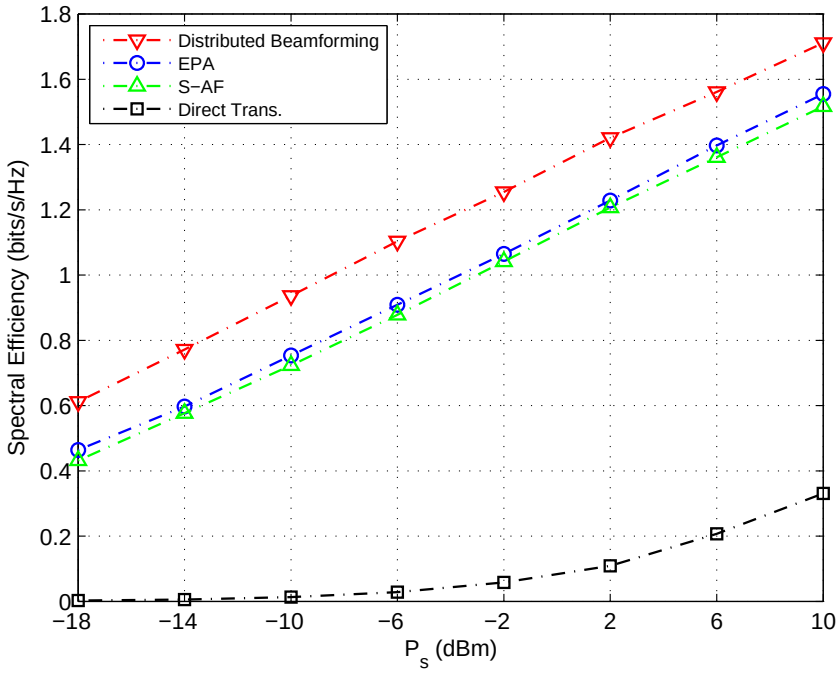

Figure 7.2: Average SE versus P_s with $L_r = 4$ in a 2-relay network.

Fig. 7.2 shows the average SE versus P_s in a 2-relay UWB based implant WBANs. For this 2-relay case, we assume that the coordinates of the two relays are set to be $\{(90, 20)\}$ and $\{(90, -20)\}$, respectively. Performance of the proposed distributed beamforming scheme is compared to those of the equal power allocation (EPA) scheme (each relay has an equal transmit power), S-AF scheme (the relay with the highest SNR is selected), and direct transmission. We can see that the proposed distributed beamform-

ing scheme outperforms all the other schemes. With perfect channel information at the relays, it is about 5dB better than the EPA scheme which needs no channel information about the second hop at the relays. Compared to direct transmission, we can see that the proposed distributed beamforming scheme can provide more than 16dB performance improvement and this improvement mainly results from the fact that the path loss of the"in-body to on-body" link is much stronger than that of the "on-body to on-body" link. From the perspective of power consumption, the transmit power at S by using the distributed beamforming scheme is much less (more than 28dB) compared to that by direct transmission when the same SE is achieved. This evidence indicates that the lifetime of the implant node can be prolonged considerably in distributed relay networks, which demonstrates the effectiveness of the proposed distributed beamforming scheme when applied to UWB based WBANs.

Fig. 7.3 depicts the average SE versus P_s with different numbers of relays and relay locations. Specifically, three cases with $m = 1, 2$, and 3 are considered, respectively. For the case $m = 1$, the coordinate of the single relay is set to be $\{(x_0, 0)\}$. For the case $m = 2$, the coordinates of the relays are set to be $\{(x_0, 20)\}$ and $\{(x_0, -20)\}$, respectively. For the case $m = 3$, the coordinates of the relays are set to be $\{(x_0, 20)\}$, $\{(x_0, 0)\}$, and $\{(x_0, -20)\}$, respectively. For all the cases, x_0 is set to be $30, 90$, and 150, respectively, where $x_0 = 30$ represents that the relays are close to P, $x_0 = 90$ represents that the relays are located near the middle of P and D, and $x_0 = 150$ represents that the relays are close to D. As shown in this figure, the SE performance improves when the number of relays is increased. This improvement benefits from the spatial diversity offered by multiple-relay channels. Thus, given a targeted SE, employing more relays can improve the power efficiency of the implant node. On the other hand, it is shown that the relay location plays an important role for the distributed relay implant WBANs. With a given P_s, the SE performance of the proposed distributed beamforming scheme is sensitive to

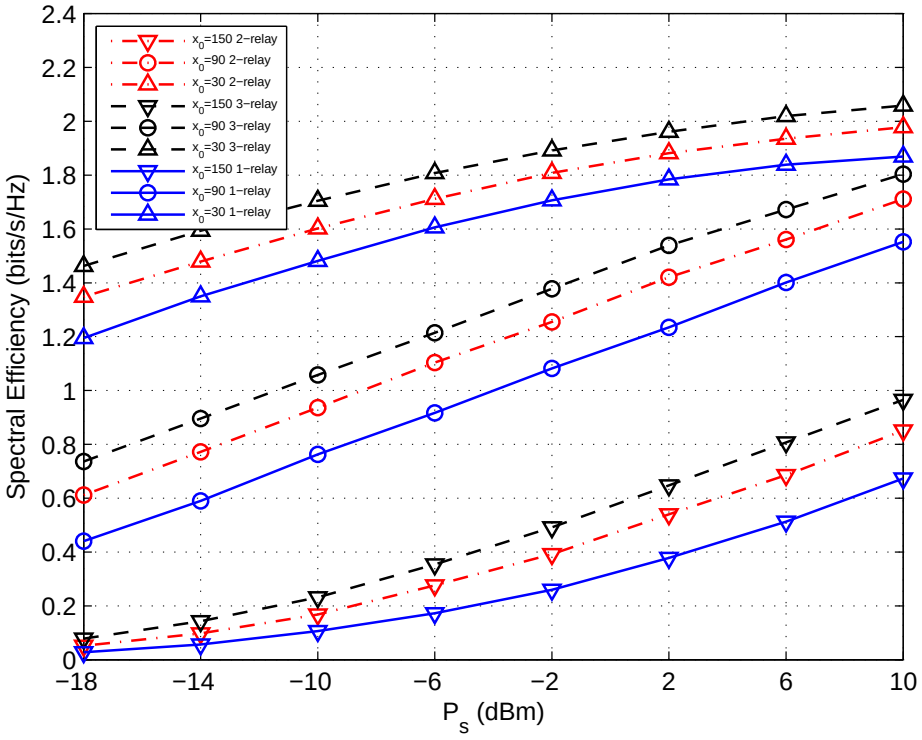

Figure 7.3: Average SE versus P_s with different numbers of relays and relay locations when $L_r = 4$.

the relay location and SE is the highest when the relays are at $x_0 = 30$ among all the three locations.

To further investigate the impact of relay location, the average SE versus x_0 with different P_s in a 2-relay UWB based implant WBANs is illustrated in Fig. 7.4. The coordinates of the two relays are set to be $\{(x_0, 20)\}$ and $\{(x_0, -20)\}$, respectively. From this figure, we notice that the optimal x_0 exists with a fixed P_s and the optimal x_0 varies with P_s. When the battery power of S is very limited and $P_s = -18$dBm, employing the relays at P can achieve the utmost SE. As P_s becomes larger, the optimal x_0 increases and choosing the relays close to P is the best option.

Fig. 7.5 presents the average SE versus P_s with different L_r in a 2-relay network, where the locations of the two relays are set to be $\{(30, 20)\}$ and $\{(30, -20)\}$, respectively.

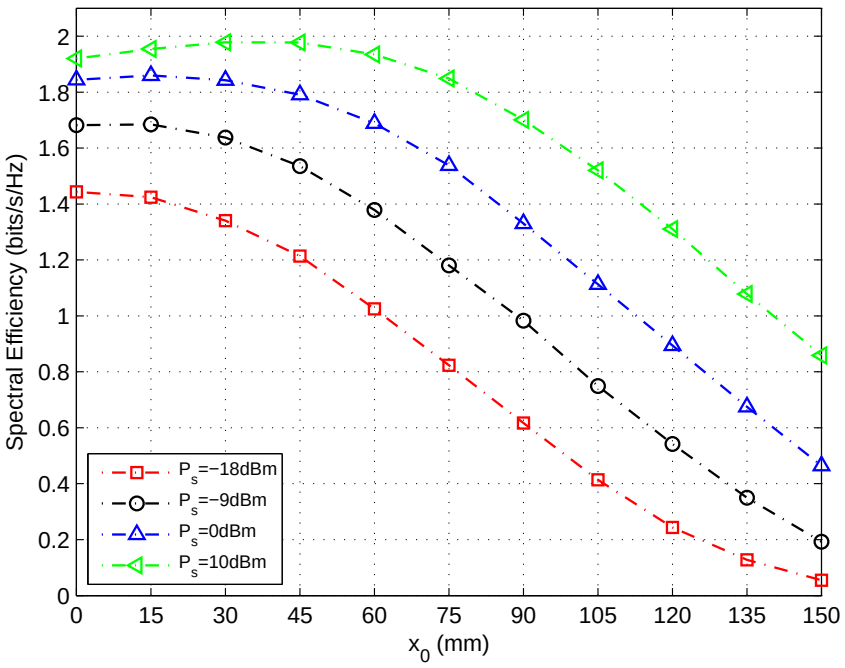

Figure 7.4: Average SE versus x_0 with different P_s in a 2-relay network.

Obviously, employing more Rake fingers can achieve better SE performance because more multipath energy can be captured. From the power consumption viewpoint, the lifetime of the implant node can be prolonged at the cost of deploying more Rake fingers at D.

In conclusion, the proposed distributed beamforming scheme can be applied to UWB based WBANs effectively, which is superior to the other transmission schemes in terms of SE. In the in-body scenario, the lifetime of the implant node can be prolonged at the cost of deploying more relays and more Rake fingers at D with a targeted SE. As the fact observed in the single-relay case, the relay location also exhibits a significant impact on the system performance in the multiple-relay case and choosing relays close to P can achieve a better SE performance compared to that with other relay locations.

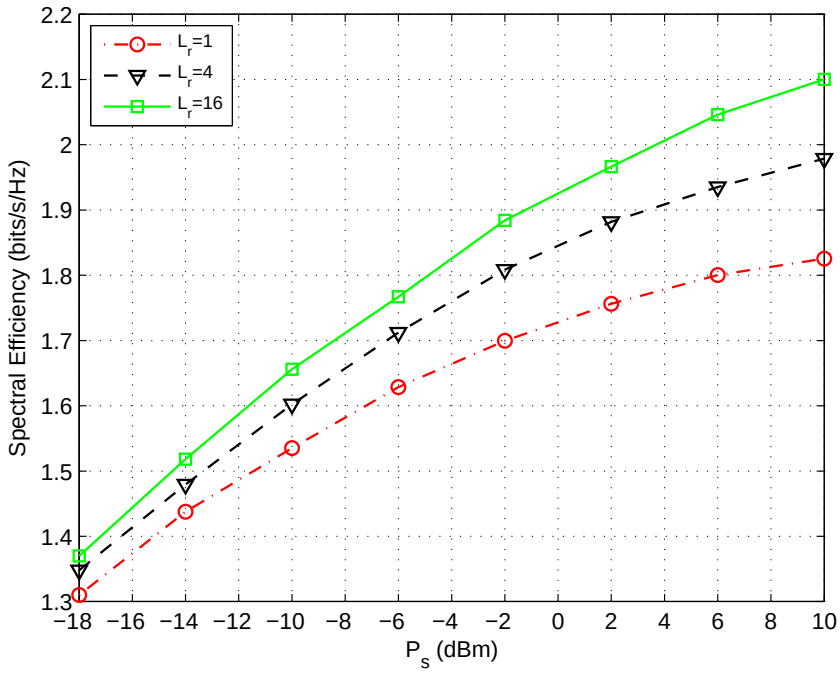

Figure 7.5: Average SE versus P_s with different L_r in a 2-relay network.

7.6.2 Energy Efficiency of Proposed Distributed Beamforming Scheme

Fig. 7.6 shows the average EE versus P_s in a 2-relay UWB based implant WBAN. For this case, the coordinates of the two relays are set to be $\{(90, 20)\}$ and $\{(90, -20)\}$, respectively. Four transmission schemes are illustrated in this figure to compare with the proposed beamforming scheme, which are the average power allocation (APA) scheme, the power-maximizing (Power-Max) scheme (every relay uses its maximum power), the SE-Max scheme and direct transmission, respectively. In the APA scheme, the power allocation weight for the relay i is set to be $\mathrm{E}\{w_i^o\}$, which denotes the average transmit power consumed by the relay i in the proposed beamforming scheme. Thus, the APA scheme uses the same amount of power resource as the proposed scheme. As shown in this figure, the proposed distributed beamforming scheme is superior to all the other schemes

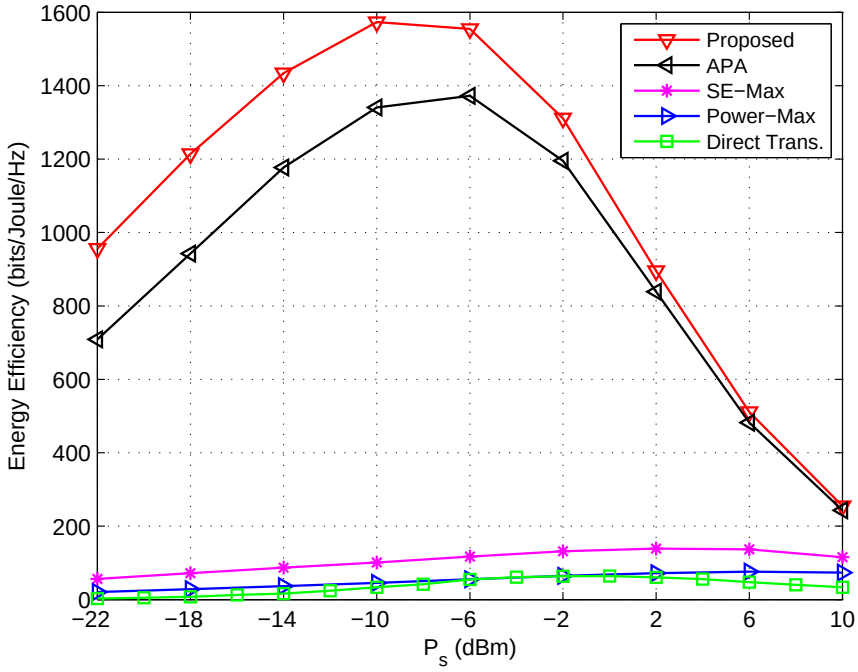

Figure 7.6: Average EE versus P_s in a 2-relay network.

in terms of EE. For the APA scheme, its performance is only slightly inferior to that of the proposed scheme, especially when P_s is in the moderate-to-high regimes. For the Power-Max and SE-Max schemes, both of them cannot achieve a satisfactory performance, which results from the fact that employing large transmit power in both schemes is deleterious to EE. Compared to direct transmission, we can see that the proposed beamforming scheme can provide a substantial performance improvement. This evidence indicates that the lifetime of WBANs can be prolonged considerably by using the proposed distributed beamforming scheme.

Fig. 7.7 depicts the average SE versus P_s in a 2-relay network. The coordinates of the two relays are the same as those in Fig. 7.6. Obviously, the SE-Max scheme has the best performance in terms of SE. Although the performance gap between the proposed scheme and the SE-Max scheme grows larger as P_s increases, our proposed scheme still

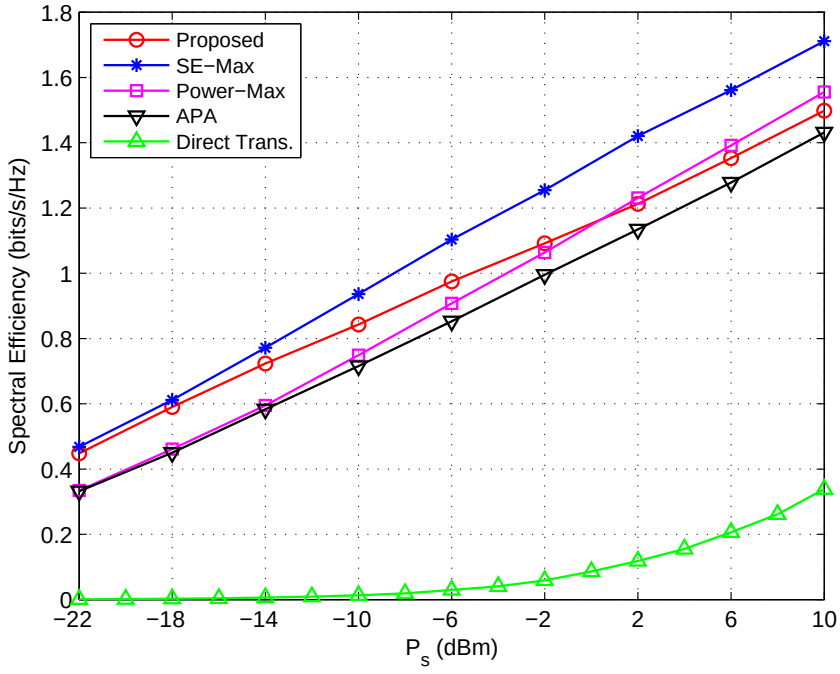

Figure 7.7: Average SE versus P_s in a 2-relay network.

has an acceptable SE, which outperforms the APA scheme with the same power resource and direct transmission.

To investigate the impact of relay location on EE, Fig. 7.8 presents the average EE versus P_s with different relay locations in a 2-relay network, where the y-coordinate of the two relays are fixed at $\{20\}$ and $\{-20\}$, respectively. For the x-coordinate, we assume that x_0 has the value of $0, 90$, and 150, respectively, where $x_0 = 0$ represents that the relays are close to P, $x_0 = 90$ represents that the relays are located near the middle of P and D, and $x_0 = 150$ represents that the relays are close to D. Based on the observations, the EE performance of the proposed scheme is also sensitive to the relay location with a given P_s. When the battery power of S is very limited, employing the relays close to P can achieve the utmost EE. As P_s becomes larger, choosing the relays close to the middle point of P and D is the best option.

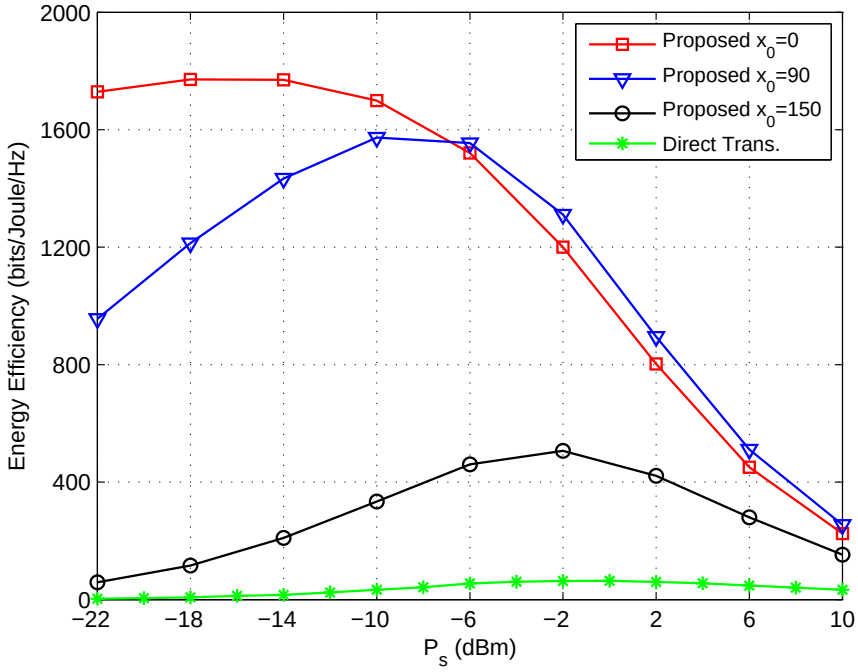

Figure 7.8: Average EE versus P_s with different relay locations.

7.7 Summary

In this Chapter, spectral efficiency optimization and energy efficiency optimization are both investigated in multiple-relay UWB based WBANs. To solve the optimization problems, network beamforming schemes are proposed. With the assumption that each relay has an individual power constraint, we prove that the proposed network beamforming schemes are equivalent to solving a distributed power allocation problem, where each relay properly adjusts its own power such that the system spectral efficiency and energy efficiency can be maximized.

In the simulations, we evaluate the performance of the proposed distributed beamforming schemes and exploit the optimal relay locations. As the fact observed in the single-relay case, the relay location also exhibits a significant impact on the system performance in the multiple-relay case. Moreover, results demonstrated the effectiveness of

the proposed distributed beamforming schemes applied to UWB based WBANs. Compared to the other relay-based schemes, the proposed distributed beamforming schemes can provide a better performance regarding spectral efficiency and energy efficiency, which allows for WBANs to deliver consistent high transmission performance to patient in various eHealth applications. The related research work in this Chapter is published in ACM BodyNets 2014 and IEEE VTC 2015.

Chapter 8

Conclusions and Future Work

This thesis proposes relay-assisted schemes to effectively achieve spectral efficiency and energy efficiency related optimization for UWB based WBANs. In this Chapter, we summarize our research work presented in the previous Chapters. The open problems and interesting future extensions of this thesis are also discussed.

8.1 Research Summary

As a new emerging type of wireless networks for telemedicine and mHealth, WBANs have drawn much attention from researchers, which target providing reliable and accurate health monitoring for patients and giving patients great experience in mobility. With the properties of large bandwidth and extremely low transmission power, UWB is able to offer several advantages when applying to WBANs. In UWB based WBANs, spectral efficiency and energy efficiency are viewed as the major challenges which need to be tackled. Moreover, the tradeoff between spectral efficiency and energy efficiency is also a prime issue worth studying. This thesis explores the spectral and energy efficiency optimization and tradeoff problems and presents joint optimal power allocation and relay location based schemes to solve the problems. The proposed joint optimal schemes can

be considered as a source of inspiration for the relay selection in WBANs, which provides an insight into the spectral-energy efficient design of WBANs with respect to selection of the proper placement of the wearable relay nodes along with the optimal transmit power levels.

Chapter 1 gives the overview of this research work, where the research background, objectives, thesis organization and contributions are presented.

Chapter 2 presents the overview of UWB and WBANs, respectively. Main challenges of UWB based WBANs are comprehensively reviewed. Along with the description of the challenges, the motivations of the research in the thesis are stated.

In Chapter 3, an energy-saving based relay-location selection criterion is developed for UWB based WBANs with a realistic nonlinear energy consumption model. The optimal power allocation with a given relay location is derived for single-relay cooperative transmission to minimize the total energy consumption. Considering the energy consumption difference between direct transmission and cooperative transmission, the energy-saving relay selection criterion is proposed and analyzed afterwards. Based on theoretical derivations and numerical results, the relay location in different regions makes a big difference on the energy-saving performance of cooperative transmission. The relay location, therefore, plays a critical role from the system optimization point of view. Hence, it is concluded that deploying a relay node optimally in terms of the relay location in UWB based WBANs is of paramount importance.

In Chapter 4 and Chapter 5, spectral efficiency optimization and energy efficiency optimization are studied thoroughly in single-relay UWB based WBANs. Three typical transmission scenarios are taken into account herein. To deploy the relay node optimally, relay-location based network models are developed. With the proposed models, optimization problems are mathematically formulated and schemes are proposed to optimize the metrics. The basic idea of the proposed schemes is to seek the optimal relay loca-

tion in WBANs together with the optimal power allocation. Based on the theoretical analysis and numerical results, some interesting results are revealed. In the along-torso scenario, we show that direct transmission is preferable to the cooperative transmission, even though the optimal relay location is selected and the optimal power allocation is achieved in cooperative transmission. In the around-torso scenario and in-body scenario, direct transmission is unable to provide an acceptable transmission performance in UWB based WBANs. The utilization of an on-body relay node is thus essential for the spectral and energy efficient transmissions. With the proposed joint optimal schemes, it is demonstrated that the two metrics can be significantly enhanced compared to other transmission schemes. Moreover, most of the power consumption can be transferred from the on-body/implant node to the on-body relay, which helps the node with a lifetime increase.

In Chapter 6, performance between energy efficiency and spectral efficiency is balanced in single-relay UWB based WBANs. To design energy-spectral efficient WBANs, we adopt a utility for the tradeoff between energy efficiency and spectral efficiency. Since the utility optimization problem is a non-concave fractional program, algorithms are proposed to obtain the globally optimal solution and a low complexity suboptimal solution, respectively. We prove the efficacy of the proposed algorithms and validate that the proposed utility, as an effective metric for the energy-spectral efficiency tradeoff, is able to balance the performance between energy efficiency and spectral efficiency with any desirable preference.

In Chapter 7, we extend the work from the single-relay case to a multiple-relay case. Spectral efficiency optimization and energy efficiency optimization are investigated in multiple-relay UWB based WBANs. Under the assumption that an individual relay power is constrained, both metric optimization problems are formulated as a distributed network beamforming problem, where each relay properly adjusts its own power to make the

metrics maximized. In the spectral efficiency optimization, the network beamforming can be reduced to a quasi-convex optimization problem, which can be solved by using convex optimization. In the energy efficiency optimization, since the problem is a non-convex and nonlinear problem, the algorithm proposed in Chapter 6 is exploited to find the global optimum. Simulations results show that the proposed beamforming scheme is superior to other transmission schemes regarding spectral efficiency and energy efficiency. A considerable improvement can be achieved not only in spectral efficiency but also in energy efficiency compared to direct transmission. Moreover, our numerical examples reveal that the optimal relay location varies with the battery power of the source node.

8.2 Future Work

The study presented in this thesis provides potential extensions for future work. Some interesting topics of open problems for future research are discussed as follows.

8.2.1 Channel Modeling

In this thesis, the state-of-the art UWB channel model in the human chest is used for designing the energy-spectral efficient transmission in the in-body scenario. This statistical model is developed by using a heterogeneous anatomical model that includes the frequency-dependent dielectric properties of different human tissues. Although this channel model has been widely used for evaluating the performance of implant WBANs via computer simulation, the limitations of this channel model implemented in real life cannot be ignored. In this model, only the chest was considered. Owing to the highly inhomogeneous structure of the human body, the proposed model may not be applied to other anatomical parts. Thus, a customised channel model for implant transmissions must be derived in the future.

8.2.2 Error Resilience and Reliability

This thesis is mainly focused on the spectral and energy efficiency optimization and tradeoff for UWB based WBANs. In fact, error resilience and transmission reliability are also important in UWB based WBANs. As we may realize, low transmission power and small antenna sizes of WBAN sensor nodes causes reduced SNR, thus causing higher bit error rates and reducing the transmission reliability. However, the reliability of data transmission in WBANs is vital, especially for some healthcare applications. Therefore, error resilient schemes for data transmission should be developed in UWB based WBANs for reducing bit error rates and increasing network reliability.

8.2.3 Interference Mitigation

This thesis only considers the design and optimization for a single WBAN. As we discussed in Chapter 4, the nodes in a WBAN can be centrally coordinated by the coordinator, thus allowing a number of sensor nodes to coexist in a single network without having them interfere with each other. In practice, several WBANs may come into range of each other (for instance, multiple people wearing WBANs are in a small room or lift). In this case, it is impossible to coordinate among different WBANs due to unpredictable people's movement and the private security issues. Therefore, interference mitigation schemes need to be proposed to minimize interference while maintaining satisfactory overall spectral efficiency or energy efficiency as well as fairness among WBANs.

Abbreviations

3G Third Generation

AF Amplify-and- Forward

AWGN Additive White Gaussian Noise

APA Average Power Allocation

BPSK Binary Phase-Shift Keying

BER Bit Error Rate

CCA Clear Channel Assessment

CIR Channel Impulse Response

DS Direct Sequence

DF Decode-and-Forward

EE Energy Efficiency

EIRP Effective Isotropic Radiated Power

ECG Electrocardiogram

EFC Electric Field Communication

EPA Equal Power Allocation

FCC Federal Communications Commission

HBC Human Body Communications

IR Impulse Radio

ISI Inter-Symbol Interference

KKT Karush-Kuhn-Tucker

MAC Medium Access Control

mHealth Mobile Health

MB-OFDM Multi-Band Orthogonal Frequency-Division Multiplexing

MIMO Multi-Input Multi-Output

MRC Maximum-Ratio Combining

OOK On-Off Keying

Power-Max Power-Maximizing

PHY Physical

PSD Power Spectral Density

PDA Personal Digital Assistant

PSDU Physical-layer Service Data Unit

PPDU Physical-layer Protocol Data Unit

PHR Physical-layer Header

PA Power Allocation

PPM Pulse-Position Modulation

QoS Quality of Service

RL Relay Location

RF Radio Frequency

SFD Start Frame Delimiter

SHR Synchronization Header

SNR Signal-to-Noise Ratio

S-AF Selection Amplify-And-Forward

SE-Max SE-Maximizing

STBC Space-Time Block Coding

SE Spectral Efficiency

TH Time Hopping

TDMA Time-Division Multiple Access

UWB Ultra Wideband

WBANs Wireless Body Area Networks

WSNs Wireless Sensor Networks

WLANs Wireless Local Area Networks

WPANs Wireless Personal Area Networks

Bibliography

[1] D. Porcino and W. Hirt, "Ultra-wideband radio technology: potential and challenges ahead," *Communications Magazine, IEEE*, vol. 41, no. 7, pp. 66–74, July 2003.

[2] B. Latré, B. Braem, I. Moerman, C. Blondia, and P. Demeester, "A survey on wireless body area networks," *Wirel. Netw.*, vol. 17, no. 1, pp. 1–18, Jan. 2011. [Online]. Available: http://dx.doi.org/10.1007/s11276-010-0252-4

[3] I. Chlamtac, M. Conti, and J. J.-N. Liu, "Mobile Ad Hoc networking: imperatives and challenges," *Ad Hoc Networks*, vol. 1, no. 1, pp. 13–64, 2003. [Online]. Available: http://www.sciencedirect.com/science/article/pii/S1570870503000131

[4] "IEEE draft standard for local area network/wide area network (LAN/WAN) node communication protocol to complement the utility industry end device data tables," *1703/D9*, pp. 1–253, April 2012.

[5] "IEEE approved draft standard for local and metropolitan area networks part 15.4: low rate wireless personal area networks (LR-WPANs) amendment: physical layer (PHY) specifications for low data rate wireless smart metering utility networks," *802.15.4g/D7*, pp. 1–258, April 2012.

[6] FCC, "Revision of part 15 of the commission's rules regarding ultra-wideband transmission systems," ET Docket 98-153, FCC 02-8, Tech. Rep., 2002.

[7] G. Breed, "A summary of FCC rules for ultra wideband communications," *High Frequency Electronics*, vol. 4, pp. 42–44, 2005.

[8] J. Fernandes and D. Wentzloff, "Recent advances in IR-UWB transceivers: An overview," in *Circuits and Systems (ISCAS), Proceedings of 2010 IEEE International Symposium on*, May 2010, pp. 3284–3287.

[9] J. Choliz, A. Hernandez-Solana, A. Sierra, and P. Cluzeaud, "Coexistence of MB-OFDM UWB with impulse radio UWB and other radio systems," in *Ultra-Wideband (ICUWB), 2011 IEEE International Conference on*, Sept 2011, pp. 410–414.

[10] R. Chavez-Santiago, I. Balasingham, J. Bergsland, W. Zahid, K. Takizawa, R. Miura, and H.-B. Li, "Experimental implant communication of high data rate video using an ultra wideband radio link," in *Engineering in Medicine and Biology Society (EMBC), 2013 35th Annual International Conference of the IEEE*, July 2013, pp. 5175–5178.

[11] M. Win and R. Scholtz, "Impulse radio: how it works," *Communications Letters, IEEE*, vol. 2, no. 2, pp. 36–38, Feb 1998.

[12] L. Lampe and K. Witrisal, "Challenges and recent advances in IR-UWB system design," in *Circuits and Systems (ISCAS), Proceedings of 2010 IEEE International Symposium on*, May 2010, pp. 3288–3291.

[13] "IEEE standard for local and metropolitan area networks - part 15.6: Wireless body area networks," *IEEE Std 802.15.6-2012*, pp. 1–271, Feb 2012.

[14] G. Aiello and G. Rogerson, "Ultra-wideband wireless systems," *Microwave Magazine, IEEE*, vol. 4, no. 2, pp. 36–47, June 2003.

[15] V. Sipal, B. Allen, D. Edwards, and B. Honary, "Twenty years of ultra-wideband: Opportunities and challenges," *Communications, IET*, vol. 6, no. 10, pp. 1147–1162, July 2012.

[16] W. Hirt, "Ultra-wideband radio technology: overview and future research," *Computer Communications*, vol. 26, no. 1, pp. 46–52, 2003. [Online]. Available: http://www.sciencedirect.com/science/article/pii/S0140366402001196

[17] V. Somayazulu, J. Foerster, and S. Roy, "Design challenges for very high data rate UWB systems," in *Signals, Systems and Computers, 2002. Conference Record of the Thirty-Sixth Asilomar Conference on*, vol. 1, Nov 2002, pp. 717–721 vol.1.

[18] M. Chiani and A. Giorgetti, "Coexistence between UWB and narrow-band wireless communication systems," *Proceedings of the IEEE*, vol. 97, no. 2, pp. 231–254, Feb 2009.

[19] A. Giorgetti, M. Chiani, and D. Dardari, "Coexistence issues in cognitive radios based on ultra-wide bandwidth systems," in *Cognitive Radio Oriented Wireless Networks and Communications, 2006. 1st International Conference on*, June 2006, pp. 1–5.

[20] B. Allen, A. Brown, K. Schwieger, E. Zimmermann, W. Q. Malik, D. J. Edwards, L. Ouvry, and I. Oppermann, "Ultra wideband: applications, technology and future perspectives," in *International Workshop On Convergent Technologies (IWCT)*, 2005. [Online]. Available: http://hdl.handle.net/10547/269833

[21] S. Roy, J. Foerster, V. Somayazulu, and D. Leeper, "Ultra-wideband radio design: the promise of high-speed, short-range wireless connectivity," *Proceedings of the IEEE*, vol. 92, no. 2, pp. 295–311, Feb 2004.

[22] L. Stoica, A. Rabbachin, and I. Oppermann, "A low-complexity noncoherent IR-UWB transceiver architecture with TOA estimation," *Microwave Theory and Techniques, IEEE Transactions on*, vol. 54, no. 4, pp. 1637–1646, June 2006.

[23] J. Fernandes and D. Wentzloff, "Recent advances in IR-UWB transceivers: An overview," in *Circuits and Systems (ISCAS), Proceedings of 2010 IEEE International Symposium on*, May 2010, pp. 3284–3287.

[24] M. Win and R. Scholtz, "Ultra-wide bandwidth time-hopping spread-spectrum impulse radio for wireless multiple-access communications," *Communications, IEEE Transactions on*, vol. 48, no. 4, pp. 679–689, Apr 2000.

[25] M. Win, "A unified spectral analysis of generalized time-hopping spread-spectrum signals in the presence of timing jitter," *Selected Areas in Communications, IEEE Journal on*, vol. 20, no. 9, pp. 1664–1676, Dec 2002.

[26] M. Win and R. Scholtz, "Characterization of ultra-wide bandwidth wireless indoor channels: a communication-theoretic view," *Selected Areas in Communications, IEEE Journal on*, vol. 20, no. 9, pp. 1613–1627, Dec 2002.

[27] R. Kshetrimayum, "An introduction to UWB communication systems," *Potentials, IEEE*, vol. 28, no. 2, pp. 9–13, March 2009.

[28] X. Chen and S. Kiaei, "Monocycle shapes for ultra wideband system," in *Circuits and Systems, 2002. ISCAS 2002. IEEE International Symposium on*, vol. 1, 2002, pp. 597–600.

[29] R. K. M. Ghavami, L. Michael, *Ultra Wideband Signals and Systems in Communication Engineering*. Wiley, 2007.

[30] R. Fontana, A. Ameti, E. Richley, L. Beard, and D. Guy, "Recent advances in ultra wideband communications systems," in *Ultra Wideband Systems and Technologies, 2002. Digest of Papers. 2002 IEEE Conference on*, May 2002, pp. 129–133.

[31] A. Giorgetti, M. Chiani, and M. Win, "The effect of narrowband interference on wideband wireless communication systems," *Communications, IEEE Transactions on*, vol. 53, no. 12, pp. 2139–2149, Dec 2005.

[32] D. Cypher, N. Chevrollier, N. Montavont, and N. Golmie, "Prevailing over wires in healthcare environments: benefits and challenges," *Communications Magazine, IEEE*, vol. 44, no. 4, pp. 56–63, April 2006.

[33] C. Baker, K. Armijo, S. Belka, M. Benhabib, V. Bhargava, N. Burkhart, A. Der Minassians, G. Dervisoglu, L. Gutnik, M. Haick, C. Ho, M. Koplow, J. Mangold, S. Robinson, M. Rosa, M. Schwartz, C. Sims, H. Stoffregen, A. Waterbury, E. Leland, T. Pering, and P. Wright, "Wireless sensor networks for home health care," in *Advanced Information Networking and Applications Workshops, 2007, AINAW '07. 21st International Conference on*, vol. 2, May 2007, pp. 832–837.

[34] R. Cavallari, F. Martelli, R. Rosini, C. Buratti, and R. Verdone, "A survey on wireless body area networks: Technologies and design challenges," *Communications Surveys Tutorials, IEEE*, vol. 16, no. 3, pp. 1635–1657, Third 2014.

[35] M. Patel and J. Wang, "Applications, challenges, and prospective in emerging body area networking technologies," *Wireless Communications, IEEE*, vol. 17, no. 1, pp. 80–88, February 2010.

[36] H. Cao, V. Leung, C. Chow, and H. Chan, "Enabling technologies for wireless body area networks: A survey and outlook," *Communications Magazine, IEEE*, vol. 47, no. 12, pp. 84–93, Dec 2009.

[37] S. Movassaghi, M. Abolhasan, J. Lipman, D. Smith, and A. Jamalipour, "Wireless body area networks: A survey," *Communications Surveys Tutorials, IEEE*, vol. 16, no. 3, pp. 1658–1686, Third 2014.

[38] S. Ullah, H. Henry, and B. Bart, "A comprehensive survey of wireless body area networks," *Journal of Medical Systems*, vol. 36, no. 3, pp. 1065–1094, June 2012.

[39] S. Gopalan and J.-T. Park, "Energy-efficient MAC protocols for wireless body area networks: Survey," in *Ultra Modern Telecommunications and Control Systems and Workshops (ICUMT), 2010 International Congress on*, Oct 2010, pp. 739–744.

[40] F. Troesch, C. Steiner, T. Zasowski, T. Burger, and A. Wittneben, "Hardware aware optimization of an ultra low power UWB communication system," in *Ultra-Wideband, 2007. ICUWB 2007. IEEE International Conference on*, Sept 2007, pp. 174–179.

[41] E. Jovanov, A. Milenkovic, C. Otto, P. De Groen, B. Johnson, S. Warren, and G. Taibi, "A WBAN system for ambulatory monitoring of physical activity and health status: Applications and challenges," in *Engineering in Medicine and Biology Society, 2005. IEEE-EMBS 2005. 27th Annual International Conference of the*, Jan 2005, pp. 3810–3813.

[42] I. Akyildiz, W. Su, Y. Sankarasubramaniam, and E. Cayirci, "A survey on sensor networks," *Communications Magazine, IEEE*, vol. 40, no. 8, pp. 102–114, Aug 2002.

[43] S. Ramli and R. Ahmad, "Surveying the wireless body area network in the realm of wireless communication," in *Information Assurance and Security (IAS), 2011 7th International Conference on*, Dec 2011, pp. 58–61.

[44] B. Gyselinckx, R. Vullers, C. Van Hoof, J. Ryckaert, R. Yazicioglu, P. Fiorini, and V. Leonov, "Human++: Emerging technology for body area networks," in

Very Large Scale Integration, 2006 IFIP International Conference on, Oct 2006, pp. 175–180.

[45] C. Poon, Y.-T. Zhang, and S.-D. Bao, "A novel biometrics method to secure wireless body area sensor networks for telemedicine and m-health," *Communications Magazine, IEEE*, vol. 44, no. 4, pp. 73–81, April 2006.

[46] K. Y. Yazdandoost and S.-P. Kamran, "Channel model for body area network (BAN)," IEEE P802.15, Tech. Rep., 2009.

[47] R. Chavez-Santiago, K. Sayrafian-Pour, A. Khaleghi, K. Takizawa, J. Wang, I. Balasingham, and H.-B. Li, "Propagation models for IEEE 802.15.6 standardization of implant communication in body area networks," *Communications Magazine, IEEE*, vol. 51, no. 8, pp. 80–87, August 2013.

[48] IEEE 802.15 WPAN Task Group 6 Body Area Networks. [Online]. Available: http://www.ieee802.org/15/pub/SGmban.html

[49] F. Martelli, C. Buratti, and R. Verdone, "On the performance of an IEEE 802.15.6 wireless body area network," in *Wireless Conference 2011 - Sustainable Wireless Technologies (European Wireless), 11th European*, April 2011, pp. 1–6.

[50] K. S. Kwak, S. Ullah, and N. Ullah, "An overview of IEEE 802.15.6 standard," in *Applied Sciences in Biomedical and Communication Technologies (ISABEL), 2010 3rd International Symposium on*, Nov 2010, pp. 1–6.

[51] N. Bradai, S. Belhaj, L. Chaari, and L. Kamoun, "Study of medium access mechanisms under IEEE 802.15.6 standard," in *Wireless and Mobile Networking Conference (WMNC), 2011 4th Joint IFIP*, Oct 2011, pp. 1–6.

[52] C. Li, L. Wang, J. Li, B. Zhen, H.-B. Li, and R. Kohno, "Scalable and robust medium access control protocol in wireless body area networks," in *Personal, Indoor and Mobile Radio Communications, 2009 IEEE 20th International Symposium on*, Sept 2009, pp. 2127–2131.

[53] C. Lee, J. Kim, H. S. Lee, and J. Kim, "Physical layer designs for wban systems in IEEE 802.15.6 proposals," in *Communications and Information Technology, 2009. ISCIT 2009. 9th International Symposium on*, Sept 2009, pp. 841–844.

[54] S. Ullah and K. S. Kwak, "Throughput and delay limits of IEEE 802.15.6," in *Wireless Communications and Networking Conference (WCNC), 2011 IEEE*, March 2011, pp. 174–178.

[55] J. Wang and Q. Wang, "Channel modeling and ber performance of an implant UWB body area link," in *Applied Sciences in Biomedical and Communication Technologies, 2009. ISABEL 2009. 2nd International Symposium on*, Nov 2009, pp. 1–4.

[56] M. Yuce, H. C. Keong, and M. S. Chae, "Wideband communication for implantable and wearable systems," *Microwave Theory and Techniques, IEEE Transactions on*, vol. 57, no. 10, pp. 2597–2604, Oct 2009.

[57] K. Katsu, D. Anzai, and J. Wang, "Performance evaluation on correlation detection and energy detection for ultra wideband-impulse radio communication with multi-pulse position modulation scheme in implant body area networks," *Communications, IET*, vol. 7, no. 13, pp. 1430–1436, September 2013.

[58] D. Anzai, K. Katsu, R. Chavez-Santiago, Q. Wang, D. Plettemeier, J. Wang, and I. Balasingham, "Experimental evaluation of implant UWB-IR transmission with

living animal for body area networks," *Microwave Theory and Techniques, IEEE Transactions on*, vol. 62, no. 1, pp. 183–192, Jan 2014.

[59] D. Smith, D. Miniutti, T. Lamahewa, and L. Hanlen, "Propagation models for body-area networks: A survey and new outlook," *Antennas and Propagation Magazine, IEEE*, vol. 55, no. 5, pp. 97–117, Oct 2013.

[60] A. Fort, C. Desset, J. Ryckaert, P. De Doncker, L. Van Biesen, and P. Wambacq, "Characterization of the ultra wideband body area propagation channel," in *Ultra-Wideband, 2005. ICU 2005. 2005 IEEE International Conference on*, Sept 2005, pp. 1–6.

[61] A. Fort, J. Ryckaert, C. Desset, P. De Doncker, P. Wambacq, and L. Van Biesen, "Ultra-wideband channel model for communication around the human body," *S-elected Areas in Communications, IEEE Journal on*, vol. 24, no. 4, pp. 927–933, April 2006.

[62] T. Aoyagi, J. Takada, K. Takizawa, N. Katayama, T. Kobayashi, K. Y. Yazdan-doost, H. B. Li, and R. Kohno, "Channel model for wearable and implantable WBANs," IEEE 802.15-08-0416-04-0006, Tech. Rep., 2008.

[63] G. Dolmans and A. Fort, "Channel models WBAN-holst centre/IMEC-NL," IEEE 802.15-08-0418-01-0006, Tech. Rep., 2008.

[64] N. G. Kang, C. Cho, S. H. Park, and E. T. Won, "Channel model for WBANs," IEEE 802.15-08-0781-00-0006, Tech. Rep., 2008.

[65] Y. Chen, J. Teo, J. Lai, E. Gunawan, K. S. Low, C. B. Soh, and P. Rapajic, "Co-operative communications in ultra-wideband wireless body area networks: Channel modeling and system diversity analysis," *Selected Areas in Communications, IEEE Journal on*, vol. 27, no. 1, pp. 5–16, January 2009.

[66] B. Zhen, M. Kim, J.-i. Takada, and R. Kohno, "Characterization and modeling of dynamic on-body propagation at 4.5ghz," *Antennas and Wireless Propagation Letters, IEEE*, vol. 8, pp. 1263–1267, 2009.

[67] A. Ghildiyal, B. Godara, K. Amara, R. Dalmolin, and A. Amara, "UWB for low power, short range, in-body medical implants," in *Wireless Information Technology and Systems (ICWITS), 2010 IEEE International Conference on*, Aug 2010, pp. 1–4.

[68] A. Khaleghi, R. Chavez-Santiago, X. Liang, I. Balasingham, V. Leung, and T. Ramstad, "On ultra wideband channel modeling for in-body communications," in *Wireless Pervasive Computing (ISWPC), 2010 5th IEEE International Symposium on*, May 2010, pp. 140–145.

[69] A. Khaleghi, R. Chavez-Santiago, R. L.vez-Santiago, and I. Balasingham, "Ultra-wideband statistical propagation channel model for implant sensors in the human chest," *Microwaves, Antennas Propagation, IET*, vol. 5, no. 15, pp. 1805–1812, December 2011.

[70] S. Benedetto, *Principles of Digital Transmission: With Wireless Applications*, E. Biglieri, Ed. Springer, 1999.

[71] Y. Liang and V. Veeravalli, "Resource allocation for wireless relay channels," in *Signals, Systems and Computers, 2004. Conference Record of the Thirty-Eighth Asilomar Conference on*, vol. 2, Nov 2004, pp. 1902–1906.

[72] K. Phan, D. Nguyen, and T. Le-Ngoc, "Joint power allocation and relay selection in cooperative networks," in *Global Telecommunications Conference, 2009. GLOBECOM 2009. IEEE*, Nov 2009, pp. 1–5.

[73] Y. Zhao, R. Adve, and T. J. Lim, "Improving amplify-and-forward relay networks: optimal power allocation versus selection," *Wireless Communications, IEEE Transactions on*, vol. 6, no. 8, pp. 3114–3123, August 2007.

[74] Y. Jing and H. Jafarkhani, "Network beamforming using relays with perfect channel information," *Information Theory, IEEE Transactions on*, vol. 55, no. 6, pp. 2499–2517, June 2009.

[75] V. Havary-Nassab, S. ShahbazPanahi, A. Grami, and Z.-Q. Luo, "Distributed beamforming for relay networks based on second-order statistics of the channel state information," *Signal Processing, IEEE Transactions on*, vol. 56, no. 9, pp. 4306–4316, Sept 2008.

[76] A. Boulis, D. Smith, D. Miniutti, L. Libman, and Y. Tselishchev, "Challenges in body area networks for healthcare: the MAC," *Communications Magazine, IEEE*, vol. 50, no. 5, pp. 100–106, May 2012.

[77] L. Wang, C. Goursaud, N. Nikaein, L. Cottatellucci, and J. Gorce, "Cooperative scheduling for coexisting body area networks," *Wireless Communications, IEEE Transactions on*, vol. 12, no. 1, pp. 123–133, January 2013.

[78] R. D'Errico, R. Rosini, and M. Maman, "A performance evaluation of cooperative schemes for on-body area networks based on measured time-variant channels," in *Communications (ICC), 2011 IEEE International Conference on*, June 2011, pp. 1–5.

[79] P. Jamjareegulgarn, "Performance evaluation for cooperative diversity-based wireless body area network," in *Networks (ICON), 2013 19th IEEE International Conference on*, Dec 2013, pp. 1–6.

[80] D. Smith, "Improved switched combining with cooperative diversity for wireless body area networks: Empirical analysis and theory," in *Communications (ICC), 2014 IEEE International Conference on*, June 2014, pp. 5682–5687.

[81] R. Sanders and M. Lee, "Implantable pacemakers," *Proceedings of the IEEE*, vol. 84, no. 3, pp. 480–486, Mar 1996.

[82] B. Gyselinckx, C. Van Hoof, J. Ryckaert, R. Yazicioglu, P. Fiorini, and V. Leonov, "Human++: autonomous wireless sensors for body area networks," in *Custom Integrated Circuits Conference, 2005. Proceedings of the IEEE 2005*, Sept 2005, pp. 13–19.

[83] J. Paradiso and T. Starner, "Energy scavenging for mobile and wireless electronics," *Pervasive Computing, IEEE*, vol. 4, no. 1, pp. 18–27, Jan 2005.

[84] B. Gyselinckx, J. Penders, and R. Vullers, "Potential and challenges of body area networks for cardiac monitoring," *Journal of Electrocardiology*, vol. 40, no. 6, Supplement 1, pp. S165 – S168, 2007, {ISCE} 32nd Annual Conference. [Online]. Available: http://www.sciencedirect.com/science/article/pii/S0022073607006632

[85] D. Hoang, Y. Tan, H. Chng, and S. Panda, "Thermal energy harvesting from human warmth for wireless body area network in medical healthcare system," in *Power Electronics and Drive Systems, 2009. PEDS 2009. International Conference on*, Nov 2009, pp. 1277–1282.

[86] T. von Buren, P. Mitcheson, T. Green, E. Yeatman, A. Holmes, and G. Troster, "Optimization of inertial micropower generators for human walking motion," *Sensors Journal, IEEE*, vol. 6, no. 1, pp. 28–38, Feb 2006.

[87] "A study of vibration-based energy harvesting in activities of daily living," in *Pervasive Computing Technologies for Healthcare (PervasiveHealth), 2010 4th International Conference on-NO PERMISSIONS*, March 2010, pp. 1–4.

[88] S. Marinkovic, E. Popovici, C. Spagnol, S. Faul, and W. Marnane, "Energy-efficient low duty cycle MAC protocol for wireless body area networks," *Information Technology in Biomedicine, IEEE Transactions on*, vol. 13, no. 6, pp. 915–925, Nov 2009.

[89] H. Su and X. Zhang, "Battery-dynamics driven tdma mac protocols for wireless body-area monitoring networks in healthcare applications," *Selected Areas in Communications, IEEE Journal on*, vol. 27, no. 4, pp. 424–434, May 2009.

[90] M. A. Ameen, N. Ullah, M. S. Chowdhury, S. R. Islam, and K. Kwak, "A power efficient MAC protocol for wireless body area networks," *EURASIP Journal on Wireless Communications and Networking*, 2012.

[91] M. Alam, O. Berder, D. Menard, and O. Sentieys, "TAD-MAC: Traffic-aware dynamic MAC protocol for wireless body area sensor networks," *Emerging and Selected Topics in Circuits and Systems, IEEE Journal on*, vol. 2, no. 1, pp. 109–119, March 2012.

[92] X. Huang, H. Shan, and X. Shen, "On energy efficiency of cooperative communications in wireless body area network," in *Wireless Communications and Networking Conference (WCNC), 2011 IEEE*, March 2011, pp. 1097–1101.

[93] C. Su, P. Wang, and R. Chai, "Joint power allocation and coordinator deployment for wireless body area network," in *Wireless Communications Signal Processing (WCSP), 2013 International Conference on*, Oct 2013, pp. 1–6.

[94] G. Ntouni, A. Lioumpas, and K. Nikita, "Reliable and energy-efficient communications for wireless biomedical implant systems," *Biomedical and Health Informatics, IEEE Journal of*, vol. 18, no. 6, pp. 1848–1856, Nov 2014.

[95] J. Elias and A. Mehaoua, "Energy-aware topology design for wireless body area networks," in *Communications (ICC), 2012 IEEE International Conference on*, June 2012, pp. 3409–3410.

[96] J. Elias, "Optimal design of energy-efficient and cost-effective wireless body area networks," *Ad Hoc Networks*, vol. 13, Part B, no. 0, pp. 560–574, 2014. [Online]. Available: http://www.sciencedirect.com/science/article/pii/S1570870513002321

[97] C. K. Ho, T. S. See, and M. R. Yuce, "An ultra-wideband wireless body area network: Evaluation in static and dynamic channel conditions," *Sensors and Actuators A: Physical*, vol. 180, no. 0, pp. 137–147, 2012. [Online]. Available: http://www.sciencedirect.com/science/article/pii/S0924424712002233

[98] Y. Chen, S. Zhang, S. Xu, and G. Li, "Fundamental trade-offs on green wireless networks," *Communications Magazine, IEEE*, vol. 49, no. 6, pp. 30–37, June 2011.

[99] C. Xiong, G. Li, S. Zhang, Y. Chen, and S. Xu, "Energy- and spectral-efficiency tradeoff in downlink OFDMA networks," *Wireless Communications, IEEE Transactions on*, vol. 10, no. 11, pp. 3874–3886, November 2011.

[100] S. Verdu, "Spectral efficiency in the wideband regime," *Information Theory, IEEE Transactions on*, vol. 48, no. 6, pp. 1319–1343, Jun 2002.

[101] O. Onireti, F. Heliot, and M. Imran, "On the energy efficiency-spectral efficiency trade-off in the uplink of CoMP system," *Wireless Communications, IEEE Transactions on*, vol. 11, no. 2, pp. 556–561, February 2012.

[102] F. Heliot, M. Imran, and R. Tafazolli, "On the energy efficiency-spectral efficiency trade-off over the MIMO rayleigh fading channel," *Communications, IEEE Transactions on*, vol. 60, no. 5, pp. 1345–1356, May 2012.

[103] D. Duan, F. Qu, L. Yang, A. Swami, and J. Principe, "Modulation selection from a battery power efficiency perspective," *Communications, IEEE Transactions on*, vol. 58, no. 7, pp. 1907–1911, July 2010.

[104] R. Nabar, H. Bolcskei, and F. Kneubuhler, "Fading relay channels: performance limits and space-time signal design," *Selected Areas in Communications, IEEE Journal on*, vol. 22, no. 6, pp. 1099–1109, Aug 2004.

[105] X. Deng and A. Haimovich, "Power allocation for cooperative relaying in wireless networks," *Communications Letters, IEEE*, vol. 9, no. 11, pp. 994–996, Nov 2005.

[106] W. Zhang, D. Duan, and L. Yang, "Relay selection from a battery energy efficiency perspective," in *Military Communications Conference, 2009. MILCOM 2009. IEEE*, Oct 2009, pp. 1–7.

[107] H.-B. Li and R. Kohno, "Introduction of SG-BAN in IEEE 802.15 with related discussion," in *Ultra-Wideband, 2007. ICUWB 2007. IEEE International Conference on*, Sept 2007, pp. 134–139.

[108] R. H. Louie, Y. Li, and B. Vucetic, "Performance analysis of beamforming in two hop amplify and forward relay networks," in *Communications, 2008. ICC '08. IEEE International Conference on*, May 2008, pp. 4311–4315.

[109] S. Boyd and L. Vandenberghe, *Convex optimization*. Cambridge University Press, 2004.

[110] V. Rodoplu and T. Meng, "Bits-per-joule capacity of energy-limited wireless networks," *Wireless Communications, IEEE Transactions on*, vol. 6, no. 3, pp. 857–865, March 2007.

[111] S. Schaible, "Fractional programming," *Zeitschrift fur Operations Research*, vol. 27, no. 1, pp. 39–54, 1983.

[112] W. Dinkelbach, "On nonlinear fractional programming," *Management Science*, vol. 13, no. 7, pp. 492–498, 1967.

[113] C. W. Cobb and P. H. Douglas, "A theory of production," *American Economic Review*, vol. 18, no. 1, pp. 139–165, 1928.

[114] Y. Chen and L. Qu, "The impact of ICT on the information economy," in *Wireless Communications, Networking and Mobile Computing, 2008. WiCOM '08. 4th International Conference on*, Oct 2008, pp. 1–4.

[115] L. Badia, C. Saturni, L. Brunetta, and M. Zorzi, "An optimization framework for radio resource management based utility vs. price tradeoff in WCDMA systems," in *Modeling and Optimization in Mobile, Ad Hoc, and Wireless Networks, 2005. WIOPT 2005. Third International Symposium on*, April 2005, pp. 404–412.

[116] L. Deng, Y. Rui, P. Cheng, J. Zhang, Q. Zhang, and M. Li, "A unified energy efficiency and spectral efficiency tradeoff metric in wireless networks," *Communications Letters, IEEE*, vol. 17, no. 1, pp. 55–58, January 2013.

[117] J. Rao and A. Fapojuwo, "On the tradeoff between spectral efficiency and energy efficiency of homogeneous cellular networks with outage constraint," *Vehicular Technology, IEEE Transactions on*, vol. 62, no. 4, pp. 1801–1814, May 2013.

[118] K. Schittkowski, "NLQPL: A fortran-subroutine solving constrained nonlinear programming problems," *Annals of Operations Research*, vol. 5, pp. 485–500, 1985.

[119] L. Yang and G. Giannakis, "Analog space-time coding for multiantenna ultra-wideband transmissions," *Communications, IEEE Transactions on*, vol. 52, no. 3, pp. 507–517, March 2004.